**ADDIS ABABA UNIVERSITY**

**COLLEGE OF HEALTH SCIENCES**

**SCHOOL OF PHARMACY**

**DEPARTMENT OF PHARMACEUTICS AND SOCIAL PHARMACY**

# Green Synthesis of Honey based Silver Nanoparticles for Ampicillin Delivery against Drug Resistance *Escherichia Coli*

**By: Engidashet Fekade Tadesse (B. Pharm)**

**August, 2023**

**Addis Ababa, Ethiopia**

Green Synthesis of Honey based Silver Nanoparticles for Ampicillin Delivery against Drug Resistance *Escherichia Coli*

By Engidashet Fekade Tadesse

A Thesis Submitted to the Department of Pharmaceutics and Social Pharmacy, School of Pharmacy, College of Health Sciences, Addis Ababa University for the partial Fulfillment of the Requirements of the Degree of Master of Science in Pharmaceutics.

Under the supervision of:

Gebremariam Birhanu (PhD)

Fantahun Molla (Asst.Prof)

August; 2023

Addis Ababa, Ethiopia

## Declaration

I, the undersigned, declare that the thesis titled "Green Synthesis of Honey based Silver Nanoparticles for Ampicillin Delivery against Drug Resistance *Escherichia Coli* ''is the result of my own research and has not been done in substance for the award of any degree at any other university. All sources of resources used in this thesis have been properly credited.

Name of the Student: Engidashet Fekade Tadesse

Signature_____Date_____

# Addis Ababa University

## School of Graduate Studies

This is to certify that the thesis prepared by Engidashet Fekade Tadesse, entitled: "Green synthesized silver nanoparticles using aqueous extract honey for ampicillin delivery against resistant *Escherichia coli*" and submitted in partial fulfillment of the requirements for the degree of Master of Science in Pharmaceutics complies with the regulations of the University and meets the accepted standards with respect to originality and quality.

Approved and signed by the examining committee:

| Name | Signature | Date |
|---|---|---|
| 1. Dr.Dereje Kebebe (External Examiner) |  | 19-Aug-23 |
| 2. Mr. Muluken Nigatu (Internal Examiner) | | |
| 3. Dr. Gebremariam Birhanu (Advisor) |  | 19-Aug-23 |
| 4. Mr. Fantahun Molla (Advisor) | | |

Chief of the department or Graduate programe coordinator

## Acknowledgement

First and above all, I would like to thank the Almighty God who gave me the courage and strength to complete my thesis. Successful completion of this thesis was possible due to the support of many people and organizations. It is therefore a pleasant opportunity for me to express my gratitude for all of them.

My sincere and profound gratitude and appreciation goes to my advisors Dr. Gebremariam Birhanu, and Fantahun Molla for their invaluable advice, comments, follow-up and words of inspiration throughout this work. And my special thanks also go to Dr.Yitayal Adimasu for his special help in this work.

I extend my sincere thanks to the Ethiopian Pharmaceutical Factory (EPHARM) (Ethiopia) P.L.C. for giving me of Ampicillin. I am grateful to the Department of Chemistry, College of Natural Sciences, Debre Berhan University for donating materials and instruments and for providing me access to the laboratory facilities to perform antimicrobial susceptibility testing. I also thank the Ethiopian Institute of Public Health for the generous gift of the necessary materials and equipment including the bacteria *E.coli*.

I also want to thank Debre Birhan University and Addis Ababa University for sponsoring of my study.

Finally, I want to thank my instructors, friends, and for their assistance, and encouragement throughout this work.

**Table of Contents**

## List of Figures

## List of Tables

## List of Abbreviation/Acronyms

Ag: Silver

AgNPs: Silver Nanoparticles

AMP: Ampicillin

AMR: Antimicrobial Resistance

API: Active Pharmaceutical Ingredient

AST: Antibacterial Susceptibility Test

ATCC*:* American Type Culture Collection

BBB: Blood Brain Barrier

CDC: Center for Disease Control

CFU: Colony Forming Unites

CLSI: Clinical Laboratory Standards Institutes

CSF: Cerebrospinal Fluids

DDD: Drug Delivery Devices

DDS: Drug Delivery Systems

DL: Drug Loading

DLS: Dynamic Light Scattering

DM: Dialysis Membrane

DNA: Dioxin Nucleic Acid

DSC: Differential Scanning Calorimetry

DW: Distilled water

E.coli: Escherichia Coli

EARS-NET: European Surveillance Antimicrobial Consumption Network

EE: Encapsulation Efficiency

EPHARM: Ethiopian pharmaceutical factory

EPHI: Ethiopian Public Health Institutes

FTIR: Fourier-Transform Infrared Spectroscopy

GDP: Growth Domestic Product

GLASS: Global antimicrobial resistance surveillance system

HIV: Human Immune Virus

ICH: International Council for Harmonization

kDA: Kilo Dalton

LC: Loading Capacity

MBC: Minimum Bactericidal Concentration

MDR: Multi Drug Resistance

MIC: Minimum Inhibitory Concentration

MS: Mass Spectroscopy

MWCO: Molecular Weight Cutoff

NPs: Nanoparticles

PDI: Polydispersion Index

PECA: Polyethylcyanoacrylate

PSD: Particle Size Distribution

RNA: Ribose Nucleic Acid

ROS: Reactive Oxygen Species

SEM: Scanning Electron Microscopy

SSA: Sub-Saharan Africa

TB: Tuberculosis

TEM: Transmissions Electron Microscope

UN: United Nation

UNSDG: United Nation Sustainable Development Goals

US: United States

USA: United States of America

USD: United States Dollar

UTI: Urinary Tract Infection

UV-Vis: Ultraviolet-Visible Spectroscopy

WHO: World Health Organization

XRD: X-ray Diffraction

ZOI: Zone of Inhibition

## Abstract

The efficiency of antibiotics is currently being limited by the critical public health issue of antimicrobial resistance. Neonatal mengitus, which is predominantly caused by Escherichia coli (*E. coli*), is the most common infection. Its management has becoming more challenging due to the emergence of antibiotic resistance.

The goal of the current study was to synthesize AgNPs from honey's aqueous extract to deliver ampicillin (AMP) and boost its potency against AMP-resistant *E. coli*. Important operating parameters were under control. One factor at a time method was employed for optimizing the effects of temperature, time, pH, silver nitrate and honey concentrations, and the ratio of the mixing amount of aqueous extracted honey and silver nitrate solutions. AMP was loaded into AgNPs by changing the incubation period and AMP concentration. The AMP-loaded AgNPs were characterized using UV-vis spectroscopy, Fourier transform infrared (FTIR), X-ray diffraction (XRD), differential scanning calorimetry (DSC), Dynamic light scattering (DLS), and Scanning electron microscope (SEM). The *in vitro* drug release profile AMP loaded AgNPs was evaluated at pH 1.2, 6, 7.3, 7.4 and 8. The *in vitro* antibacterial capability of AMP, AgNPs and AMP loaded AgNPs and honey against *E.coli* was examined using the disc diffusion method.

The optimized AgNPs had a $49 \pm 0.572$nm crystal size and a spherical and uneven shape. X-ray energy dispersive spectroscopy, verified the purity of the manufactured AgNPs. UV-visible and FTIR spectra of the AMP loaded AgNPs revealed separate bands for both the AMP and AMP loaded AgNPs. Optimized AMP-loaded AgNPs had loading contents of 48.08 % and 96.3% entrapment efficiency. A regulated release of AMP over 24 hours was achieved with a pH medium of 7.3 and pH 7.4. Inhibitory zones for AgNPs, and AMP loaded AgNPs were 10.00± 0.6673 and $17.2 \pm 1.686$mm, respectively where it was null for honey and AMP. AMP loaded AgNPs demonstrated substantially potent antibacterial action as compared to AMP and AgNPs alone. Thus, against AMP-resistant *E. coli*, the AMP-loaded AgNPs has shown encouraging results.



**Keywords:** Ampicillin, Ampicillin loaded silver nanoparticle, Antimicrobial resistance, Green synthesis, Honey extract, Silver nanoparticles

# 1. Introduction

## 1.1. Background

Microorganisms are a common ally of humans but can be the worst if they are not handled appropriately (Puzniak *et al*., 2021). Throughout human history, microbial infections have been a major source of disease (Geta, 2019). By way of illustration, women who received postpartum treatment, showed a markedly greater incidence of bacterial infection. These illnesses are frequently caused by common bacteria strains such as *S. aureus, E. coli, K. pneumoniae, Citrobacter, Enterobacter*, and S. *pyogenes* (Bitew *et al.*, 2019).To combat bacteria-caused illnesses, antibiotics were developed in the late 19th century. Indeed one of human's greatest achievements in the 20th century was the development of antibiotics (Ahmad and Khan, 2019; Friedman, Temkin, and Carmeli, 2016).

Antibiotics are chemicals that are crucial for eradicating or inhibiting the growth of microorganisms (Geta, 2019). In the "golden period" of antibiotic discovery, the majority of antibiotics were found in 1941. Alexander Fleming originally isolated penicillin from the fungus Penicillium notatum in 1928, making it the first antibacterial substance. Numerous antibiotics have been found since the beginning of 1941, and today they are primarily produced semi-synthetically or synthetically by chemical alterations of natural antibiotics that already exist to increase their efficacy (Sanseverino *et al.*, 2018).

The development of antibiotics allowed us to save the lives of numerous individuals around the globe (Geta, 2019). For the past 73 years, infectious diseases have been treated with antibiotics caused by bacteria that can be fatal (Molchanova, Hansen, and Franzyk, 2017). The development of effective antibiotics transformed bacterial treatment in contemporary biomedicine. Even though the discovery of these antibiotics was a significant development for the medical field, another heartbreaking development like antimicrobial resistance (AMR) was on the horizon. Sadly, the emergence of resistance these days restricts the efficacy of any treatment intervention (Ahmad and Khan, 2019).

Microorganisms' capacity to withstand the effects of medications is known as AMR. Whereas before they were sensitive, microorganisms developed a tolerance to the antibiotics (Geta, 2019).

One of the greatest concerns for humankind today is AMR, which poses a massive threat to world health (Hasan and Al-Harmoosh, 2020; Hernando-Amado *et al.*, 2019; Jubeh; Breijyeh and Karaman, 2020). It is an issue that affects the entire world and is also associated with prolonged hospital stays, increased medical expenses, high morbidity, and death (Geta, 2019).

There are other potential explanations for subpar client treatments, so AMR isn't just concerned with combating infections. For instance, widespread anthropogenic antibiotics, biocides, heavy metals, and other pollutants may cause imbalances in the microbial communities' homeostasis throughout the biosphere (Hernando-Amado *et al.*, 2019). Bacteria of the gram-positive and gram-negative type's varieties showed signs of resistance to the most regularly used medicines examined *in vitro*. In moms who are more susceptible, antibiotic-resistant strains represent a serious hazard, according to multidrug-resistant (MDR) bacteria (Bitew *et al.*, 2019). Figure 1 shows us that antibiotic resistance is occasionally rising.

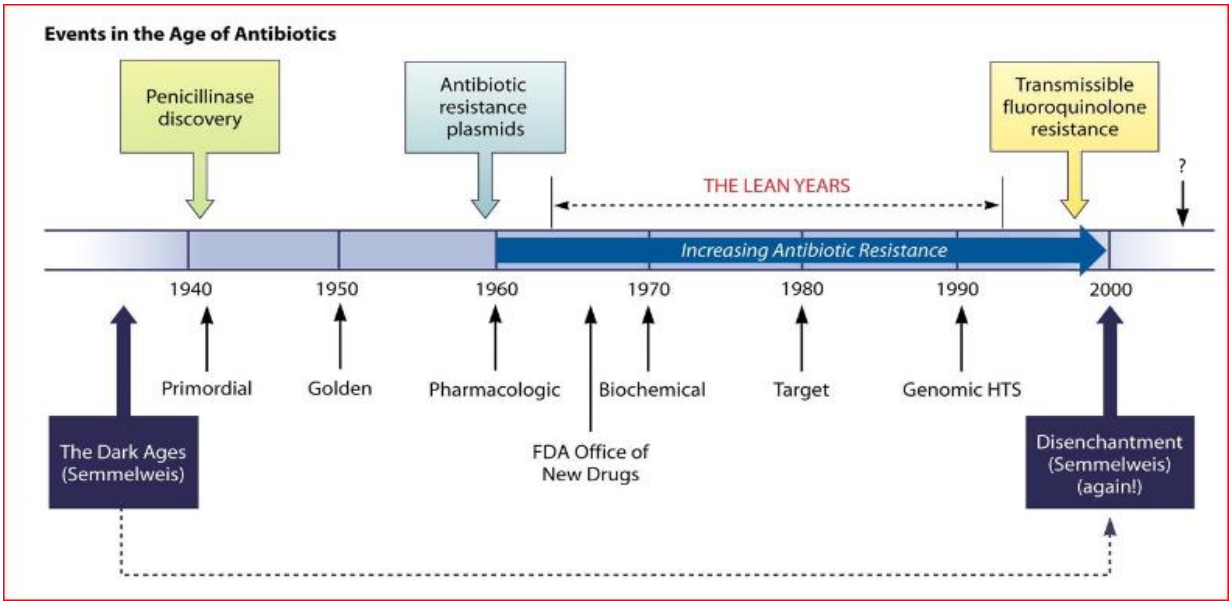


**Figure 1:** The history and the discovery of antibiotics then the concurrent emergence of AMR (Adapted from (Geta, 2019))

Until now, the first class of therapeutic medications that have been proven to successfully treat infections has been antibiotics. One of the deadliest infectious diseases in human history is AMR. The level of drug resistance has been rising since the 1940s (Geta, 2019).

### 1.1.1.Neonatal meningitis

Acute bacterial meningitis is associated with severe morbidity and death, and it occurs more commonly during the first month of life than in any other month. Neonatal meningitis (NM) is a condition marked by a meningeal infection that typically affects newborns in their first 28 days of life (Reta and Zeleke, 2016). In SSA, NM is a major cause of morbidity and necessitates immediate empirical treatment with parenterally administered antibiotics (Swann *et al*., 2014).

Neonatal meningitis occurs between 0.2 and 0.5 times per 1,000 live births in Western nations, although rates of 1.1 to 1.9 times per 1,000 births have been recorded in poor nations. Treatment-related mortality varies, with survival rates ranging from 17 to 29% and complication rates from 15 to 68%. Children under the age of 15 make up about two-thirds of meningitis fatalities in low-income nations (Reta and Zeleke, 2016).

Low birth weight, preterm membrane rupture, maternal chorioamnionitis, and low socioeconomic level are all neonatal and maternal risk factors for meningitis in newborns (Reta and Zeleke, 2016). The most significant bacteria responsible for NM were found to be *S. pyogenes* (20%) and *E. coli* (18%) (Reta and Zeleke, 2016). Therefore, according to the research of Reta and Zeleke (16), *E. coli is the* second most common reason for infant meningitis. Among the eight pathogens chosen for the Global AMR Surveillance System (GLASS)'s first phase of implementation is *E. coli*, which is a frequent reason for hospitalization and community-based infections globally (Department of Health South Africa, 2017). Additionally, as part of WHO's initial GLASS implementation, it is one of the three pathogens that Ethiopia is most concerned about monitoring (Ibrahim et al., 2019).

### 1.1.2.Ampicillin trihydrate

An effective treatment for gram-positive and gram-negative bacterial infections caused by *Streptococcus, Bacillus anthracis, Haemophilus influenzae, Neisseria gonorrhoeae, and Escherichia coli* is AMP trihydrate; broad-spectrum semisynthetic penicillin. This antibiotic is used to treat otitis media in children and upper respiratory tract infections (US Department of Health and Human Services, 1992). Its molecular weight is 371.39 g/mol.

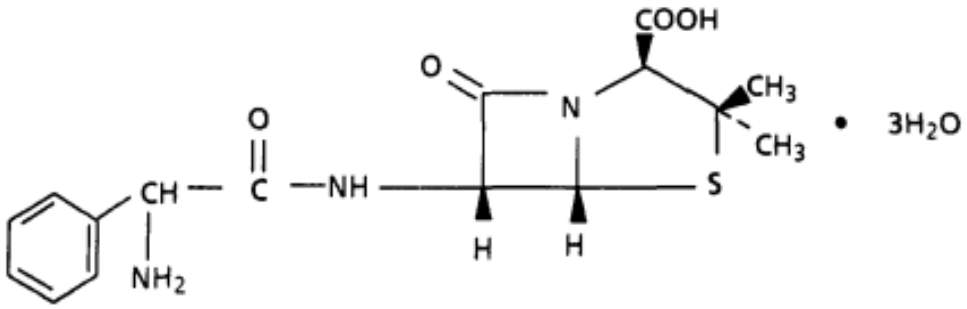


**Figure 2:** Ampicillin trihydrate Chemical Structure

AMP trihydrate, which shares a chemical formula with the substance $C_{16}H_{19}N_3O_4S$ 3H2O, is a semi-synthetic material of aminopenicillin composed of the element penicillin core, 6-aminopenicillins acid (Khan *et al.*, 2015).

The chemical stability of β-lactam units has long been a source of concern. AMP instability rapidly lowers its antibacterial activity. It is a white, odorless microcrystalline powder with a bitter flavour. Temperature and pH appear to have the greatest influence on AMP's aqueous stability. When AMP is stored in an alkaline environment, it loses its antibacterial activity and becomes easily soluble in alkaline solutions. Furthermore, at pH 8, AMP exhibits a charged state, i.e., it is water soluble, and a reversal voltage permeation experiment can be directly performed to assess AMP flux (Ghai *et al.*, 2018).

The most popular antibiotic for treating bacterial infections like *E. coli* and Neisseria meningitis is AMP, which has wide antibacterial activity. Particularly when the meninges are inflamed, it reaches the cerebrospinal fluid (CSF). For the first week of life, 50 mg/kg of AMP should be administered every 12 hours; for children aged 1-3 weeks, it should be administered every 8 hours; and for infants aged 4 weeks and older, it should be administered every 6 hours. In divided dosages, this AMP is given to treat meningitis at a dose of 300 to 400 mg/kg/day (Pacific, 2017).

1.1.3.Ampicillin treatment challenges

The effectiveness of prescribed drugs in treating bacterial meningitis is one of two key therapy con cerns.Size, load, lipophilicity, protein binding ability, interactions with the antibiotic's efflux pump

s, and the degree to which the bloodbrain barrier (BBB) is compromised by inflammation all have an impact on how well the drug crosses the BBB.However, the antibiotic's CSF concentration and bactericidal activity against the causing microbes also affect clinical effectiveness (Van De Beek et al., 2012).

The pH of CSF is 7.3 (Siesjö, 1972), which is almost similar to pH 7.4. Similarly, AMP doesn't directly penetrate in normal meningitis. To curb the developments of resistance, novel technology is being developed, i.e., nanoparticles (Liu *et al.*, 2021).

The predominant cause of NM is still *E. coli*. When compared to infants with late-onset meningitis, the percentage of multidrug-resistant *E. coli* recovered from neonates is substantially lower. Clinicians should consider this pattern when selecting effective and suitable antibiotics as an empirical treatment for NM. Between 10% and 15% of people die, particularly during the newborn period. Extraintestinal pathogenic *E. coli* is one of the most common bacteria that cause extraintestinal disorders such as NM, septicemia, and urinary tract infections (UTI) (Liu *et al.*, 2021).

Use of broad-spectrum antibiotics is known to increase the danger of *enterobacteriaceae*, notably *E. coli*, which are resistant to medicines, colonizing new areas and spreading. According to the European Surveillance of Antimicrobial Consumption Network (EARS-Net), national *E. coli* resistance levels have been related to national antibiotic usage in the hospital and community sectors. There are large inter-country disparities in the use of broad-spectrum antibiotics, according to the most recent data from the EARS-Net, necessitating a stronger emphasis on antibiotic stewardship and more chances for reducing antimicrobial consumption (Livermore, Macgowan and Wale, 2018).

More than half of the *E. coli* isolates reported to the EARS-Net in 2018 were resistant to at least one type of antibiotic, including carbapenems, aminoglycosides, fluoroquinolones, third-generation cephalosporin's, and aminopenicillin. The resistance to AMP increased significantly between 2015 and 2019. AMR *E. coli* was the major source of cases and sickness in Europe, accounting for the majority of the burden of AMR(Livermore, Macgowan and Wale, 2018).

## 1.2.Nanotechnology

Nanotechnology uses small-scale interactions to synthesize new applications (Pal *et al*., 2011). Preventive measures and comprehensive strategies are needed to address *E. coli* resistance(Tuem *et al.*, 2018). It may help to treat bacterial infections and prevent diseases(Singh *et al.*, 2021). The most promising strategy for combating AMR is nanoparticles (NPs) (Prasad, 2008). Nano is any product with dimensions between 1 and 100 nm(Vallet-Regí, González and Izquierdo-Barba, 2019). NPs are effective in combating bacterial infections due to their bactericidal activity. In order to eliminate AMP resistance, NPs are preferred because of their high surface-to-volume ratio and crystalline surface structure, which encourages chemical activity against *E.coli* (Prasad, 2008).

Nanotechnology creates new antibacterial agents to stop AMR and eradicate resistant germs. About 99,000 scientific papers about the hunt for novel antimicrobial compounds were published between 2018 and 2020, of which 5,900 dealt with the search for antimicrobial compounds based on metallic components like zinc, copper, nickel, cobalt, manganese, chromium, and silver (Bahiru, 2022).

Nanomedicine is emerging to combat AMR and international research and commercial endeavors are being undertaken to release antibiotics resistant to common infections(Boisseau and Loubaton, 2011; Morigi *et al.*, 2012; Prasad, 2008). Investigation of bactericidal nanomaterials is essential to avert AMR, with AgNPs being a front line form(Prasad, 2008; Stabryla *et al.*, 2021). Entry feasibility is assessed by market category, size, structure, competitors, and market share. Silver ions and AgNPs have effects on gram-positive Vs gram-negative bacteria that are dose- and size-dependent(Prasad, 2008; Morigi *et al.*, 2012). In general, using AgNPs to deliver drugs is a good strategy for combating the issue of drug resistance (Wang, Hu and Shao, 2017).

### 1.2.1. Nanoparticles

Antibiotic-resistant bacterial strains are a public health issue(Hadiya *et al.*, 2018). Studying the bioactivity and uses of metal NPs is necessary to find a solution to this problem. Nanotechnology is expected to have an economic impact of $3.1 trillion by 2020(Singh *et al.*, 2021). Nano-sized metal particles have distinct chemical, physical, and biological properties (Id *et al*., 2018). Designing and creating novel methods that use NPs to eradicate the resistant strain of bacteria is

currently receiving a lot of attention(Pal *et al.*, 2011). As a result, there should be a compelling reason to prepare novel bactericides and dosage formulations employing nanotechnologies (Hadiya *et al*., 2018).

NPs have significant benefits over conventional drug design in terms of their high stability, high specifity, high drug carrying capacity, ability for controlled release, potential of use in a variety of administration routes, and capacity to deliver both hydrophilic and hydrophobic drug molecules (Pal *et al*., 2011). Future NPs want to stay away from AMR. NPs are preferred because they interact directly with the bacterial cell wall to stop AMR (Wang and Hu, 2017). According to Blanco Massani *et al*. (2018), the apoptotic response against *E. coli* is the mechanism of silver ions (Ag+) (Blanco Massani *et al.*, 2018). However, Jubeh *et al*. (2020) and Id *et al*. (2018).'s study claim that the specific mechanism of action is uncertain (Id *et al.*, 2018; Jubeh, *et al*., 2020). According to another study by Singh *et al.* (2020), free metal NPs have detrimental impacts on the bacterial surface's outer membrane breakdown. While the primary mode of action for metal oxide NPs is oxidative stress brought on by reactive oxygen species (ROS)(Chmielewska *et al*., 2021).

Studies have shown that the release of ions from AgNPs causes the formation of pits and gaps on the surface of bacterial membranes. These ions subsequently interact with the disulfide or sulfhydryl groups of enzymes to disrupt the metabolic pathway, which ultimately causes bacterial cell death (Singh *et al*., 2020).

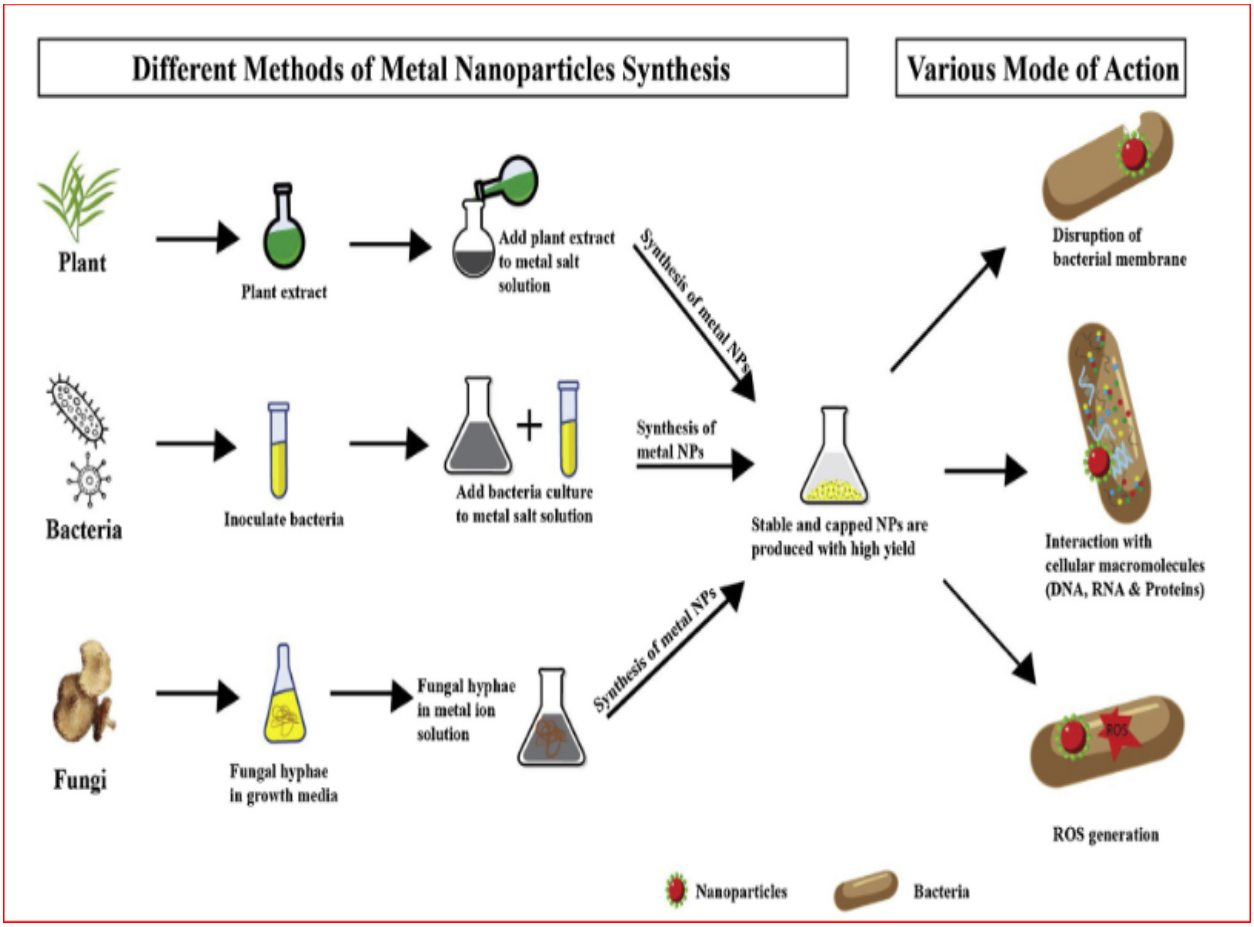


**Figure 3**: Green synthesis of metallic NPs using bacterial, fungal, and plant sources(Singh *et al.*, 2020)

An important function for NPs in halting the global spread of AMR is in its containment. These NPs can also be used to salvage antimicrobials from existing resistant strains(Gupta *et al.*, 2020). Contrarily, according to a study by Morigi *et al.*, (2012), Gram-negative bacteria have a thin peptidoglycan layer between the cytoplasmic membrane and the outer membrane, which makes NPs more effective bactericides than gram-positive bacteria.

### 1.2.2.Green metallic nanoparticle synthesis

NPs can be prepared using either a top-down or bottom-up approach. The top-down approach involves formulating or synthesizing a nanoscale structure starting from the largest ones by "cutting" the size to the required values. This is in contrast to the bottom-up approach, which starts with the molecular, atomic, or ionic level and precisely controls the molecular structure (Pryshchepa, Pomastowski and Buszewski, 2020).

Based on the procedures used, synthesis techniques can be categorized into three types: physical, chemical, and biological procedures, with the first two methods being regarded as conventional methods. For the synthesis of nanomaterials, physical techniques use physical agents like heat, electrical discharge, plasma, or electromagnetic radiation(Pryshchepa, Pomastowski and Buszewski, 2020)

Mechanical milling and ball milling, laser ablation, sputter deposition, lithography, and spray pyrolysis are all included in this process. On the other hand, the chemical method is based on the premise that the initial components metal precursor, reducing agent, and stabilizing (capping) agents are chemically changed to yield NPs. It encompasses micro-emulsion synthesis, chemical reduction, hydrothermally mediated precipitation, and sol-gel synthesis(Pryshchepa, Pomastowski and Buszewski, 2020). However, both physical and chemical methods have drawbacks, including high costs, low production rates, requirements for a highly constrained laboratory environment, high temperature and pressure requirements, high energy requirements for synthesis, production of toxic by-products, and in the case of chemical methods, the possibility of toxic chemicals being adsorbed on the surface, which makes biological applications of NPs challenging(Akbar *et al.*, 2020). In these methods, additional capping and stabilizing compounds are also necessary (Sharma, Garg and Kumari, 2020).

It is evident that a different approach that is economical, secure, and environmentally friendly is required to address these limits in NP synthesis. A workable alternative in this case is the green synthesis approach. Bottom-up approaches can be microbiological (using bacteria and bacterial extracts), natural (using plant or algal extracts), or biomolecular/biopolymer (using structural biopolymers or biomolecules obtained from living organisms)(El Shafey, 2020).

Plant-mediated green synthesis is becoming more and more popular due to the challenges involved in choosing and growing a good bacterial strain, scaling laboratory processes to industry, and adding another stage of purification to the preparation of microorganism-mediated NPs(Mokhena *et al.*, 2018). Additionally, this microbe-mediated synthesis requires the upkeep of microorganism cultures, extremely sterile settings, and expensive media and process costs (Agarwal, Venkat Kumar and Rajeshkumar, 2017). The plant-mediated green synthesis method uses natural extracts, primarily phytochemicals (including sugars, lignans, polyphenols, flavonoids, aromatic acids, xanthones, terpenes, quinones, proteins, and alkaloids) obtained from plants, leaves, fruits, peels, flowers, and seeds, to synthesize inorganic NPs, including metal oxide NPs (Mokhena *et al.*, 2018).

The riskiness of nanotechnology is generally decreased by the green synthesis process; this also mitigates the adverse impacts of the production and application of nanomaterials. It is an environmentally friendly method that uses biological components to lower synthesis costs and serve as capping or reducing agents, consumes less energy, and may be applied to the large-scale manufacturing of NPs(El Shafey, 2020). However, this method has limitations, including the inability to pinpoint the precise phytochemical molecule that causes the preparation of NPs and the unpredictability of phytochemical levels in plants as a result of environmental factors like location and temperature change (Mokhena *et al.*, 2018).

### 1.2.3.Green synthesis of silver nanoparticles

Silver nanoparticles (AgNPs) can be produced by utilizing microbes and plants that have biomedical uses through a process called green synthesis. This strategy is economical, environmentally responsible, biocompatible, safe, and green(Agarwal, Venkat Kumar and Rajeshkumar, 2017).However, the other methods of AgNPs synthesis aren’t economical, environmentally friendly, safe and green.

### 1.2.4.AgNPs as drug delivery devices (DDDs)

Metallic NPs are reliable drug delivery mechanisms due to phytochemicals(Sreedharan and Singh, 2019). NPs offer tailored delivery of the ideal dose with decreased toxicity, solubility, and bioavailability. Among these NPs, AgNPs provide passive or active targeting to tumor tissue, increasing anticancer therapy effectiveness *in vivo* through drug accumulation and receptor-mediated endocytosis(Mokhena *et al.*, 2018).

### 1.2.5.Silver nanoparticles as antimicrobial agent

AgNPs are used to treat resistant strains, low in toxicity (Lim *et al*., 2016; Rogowska et al., 2017). AgNPs have antibacterial properties because of their nanoscale (Id *et al*., 2018). AgNPs is thought to be a new weapon against certain infectious disorders, such as MDR bacteria(Thapa *et al.*, 2017). The most widely utilized metal NPs for anticancer, bactericidal, fungicidal, and antiviral purposes (Blanco Massani *et al.*, 2018). AgNPs can be used to deliver antibiotics and create sanitizing filters. AgNPs have bactericidal properties due to their stability in the growing medium (Jubeh, et al., 2020; Morigi et al., 2012).

One of its prospective uses is the use of antibiotics in conjunction with AgNPs. AgNPs containing AMP, when developed, will greatly enhance AMR (Skiba-kurek, 2020). Green synthesis of AgNPs is essential for biogenic production of nanomaterials(Mohammed *et al.*, 2010).The silver cation ($Ag^+$) is still widely used in the healthcare context as an antibacterial agent for bacterial infection prevention and treatment (Elkrewi *et al.*, 2017). Topical application is crucial, which is the main point (Percival, Salisbury and Chen, 2019), where incidences of bacterial resistance to the biocidal activity of silver are uncommon (Lim *et al*., 2016).

Silver has been found to have antibacterial properties (Lim *et al*., 2016). A different study discovered that the high antibacterial action is related to doses (>40 μg/ml), yet these concentrations have been reported as hazardous to aquatic organisms like algae and mammalian cells (Id *et al*., 2018). Another study, however, shown that while AgNPs are hazardous to mammals and host animals at high concentrations (>10 μM), silver has significant potential against microbes at low quantities (Morigi *et al.*, 2012). Whereas, Khan *et al* (2019).'s study showed that

nanosilver (1nm to 100 nm) is harmless to humans and is approved for use in pharmaceuticals (Khan *et al.*, 2019).

At a concentration of 40µg/ml, NPs with diameters ranging from 5 to 100 nm have been found to exhibit bactericidal effects on tested bacteria. Smaller NPs (<30nm) sizes have more activity than larger NPs, and it is believed that this is because the smaller particles can more easily release silver ions (Id *et al*., 2018). Many bactericidal applications have made substantial use of silver-based compounds (Id *et al*., 2018; Morigi *et al*., 2012; Percival, *et al*., 2019). Silver salts and derivatives are used as antibacterial agents. AgNPs interact with bacteria size-dependently using electron microscopy (Morigi *et al*., 2012).

AMR is reducing the number of effective medications used to treat infectious diseases. In order to reduce this problem, use nanocarriers like AgNPs (Stabryla *et al.*, 2021). AgNPs without AMP, AMP polymersomes without AgNPs, and free AMP had no impact on bacterial growth. At a silver-to-AMP ratio of 1: 0.684, it was found that the synergistic interaction between the AgNPs and AMP completely inhibited growth(Geilich *et al.*, 2015).

The preparation of fresh, efficient antibacterial tactics will receive special attention (Pal *et al*., 2011). AMP's sensitivity will rise as a result of the preparation of AMP-loaded AgNPs. *E. coli, Klebsiella pneumoniae, S. aureus, Pseudomonas aeruginosa, and Staphylococcus epidermidis* gram (-) and the gram (+) bacteria strains respectively that the AMP-loaded AgNPs demonstrated high sensitivity against them (Rogowska *et al*., 2017).

Numerous studies showed that combining antibiotics with AgNPs increases the antibacterial therapy's efficacy (Pal *et al*., 2011). AMP loaded AgNPs improve effectiveness against resistant germs. AMP and green synthetic AgNPs have a proven synergistic antimicrobial action against *E. coli.* AgNPs and AMP can be used to treat skin and mucous membrane infections (Rogowska *et al*., 2017). AgNPs are promising drug carrier for overcoming antibacterial resistance (Kora and Rastogi, 2013).

Finally, combining AMP with AgNPs has synergistic effects. Even at its greatest concentration (equivalent to 32 mg/l), AMP without AgNPs has no antibacterial activity against *E. coli*. This is a result of *E. coli's* AMP resistance. According to the database of the European Committee on

Antimicrobial susceptibility testing(AST), the AMP breakpoint against *E. coli* is 8 mg/L, while MICs (5 mg/L and 2.5 mg/L) higher than the breakpoint indicate bacterial resistance (Kolár *et al.*, 2016).

AMP and AgNPs can restore or enhance antibacterial properties. Silver does not need to be present in in large concentrations to make *E. coli* susceptible to AMP again(Kolár *et al.*, 2016). The main goal of this thesis was to use honey and AgNPs and then to show that *E. coli* has developed sensitivity to AMP loaded AgNPs. To achieve a stabilized effect in the intended formulation, the functions of silver for AMR resistance *E.coli* curving were coordinated with local honey.

### 1.3. Effects of Honey

Honey is a naturally sweet material used to heal wounds(Tsang *et al.*, 2017; Combarros-Fuertes *et al.*, 2020). The honey's content varies based on its source, as well as external elements like the season and location, as well as internal factors like processing, manipulation, packing, and storage conditions (Combarros-Fuertes *et al*., 2020). It has antibacterial, anti-inflammatory, anti-oxidant, and immune system-boosting properties(Y. *et al.*, 2013). Honey's multifaceted antibacterial effect, which poses no threat to bacterial resistance development, is one of its key characteristics(Y. *et al.*, 2013; Juraj M. *et al*., 2020).

Gram-positive bacteria respond better to honey than Gram-negative bacteria do (Juraj Majtan, *et al*., 2020; Y., E., *et al*. 2013). Due to its broad-spectrum action, honey is an attractive source for drug development(Israili, 2014). It's cellular targets and underlying mechanisms of action are still unknown(Brudzynski and Sjaarda, 2014). According to a study by Laallam *et al.* (2015), *C. perfringens* was the species that was least sensitive to honey, while *E. coli* was the most sensitive. Intermediate findings were found when honey's antibacterial activity against *B.subtilis* and *S.aureus* was tested (Laallam *et al.*, 2015).Honey has antibacterial properties, but it is unclear how it interacts with bacteria ( Green, Dods and Id, 2020; Nishio *et al.*, 2016 ).

High levels of sugar, little water, a low pH, and a high concentration of flavonoids in honey are all factors that contribute to its powerful effects. These parameters are further adjusted due to the botanical sources of honey and the ecological factors that affect melliferous plants in general as

well as the behavior, physiology, and fitness of bees and melliferous plants in particular ( Cokcetin *et al.*, 2016; Laallam *et al.*, 2015).

Due to the lack of evidence of microbial resistance to it, honey is a very promising topical antimicrobial agent against the infection of bacteria that are resistant to antibiotics as well as the treatment of chronic wound infections that do not respond to antibiotic therapy (Juraj Majtan, *et al*., 2020; Y., E., *et al*., 2013). It has so been utilized as a last-resort treatment since resistance issue is rare. Honey can be used as a substitute for conventional treatments in medical diseases (Juraj et al., 2020), available antibacterials against bacterial infections(Mandal and Mandal, 2011).

### 1.4. Effects of honey and silver combination

Honey has comparable antibacterial activity when combined with AgNPs(Guruvu *et al.*, 2022). AgNPs have recently attracted a lot of interest due to their potential applications in many different disciplines, including medicine and gene transport, antimicrobial defense, and biological applications. The evaluation of honey synthesis agent, and choice of non-toxic materials for AgNPs stability throughout production(Haroon Haiza *et al.*, 2013). In healing wounds, the combination of honey and silver has a greater synergistic impact (, Guruvu *et al*., 2022; Tsang *et al*., 2017). However, in this thesis, honey is employed to prepare AgNPs as a reducing agent. A synergistic impact was achieved when green prepared AgNPs were combined with AMP (Kolár *et al*., 2016).

Finally, AMP and honey prepare better dosage form for silver. Green synthesis AgNPs with aqueous extract honey exhibit weak antibacterial activity. To the best of my knowledge, no studies on the antibacterial properties of AgNPs have been conducted and AMP-loaded AgNPs made using aqueous extracted honey particularly in Ethiopia. Additionally, the potential for medication administration of AgNPs produced through green synthesis has received less attention. Based on these facts, this study's goal was to synthesize AgNPs for the delivery of AMP using aqueous extracts honey and to assess the AgNPs that have been loaded with AMP have antibacterial efficacy against AMP-resistant *E. coli.* As we've shown above, silver has a high effect on gram negative bacteria while honey has a broad range effect but it has a lot of impact on gram positive bacteria. In order to increase the treatment coverage of the newly prepared dosage forms, these two elements were combined.

Honey not only has an antimicrobial function but also stabilizes our dosage formulations. Since honey already has an antibacterial impact, this effect was investigated before to any honey combinations to determine how much honey would be included in the final dosage form. With data already obtained from published results, the final dosage form of was capsule and its impact on *E. coli* were compared with AMP-loaded AgNPs. Consequently, an assessment of the final dosage form was made.

### 1.5.Research Questions

Accordingly, this finding answered the following research questions:

- ✓ Does honey have stabilizing or reducing properties?
- ✓ Does AgNPs have good AMP encapsulation efficiency (EE) and loading capacity (LC)?
- ✓ Does AgNPs alone effective against AMP resistant *E.coli*?
- ✓ Does the AMP-AgNPs demonstrate good compatibility?
- ✓ Does AMP-loaded AgNPs improve the effect of AMP against AMP-resistant *E. coli*?

### 1.6.Statement of the problem

Resistance to antibiotics is a major threat to all living beings, caused by antibiotic abuse and the transmission of gene resistance between microorganisms. It is predicted to cause 10 million annual fatalities by 2050(Ahmad and Khan, 2019; Friedman, Temkin, and Carmeli, 2016; Geta, 2019; Jubeh, Breijyeh, and Karaman, 2020; Sanseverino *et al.*, 2018; Samuel Kariuki, 2015). It is a growing crisis in clinical medicine, resulting in increased morbidity and mortality due to increased resource use, higher expenses, and decreased hospital activity (Friedman, Temkin, and Carmeli, 2016). It is a global health problem that threatens to combat bacterial infections in Sub-Saharan Africa (SSA), and has a significant economic impact, leading to a decrease of 11 million to 444 million in the world population by 2050( Ahmad and Khan, 2019; Kariuki, Wairimu, and Mbae, 2021; Laallam *et al.*, 2015).

Antimicrobial resistance (AMR) is a major obstacle to the 2030 United Nations (UN) Sustainable Development Goals due to its spread and high cost (Dadgostar, 2019; Gemeda et al., 2021). Low-income nations, like Ethiopia, are particularly vulnerable to AMR due to inadequate antibiotic usage, poor medication quality, and poverty ( Puzniak *et al.*, 2021; Regea, 2018; Sanseverino *et*

*al.*, 2018). It is estimated to cost $55 billion annually in the United States (US), with an annual decline in world growth domestic product (GDP) of 1% in low-income nations and 5-7% in underdeveloped nations (Dadgostar, 2019). AMR is a major cause of situational and intergenerational poverty, as seen below in Figure 2, in low-income groups (Ahmad and Khan, 2019).

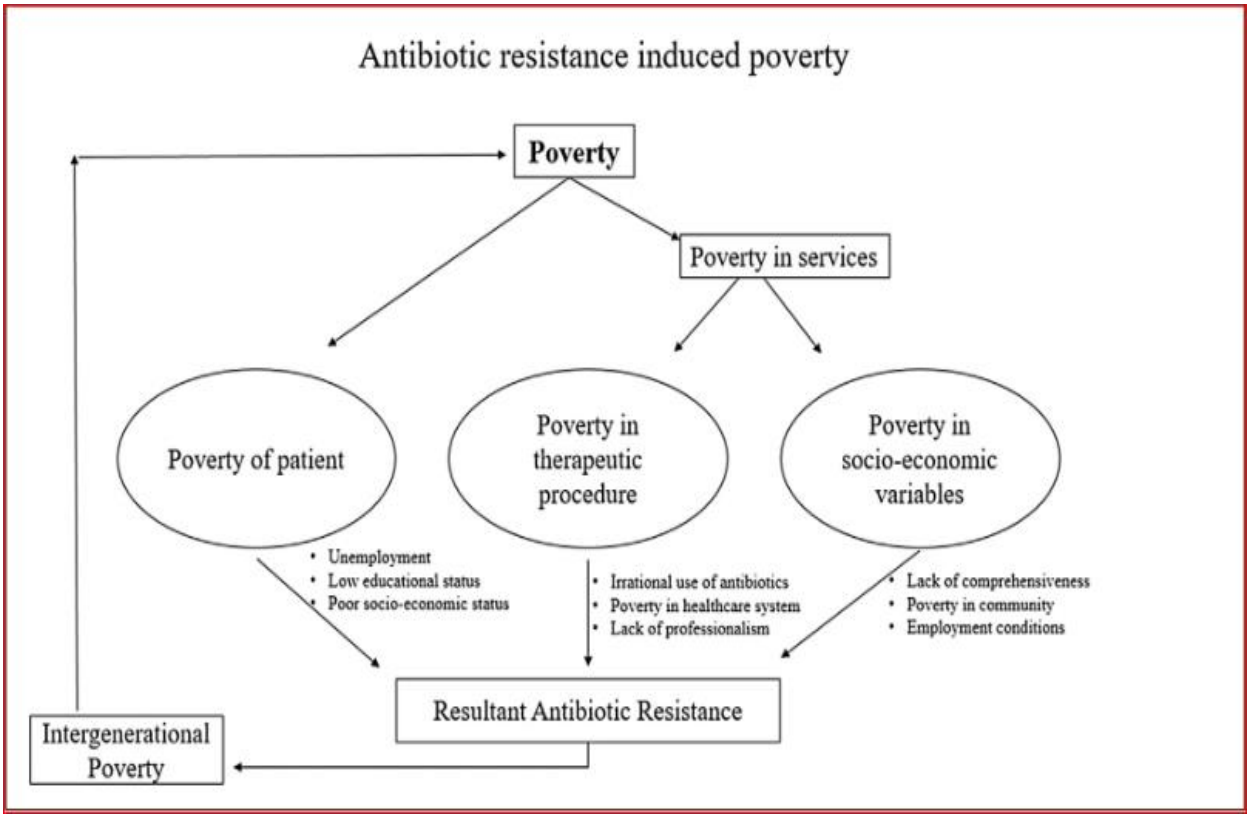


**Figure 4:** Relationship between poverty and antibiotic resistance (Ahmad and Khan, 2019).

In Europe, 32 % of *E. coli* was resistant to AMP (Livermore, Macgowan, and Wale, 2018), while it was discovered that 94.9% of *E. coli* in Ethiopia's Tigray Region are AMP resistant (Tuem *et al.*, 2019). According to a study conducted at Ayder Comprehensive Specialized Hospital in the Tigray Region of Ethiopia over a six-year period beginning in 2012 to assess the AMR patterns of bacteria isolated from urine samples, there is a high level of AMR to commonly prescribed antibiotics. Additionally, this research showed that *E. coli* had considerable resistance to all tested antibiotics, including AMP (Tuem *et al.*, 2019).

Numerous studies from various clinical settings conducted in Ethiopia found an increase in the frequency of *E. coli* AMR patterns (Tuem *et al.*, 2018). *E. coli* resistance to AMP was 82% according to a study by Kariuki, Wairimu, and Mbae from the year 2021 (Kariuki, Wairimu, and Mbae, 2021), While Tuem *et al.* (2018) discovered that *E. coli* had a maximal AMP resistance of 83.81%. However, a study conducted by Moges *et al. (2014*) found that the resistance to AMP was 100%.

Therefore, in the era of AMR development, it is critical to design efficient alternative strategies. These methods can include the creation of next-generation antibiotics, combination therapy, the use of organic antibacterial agents like plant extracts, and the application of nanotechnology, in addition to the effective use of already available antibiotics (Jelinkova et al., 2019).

### 1.7. Significances of the Study

In the past, developing new medications, giving antibiotics in high doses, and combining several antibiotics were all the approaches used to combat antibiotic resistance. Unfortunately, the development of novel antibiotics was unable to keep up with bacterial evolution, high-dose therapy was always accompanied by unbearable toxicity, and treatment methods also encouraged antibiotic abuse as well as the development of resistance strains (Merker *et al.*, 2020; Murugaiyan *et al.*, 2022).

Antibiotic resistance is on the rise and a major global concern, to overcome it, it is necessary to find new and potent antibacterial treatments. Discovering methods to stop the spread of a serious global worry for the medical industry is the development of antibiotic resistance. A broad spectrum antibiotic called AMP is becoming less and less effective as drug-resistant organisms, endangering the capacity to treat common diseases. Hence, here we aimed to demonstrate the potential of AgNPs as a promising AMP delivery strategy against *E.coli*.

The delivery method helps to preserve antibiotic efficacy and boost its antibacterial action. Many traditional AgNPs synthesis methods, such as physical and chemical ones, are expensive, call for extreme temperature and pressure conditions, and use chemicals that are difficult to dispose of since they are not environmentally friendly. As a result, AgNPs synthesis processes that use environmentally friendly methods and do not involve hazardous chemicals are becoming more and

more popular. In keeping with this, we here synthesis AgNPs from honey extracts using that is inexpensive, straightforward, quick, and safe.

## 1.8. Objectives of the study

### 1.8.1.General Objective

- ✓ To prepare AgNPs using aqueous extracted honey for AMP delivery against AMP resistant *E. coli*.

### 1.8.2. Specific Objectives

- ✓ To synthesize AgNPs by using honey extract and characterize them using various analytical techniques.
- ✓ To optimize operational elements for AgNPs synthesis,
- ✓ To load AMP on AgNPs and to characterize AMP loaded AgNPs using various analytical instruments.
- ✓ To determine the AgNPs loaded with AMP loading and EE.
- ✓ To evaluate the AMP-loaded AgNPs' in vitro drug release characteristics and
- ✓ To evaluate the effectiveness of AMP-loaded AgNPs against AMP-resistant *E. coli, in vitro* as compared with AMP and AgNPs alone.

# 2. Methodology

## 2.1. Materials and chemicals

Local honey sourced from honey bees was collected from Debre Berhan, North Shewa, Amhara region, Ethiopia. AMP trihydrate (98.2% assays, M843068 India) was kindly donated by Ethiopian Pharmaceuticals Factory (EPHARM), an Ethiopian private limited company (P.L.C.). Clinical isolates of AMP-resistant *E. coli* were obtained from microbial stem cultures at, Ethiopian Public Health Institutes (EPHI).

Other materials and chemicals used in the study include silver nitrate ($AgNO_3$) (99.99% UN 1493, BDH, GPRTM, Prod: 30087, Lot: 228K17757537), absolute ethanol (96%, Dallul Pharmaceuticals PLC ), chloroform AR (Reagent Chemical Services Ltd., UK), hydrochloric acid(HCl) (35.4%, Loba Chemie Pvt. Ltd., India, Lot: A213001611), ferric chloride (98%, Sisco research laboratories Pvt. Ltd., India), iodine (Reagent Chemical Services Ltd., UK, Lot: 1344206), sodium hydroxide (NaOH)(99.8% Norbright, China), distilled water, Whatman No. 1 and Whatman No. 3 filter paper, dialysis bag (medium dish 35 mm width and 12 kilo Dalton (KDa) molecular weight limit (SIGMA-ALDRICH, USA), thermometer, petri dish, Müller-Hinton agar (HMedia Research Laboratories Pvt. Ltd-India) were obtained from various institutions.

The working solutions of the AMP disk (10 μg AMP) were received as a donation from the University of Gonder. Analytical-grade materials were utilized throughout this project without further purification. Additionally, distilled water was used to prepare all aqueous solutions.

## 2.2.Bee Honey samples collection

The honey for this study was collected from Debre Berhan, North Shewa zone, Amhara region, Ethiopia, Debre Berhan City (Latitude: 9.6752° or 9° 40' 31" N and Longitude: 39.5325° or 39° 31' 57" E). The honey was purchased directly from the farmer from September to October, 2021. Before being used for the extraction, the obtained honey sample was kept at room temperature in a glass jar. According to the source, location, and date of collection, samples were given labels. Before an examination, the samples were strained to eliminate unwanted material such as wax sticks, dead bees, and comb fragments.

## 2.3.Preparation of Honey extract

The honey was extracted using 50 ml of water with 100gm of honey and centrifuged for 10 minutes at a speed of 3000 rpm to separate the pure honey from the wax and other impurities (Shah, 2022). Then the supernatants were removed, and the remaining portion was stored in the refrigerator (4 to 8°C) until it was used for further study.

Honey was extracted to obtain pure honey. It was used as a reducing agent. Then the honey was centrifuged in the machine, and the honey was extracted while utilizing 50 ml of water as a solvent. It was filtered via mesh sizes 10 and 60 prior to centrifugal extraction. Then, it was easily distinguished into its pure (welela) component. The centrifuge was thereafter run for 10 minutes at a speed of 3000 rpm. The wax was collected on the top of the centrifuge tube and scraped off to check whether the extracted honey contained any active pharmaceutical ingredients (API) of it by using phytochemical analysis. Next, a phytochemical analysis was performed on the samples of honey.

## 2.4. Phytochemical analysis of Honey extract

### 2.4.1.Qualitative analysis of Honey extracts

With a minor modification, the standard techniques were used to analyze the phytochemical composition of the honey samples. Tests were performed to determine the contents of alkaloids, phenolic compounds, saponins, glycosides, triterpenoids, and flavonoids (Shah, 2022).

#### 2.4.1.1.Tests for glycosides

A. Keller-Kiliani test

A glacial acetic acid solution of 4 ml was put into a test tube, and then 1–2 drops of a 2% $FeCl_3$ solution were added. The test tube was then filled with 2 ml of concentrated sulfuric acid ($H_2SO_4$) and 10 ml of extracted honey. Glycosides are present when a brown ring appears at the boundary of two immiscible solutions (Shah, 2022).

B. Salkowski’s test

To aqueous extracted honey of 10 ml, $H_2SO_4$ solution of 2 ml was added with continuous stirring. Reddish-brown coloration suggests the presence of glycosides when it forms (Shah, 2022).

2.4.1.2. Tests for alkaloids

A. Wagner’s test

Wagner's reagent and HCl of 1 ml each was added into 5ml of the aqueous extracted honey. Alkaloids are present because of the formation of a reddish-brown color(Shah, 2022).

B. Dragendorff’s test

2 ml of the Dragendorff's reagent and 4 drops of HCl were added to 5 ml of extracted honey. Precipitate that is orange or red in color forms when alkaloids are present (Shah, 2022).

2.4.1.3. Tests for saponins

A. Foam test

1 ml of extracted honey was combined with 9 ml of distilled water, vigorously shaken, and left to stand for 10 minutes. The development of stable foam demonstrates the presence of saponins (Shah, 2022).

2.4.1.4. Tests for phenolic compounds and tannins

A. Test for Lead acetate

A 50ml of test tube was filled with 2 ml of the extracted honey and 30ml of 10% lead acetate solution. The test for tannins and phenolic compounds is confirmed by the appearance of white precipitate (Shah, 2022).

B. Test for Ferric chloride

A test tube containing 5 ml of honey extract was filled, and 2% $FeCl_2$ solution was added drop by drop until a clear, dark-blue or dark-green color emerged. The presence of tannins and phenolic compounds is indicated by the production of the aforementioned color (Shah, 2022).

2.4.1.5. Tests for steroids

A. Ring test

In a test tube, extracted honey, chloroform, and acetic anhydride (UN 1715) were combined in the following ratios: 2:10:1 respectively. Then, 2ml of concentrated $H_2SO_4$ was slowly and slantingly poured along the test tube's side. The ring that formed at the solution's edge (Shah, 2022).

A. Methanol test

The extracted honey was mixed with methanol in 2:1 ratio. A spot plate was used to titrate 5 drops of the mixture with anhydrous acetate and $H_2SO_4$.The formation of the red color indicated the existence of tri-terpenoids (Shah, 2022).

2.4.1.6. Proteins test

A. Ninhydrin test

The combination of 5 ml of the extracted honey and 2 ml of ninhydrin 0.2% solution was heated on the fire. The presence of proteins was shown by the emergence of the violet color (Shah, 2022).

2.4.1.7. Tests for flavonoids

A. Shinoda test

A test tube was filled with 5 ml of extracted honey, 3 ml of strong HCl, and roughly 10 mm of magnesium ribbon. Reddish-pink coloration is caused by the presence of flavonoids (Shah, 2022).

2.4.1.8. Carbohydrates test

A. Fehling's Test

5 ml of honey extract were hydrolyzed with 1M HCl, and then neutralized with 1M NaOH. After adding an equal volume of Fehling's solutions (5 ml), the substance was heated. A red precipitate appeared, indicating that there are carbohydrates presented (Shah, 2022).

B. Benedict's test

A test tube was filled with the test solution, 5ml of extracted honey. The test tube was then heated on a water bath with a few drops of Benedict's reagent added. Reddish-brown precipitate's appearance suggests the presence of carbohydrates (Shah, 2022).

2.4.2. Quantitative analysis of Honey extract

2.4.2.1. pH Analysis

To determine the pH, a 10% (w/v) solution of honey was made (pH-016, pH meter)(Asaduzzaman *et al.*, 2015).

2.4.2.2. Moisture content

In a hot air oven set at 70°C for a total of 2 hours, a 2.0g sample was dried to a constant weight, and the moisture content was determined on a dry basis in accordance with Association of Official Agricultural Chemists (AOAC) (1990; 2000) methodology (Asaduzzaman *et al.*, 2015).The percentage of moisture content was calculated as follows:

$$\%ofAshContentLost = (\frac{WtOfSample - WtofFinalcontentAftertDried)*100}{WtofHoneySampe} .....equ(1)$$

2.4.2.3. Ash content

By drying 5.0g of honey samples in porcelain crucibles at 105°C for 3 hours in a hot air oven, the ash content was first ascertained. The dried samples were then heated to a consistent weight in a

furnace at 550–600°C, cooled, and weighed (Asaduzzaman *et al.*, 2015).Then, the ash content was calculated as follows:

$$\%ofAshcontent = \frac{(Wtofsample - WtofAsh)}{WtofhoneySample} \ldots\ldots\ldots\ldots\ldots\ldots equ(2)$$

### 2.5. UV-Visible analysis of the extracted Honey

A 1:20 dilution of the honey extract sample with distilled water was used. The UV spectrum (190-400 nm) at 1 nm intervals was then acquired using a UV-Vis spectrometer (Spectrophotometer Carry 60, Agilent Technologies USA) using 2 ml of diluted honey in a 10 mm quartz cuvette. Deionized water served as a negative control. The most sensitive wavelengths for determining whether honey is present or not are presented at wavelengths of 266, 270, 280, 290, 300, 335, and 360 nm (Suhandy and Yulia, 2021).

### 2.6. Green synthesis of silver nanoparticles

The preparation of AgNPs was done according to Habsi *et al.* (2019), with a few minor adjustments. First, the aqueous extracted honey was centrifuged (Gemmy Industrial Corp., Taiwan, Serial No.: 220 VAC/50 HZ; 0.7 A) for 10 minutes at 3,000 rpm to get rid of the honey waxes. Next, mix 15 ml of 6% aqueous extracted honey with 20 ml of a 20 mM silver nitrate (UN 1493, BDH, GPRTM, Lot: 228K17757537) solution. Then 0.1 M NaOH and 0.1 M HCl were added drop by drop into the mixture until the pH of the mixture reached 8. Then, the resulting mixture was stirred continuously at 200 rpm using a magnetic stirrer for 1 hour without heat. After 1 hour of stirring, the suspension was yellowish-brown. Following that, the suspension was centrifuged for 20 minutes at 10,000 rpm to separate the black-colored AgNPs, followed by numerous washes with distilled water to remove contaminants. Finally, the prepared AgNPs were dried in an oven at 80°C for 2 hours before being crushed in a crusher and pestle to obtain an estimated finer size for the AgNPs' subsequent characterization and application.

### 2.7. Optimization of silver nanoparticles synthesis

The effect of temperature, reaction time, pH of the mixture, the concentration of $AgNO_3$, honey concentration, and the volume ratio of honey to $AgNO_3$ on the AgNPs synthesis was studied based on the formulas shown in Table 1, and optimization of these factors was conducted using the one

factor at a time technique. The formation of AgNPs was checked through visible color changes and UV/VIS spectrophotometer analysis. Next, optical properties, crystal structure, shape, and size were examined to characterize the synthesized AgNPs under optimal conditions.

**Table 1:** Factors influencing optimization techniques

| Parameters | Temperatures(°C) | Reaction times(min) | pH | $AgNO_3$ concentration(mM) | Honey extracts concentration (%) | Ration of honey to $AgNO_3$ |
|---|---|---|---|---|---|---|
| 1 | 20 | 10 | 5 | 2 | 2 | 0.5:1 |
| 2 | 30 | 20 | 6 | 4 | 4 | 1:1 |
| 3 | 40 | 30 | 7 | 6 | 6 | 1:1.5 |
| 4 | 50 | 40 | 8 | 8 | 8 | 1.5:1 |
| 5 | 60 | 50 | 9 | 10 | 10 | |
| 6 | 70 | 60 | | | | |
| 7 | 80 | | | | | |
| 8 | 90 | | | | | |

### 2.8. Characterization of the optimized AgNPs

The following techniques and tools utilised to examine and describe the prepared NPs: visual, UV, XRD, FTIR, DLS, DSC and SEM.

#### 2.8.1. Visual characterization

Equal volume of 20mM of $AgNO_3$ and 6% aqueous extracted honey were mixed. Then, the mixture was exposed to sun light for a total of 30 minutes with evaluation of color change every 10 minutes for a total of three times. Solution samples were thereafter visually inspected.

#### 2.8.2. UV–Visible Spectrophotometry Analysis

The AMP-loaded AgNPs' optical characteristics and those of synthetic AgNPs and aqueous extracted honey were investigated using UV-vis absorption spectrophotometer (Spectrophotometer carry 60, Agilent Technologies) in the 200-800 nm range.

### 2.8.3. Fourier Transform-Infra Red (FTIR) analysis

FTIR is a useful technique for determining the presences of specific functional groups in an organic molecule.The vibration frequency of functional groups are unique to that functional group. These vibration frequencies are in the FTIR band.As a result, transmitting an infrared signal throug h the organic complex causes the functional groups to vibrate at different frequencies.In other wor ds, an infrared signal that passes through an organic compound will be absorbed at these specific fr equencies, resulting in a distinct spectrum. The beam from an infrared source is routed through a monochromatic controller with a selection, guaranteeing that only specified wavelengths, ranging from 4000 to 400 cm-1, are emitted.

The sample was prepared by utilizing the AgNPs synthesis procedures. Then, a spoonful of the prepared sample was added on the pan. The background was adjusted before the ray was applied. Then; the ray was runned after the sample was placed on the pan. The sample is placed in a holder directly in front of the FTIR source. The analog signal is read by a detector and converted to a spectrum. The signals are analyzed and the peaks are identified using a computer.

The compatibility between honey and silver was investigated using FTIR spectra (Haiza et al., 2013). The FTIR spectra of the honey extract, AgNPs, AMP, and AMP-loaded AgNPs were collected in order to identify the functional groups used in the synthesis of AgNPs and the functional groups implicated in the preparation of conjugated NPs. The samples were prepared by drying the centrifuged AgNPs. Then, the functional group was determined in the range of 4000-400 cm-1 using an FTIR spectrophotometer (Bruker, *Ettlingen, and Leipzig, Germany*).

### 2.8.4. Powder X-ray Diffraction (XRD) analysis

First, check the calibration of the XRD equipment with a silicon (Si) standard at the start of the day. Install the silicon standard into the XRD. In data scan, navigate to Controller. Navigate to scan line under controller. Ensure that the silicon standard peak is scanned (configure the scan range so that the Si peak is covered). When the machine stops, it will show a single peak with a vertical line. The vertical line represents the computer-generated position of the Si (111) peak. This should correspond to the XRD peak. If the two do not match, the vertical line must be moved to calibrate the XRD to the Si standard. The computer will prompt you to adjust the established angle

to the new value. If the new number is acceptable, use the mouse to push the YES button; otherwise, use the NO button and adjust the vertical line until it meets the peak.

Then, fill out the file identification and scan identification fields. The file identification is the name of the computer file that will be used to store the data, and the scan identification is the sample number or name. With a s step size of 0.03 degrees and a dwell period of 0.5 seconds, scan from 2.0 degrees to 35.0 degrees 2. Scan with the axes always connected.

The standard sample holder can be utilized if there are 200 mg or more of the sample available. The sample can be preserved and used again because XRD is a non-destructive technology; therefore, it will remain intact after data collection. The sample's height has a big impact on the observed peaks' 2° angles, so the instrument is set up so that the sample's top should be flush with the top of the outer ring on the sample holder. It is simple to flatten a sample such that it is flush with the top of the sample holder by using a glass microscope slide as a tamper.

The XRD pattern of the synthesized AgNPs was determined using an X-ray diffractometer (XRD-7000 X-RAY DIFFRACTOMETER, Corporation, Japan) operating at a voltage of 40 kV and a current of 30 mA with radiation CuKα (k = 1.541 Ω) operated from 2θ angles and with a sweep range between 100 to 800. The scanning speed was set of at $3^0$ per minute. The result was analyzed with X'Pert High Score Plus software (version 2.1, PAN analytical B.V. Almelo, The Netherlands). The crystallite size(t) of the NPs was estimated as shown in equ(1) (Thiruvengadam and Bansod, 2020):

$$t = \frac{0.9\lambda}{\beta Cos\theta} \ldots\ldots\ldots\ldots\ldots\ldots\ldots\ldots Equ(3)$$

Where, t is the mean size of the particle, λ is the wave length of X-ray, β is full width at half maximum intensity and θ is the diffraction (Bragg) angle.

2.8.5. Scanning Electron Microscope (SEM) analysis

Using double adhesive carbontape, secure your samples to the aluminum holder stub. Use silver paint to electrically ground the sample as well.This procedure is not required for conduc tive samples.If you have a lot of samples that appear the same, make marks on the sample stubs or samples.In the SEM, it is extremely difficult to distinguish comparable samples.The sample should

next be completely dried in a drying oven at 60$^{o}$C for at least 3 hours, depending on the sample cir cumstances. The general practice is to keep them in the drying oven overnight.

Then, smooth surfaces of industrial samples can be investigated using SEM. The samples are adhered to a metal stub, coated with 40–60 nm of metal, such as Palladium, and then examined under a microscope. The morphological size of AgNPs was then determined using the specifications of the institutions. Then after, surface morphology of green synthesized AgNPs was investigated using SEM (TESCAN VEGA3 SBU, Brno, Czech Republic).

### 2.8.6. Dynamic Light Scattering (DLS) analysis

AgNPs and AMP-AgNPs sample might need to be diluted by sonicating AgNPs for 20 min to decrease for simple particle size determination.This assessment was made for both the loaded and unloaded AgNPs.The sample should be diluted with the appropriate liquid if it is very concentrated. A drop of the plain sample in 20ml of liquid or a 1:100 dilution usual suffices. Then, AgNPs' and AMP loaded AgNP's size in the colloidal solution was determined using DLS. The hydrodynamic diameter and Polydispersion index (PDI) of AgNPs and AMP loaded AgNPs were evaluated with a 90 plus particle size analyzer (Brookhaven Instruments Corporation, USA). The aqueous suspensions of AgNPs and AMP loaded AgNPs were filtered through a 0.22µm syringe filter unit and their size distribution was measured.

### 2.8.7. Differential Scanning Calorimetry (DSC) Analysis

One to ten milligrams of AgNPs and AMP-AgNPs should be evenly distributed in an aluminum Tzero pan before using the Sartorius Microbalance to weigh and record the mass to four significant figures. Finally, the pan was sealed using the Tzero Press once the sample had been sealed, the pan had been placed in the blue die, a lid had been placed on it, and the sample had been sealed. Then, put an empty pan (with a shut cover) to be used as the reference mass in the auto-sampler in one of the places designated.

Then finally, the melting point of the prepared AgNPs were determined using DSC (instruments SDT Q600 V20.9 Build 20, Universal V4.5A TA) by heating the sample between 35 to 600 °C at a rate of 10 °C per minute (Sanmuham *et al.*, 2021).

## 2.9. Preparation of ampicillin loaded silver nanoparticles

### 2.9.1. Calibration curve for determining $\lambda$ max of standard Ampicillin

Initially, a stock solution of 1mg/ml standard AMP was prepared. From this stock solution, serial dilutions were made to obtain 5, 10, 15, 20, and 25µg and, then centrifugation was made to screen the loaded and unloaded AMP from the solution. At each stage of the centrifugation, analysis was used to filter the fluid to remove unloaded AgNPs and AMPs that were improperly charged or sized for one another. The Beers-Lamberts equation was used to obtain the EE and LC in order to calculate the concentration of AMP in the supernatant.

The maximum concentration of AMP loaded on AgNPs was determined from the calibration curve. To determine the maximum concentration of AMP loaded on AgNPs, 222 nm was selected as the maximum wavelength of absorbance. The graph was then constructed with concentration on the x-axis and absorbance on the y-axis.

### 2.9.2. Ampicillin loading on silver nanoparticles

The AMP was loaded onto the AgNPs according to a previously utilized technique with a small adjustment (Rogowska *et al*., 2017). The AMP and AgNPs solutions were mixed in equal amounts and incubated for three days. To evenly mix the solutions, AgNPs and AMP were stirred for 6 hours on a magnetic stirrer. The AMP suspension in water was sonicated for 2–5 minutes. Then, 1 mL of AMP solution (0.5mg/ml) was combined with 1 mL of AgNPs (0.8mg/ml), which had been sonicated for 10 minutes, in a 2 mL Eppendorf tube. After 72 hours of incubation, the solutions underwent centrifugation (at 10,000 rpm for 20 minutes). Using a UV-vis spectrophotometer, the absorbance was determined at 222 nm. Then the quantity of AMP in the supernatant was determined using the Beer-Lamberts equation.

#### 2.9.2.1. Optimization for drug loading

To study the impact of time and focus on EE and DL, 12mg of AgNPs was added to 15 ml of water solvent, and an equal amount (15 ml) of AMP, i.e., 7.5mg in 15 ml to be loaded, was added, where the concentrations of AgNPs and AMP were similar with the above procedures (0.8mg/ml and 0.5mg/ml, respectively). The temperature of incubation was set at room temperature.

Table 2: Optimization of silver nitrate concentration and time

| No. | Concentration of AMP(mg/ml) | Time(hr.) |
|---|---|---|
| 1 | 1.5 | 6 |
| 2 | 2 | 12 |
| 3 | 2.5 | 18 |
| 4 | 3 | 24 |
| 5 | 5 | 36 |

2.9.2.2.Drug loading (Dl) and encapsulation efficiency (EE) determination

DL and EE were evaluated using a UV-Vis spectrophotometer (Spectrophotometer Carry 60, Agilent Technologies, USA). A standard curve was used to quantify the concentration of free AMP in the supernatant. The supernatant solution was obtained from centrifuged loaded solutions (Famuyiwa *et al.*, 2021; Weng, Tong, and Chow 2020), and indirectly, the amount of DL on AgNPs was measured using UV-Vis spectroscopy. To recalculate the DL and EE, the two related equations (Eqs. 2 and 3) below were employed.

$$EE(\%) = \frac{(\text{Total dosage of Drug} - \text{Amount of Free Drug}) \times 100\%}{\text{Total Amount of Drug}} \quad \ldots\ldots\ldots\ldots\ldots\ldots Equ(4)$$

AND

$$DL(\%) = \frac{(\text{Total Amount of Drug in Nanoparticles}) * 100}{\text{Total Amount of Nanoparticles}} \quad \ldots\ldots\ldots\ldots\ldots\ldots\ldots Equ(5)$$

Where % DL is the percentage of drug loading and% EE is the percentage of encapsulation efficiency.

## 2.10. *Invitro* drug release

An equal mixture of phosphate buffer solution (5 ml) and AMP-loaded AgNPs (5 ml) solution (Shaker and Shaaban, 2017; Jin *et al.*, 2021) was dialyzed for four days. A molecular weight cutoff (MWCO) of 12 kilodaltons (kDa) membrane size was used to dialyze the solution and examine the release of the AMP over the course of four days.

### 2.10.1. Determination of λmax and drawing of the calibration curve

At five different pH values (1.2, 6.0, 7.3, 7.4, and 8), the AgNPs' release of AMP was examined, and the maximum amount of AMP that was absorbed in buffer solutions was identified. Stock solutions with various AMP concentrations were made in order to make the working solutions. The maximum quantity of AMP present in all buffer solutions was then determined by scanning these completed solutions in the 200–400 nm range.

In buffer solutions with pH values of 1.2, 6.0, 7.3, 7.4, and 8, respectively, the wavelengths at which AMP absorbance was maximum were 222, 224, 220, 218, and 222 nm. The calibration curve was prepared in a manner that was comparable for each pH level. To do this, AMP stock solutions of 0.4, 0.2, 0.1, 0.05, and 0.025 mg/mL, respectively, were prepared using buffer solutions with pH values of 1.2, 6.0, 7.3, 7.4, and 8. The final AMP concentrations in each buffer solution after being serially diluted were accordingly 2, 4, 6, 8 and 10 µg/mL.

After that, each buffer solution's absorbance was measured at the predefined maximum AMP concentration in each of the matching buffer solutions. To produce the calibration curve for all buffer conditions, the data were then plotted against concentration. Finally, a UV-Visible spectrophotometer (Spectrophotometer Carry 60, Agilent Technologies, USA) was used to measure the absorbance for all buffer solutions with changing pH values and to calculate the maximum absorbance.

### 2.10.2. Drug release test

The release of AMP from AMP-loaded AgNPs *in vitro* was investigated using the dialysis bag approach (Shaker and Shaaban, 2017). The dissolution was conducted at pH 1.2, 6, 7.3, 7.4, and 8 to simulate stomach, *E. coli*, duodenum, CSF, blood, and jejunum pH, respectively. To each 5 ml

dissolution, medium, 6 mg/mL of AMP-loaded AgNPs was dispersed, and the mixture was placed within dialysis bags overnight (MWCO 12 KDa SIGMA-ALDRICH, USA). The sacks were then knotted with thread at both ends and placed in an Erlenmeyer flask that was placed on a shaker (Dragon Lab, SK-0180, E-China) with 50 mL of external buffer medium (whose pH value was the same as the solution within the sacks) at a 100 rpm speed.

A UV-Vis spectrophotometer was used to track AMP release by taking the absorbance of 5 mL of samples from external buffers. Every time a sample was collected, an equivalent volume of fresh buffer was replaced to maintain the sink condition. The sample was subsequently obtained at intervals of 6, 12, 24, 48, 72, and 96 hours following the initial three consecutive times it was taken every hour. Using UV-visible spectroscopy, each sample's absorbance was measured at a pre-set maximum for each corresponding pH medium. Each measurement was made quickly, and the average result was taken.

The calibration curve, which had already been prepared, was used to compute the concentration of released AMP. Each experiment was completed in triplicate, with findings provided as mean values and ±SD. Then, finally, the conventional formula was $\text{Ampicillin released}\,(\%) = \frac{\text{Amount of ampicillin released}}{\text{Initial amount of ampicillin used}} \times 100$ was used to calculate the percentage cumulative AMP release.

### 2.11. *In vitro* antibacterial activity

Using the disc diffusion method, the bactericidal activity of honey, AgNPs, AMP, and AMP-loaded AgNPs was investigated individually. The procedures, except for the preparation of the filter paper discs, were performed using official testing for AST procedures for honey, AMP, and AgNPs (Mohammed et al., 2010). The bactericidal activity of honey, AgNPs, free AMP, and AMP-loaded AgNPs against EPHI-resistant *E. coli* strains was examined. Both free AMP and AMP-loaded AgNPs were tested on the same plates to compare their efficacy against resistant *E. coli* strains. To compare the effectiveness of the free AMP and the AMP-loaded AgNPs against resistant *E. coli* strains, both of them were tested on the same plates. Calculating the ZOI of the AgNPs' antibacterial activity was examined against *E. coli* before and after AMP loading (Rogowska *et al.*, 2017). Here also, a negative (deionized water) and positive (AMP) control test was done for AMP-loaded AgNPs to confirm their effect and then to compare their individual effects.

2.11.1. Preparation of standard discs

To determine synergy, each antibiotic standard disc was additionally impregnated with 10µl of AgNPs for a final content of freshly prepared AgNPs of 10µg AgNPs per disc, which is taken to make it similar to AMP concentration. In the Mueller-Hinton liquid medium, a single colony of each test strain was grown overnight at 37 °C on a rotary shaker (200 rpm). The overnight culture was diluted in order to prepare an inoculum to a 0.5 McFarland standard with distilled water, and discs with various AgNPs concentrations were prepared by plating on plates along with the standard. Following incubation for 24 hours at 37°C, ZOI was measured using calipers. Assays were performed in triplicate (Mohammed *et al.*, 2010). The amount of AMP was also equal to AgNPs and was 10µg (Mohammed *et al.*, 2010).

The filter paper discs were prepared locally by using a method from (Vineetha *et al*.,(2015). Briefly, Whatman No. 3 filter paper was punched using an office paper punch to produce holes approximately 6 mm in diameter. The resulting filter paper discs were then autoclaved at 15 pounds per square inch pressure for 30 minutes.

Next, the working solutions for AgNPs and AMP-loaded AgNPs were prepared, and then loaded onto the autoclaved paper discs (20 µg of AMP-loaded AgNPs and 10 µg of AgNPs per disc), and the paper disc-loaded filters were dried for 4 hours at 37 °C in the incubator. The amount of AMP to impregnate the disc was taken from Institute for Clinical and Laboratory Standards (CLSI) guidelines based on a dosage regimen of 500 mg given orally every 6 hours (CLSI, 2020). Then, the amount of AMP and AgNPs ratio was determined based on the LC of AgNPs.

2.11.2. Inoculum preparation

Three colonies well isolated from isolates subcultured for 24 hours of the same morphological type were picked. A loop was used to touch the top of each colony and suspend it in 2 ml of distilled water (DW). The suspension was then modified to achieve the McFarland turbidity standard of 0.5 (1-2 x $10^8$ colony forming units (CFU)/ml) by vortexing the water tube to prepare a smooth suspension.

2.11.3. Test plates inoculation

A sterile cotton swab was dipped into the inoculum suspension after it had been adjusted for turbidity within 15 minutes. A Petri dish was then prepared with inoculated Muller Hinton Agar by running the swab over its surface three times and turning the plate at approximately 60°C each time. Finally, the lid was left in a jar for 5 minutes and prepared for disc application.

2.11.4. Disc applications to inoculated agar plates

To apply the slides to the surface of the inoculated agar plates, forceps were used after immersion in alcohol and turned on. Then, all discs (a control disc inoculated with DW and discs inoculated with AMP, AMP conjugated AgNPs and bare AgNPs were carefully placed on the plate with sufficient distance between their centers and pressed with forceps. Finally, the plates loaded with those discs were turned over and left to incubate for 24 hours at 37°C.

After a period of 24 hours, the resulting diameters of ZOI, including the diameters of the discs, were measured using a ruler on the Petri dish's reverse side. The susceptibility or resistance of the organism was then determined by using CLSI's (2020) guidelines to compare the results obtained. The AST experiment was carried out three times, and the mean values were recorded.

## 2.12. Statistical analysis

Following triplicating the tested data, the standard deviation was determined in order to ascertain the data's divergence from one another. Effective data analysis was performed using UV-Vis, FTIR, XRD, DSC, and cumulative AMP release information. Lastly, using the Origin 9 software, the findings from the UV-Vis, FTIR, XRD, and DSC and graphs showing cumulative AMP release data vs. time at each pH medium measurement were plotted.

## 3. Results and Discussion

### 3.1.Qualitative phytochemical analysis of the extracted Honey

The outcomes of the phytochemical assessment of the honey extract are depicted in Table 3.

**Table 3:** Phytochemical assessment results of honey samples

| S.No | Phytochemical | Test Performed | Color formed | Results |
|---|---|---|---|---|
| 1. | Glycosides | Killer-Kiliani Test | Brown ring | Positive |
| | | Salkowski's test | Reddish brown | Positive |
| 2. | Alkaloids | Dragendorff's Test | Reddish brown | Negative |
| 3. | Saponins | Foam Test | Stable foam | Positive |
| 4. | Tannins and Phenolic compounds | Lead acetate test | White precipitate | Positive |
| | | Ferric chloride test | Brownish green | Positive |
| 5. | Steroids | Ring test | Ring formed | Positive |
| 6. | Tri-terpenoids | Methanol test | Black color | Negative |
| 7. | Flavonoids | Shinoda test | Reddish pink | Positive |
| 8. | Carbohydrates | Fehling's test | Red precipitate | Positive |
| | | Benedict's test | Reddish brown | Positive |

The phytochemical evaluation of aqueous extracted honey showed that tannins, phlorotannins, flavonoids, glycosides, and saponins were present. These results are in line with previous studies done elsewhere (Mandal and Mandal, 2011; Israili, 2014, Asaduzzaman *et al.*, 2015; Shah, 2022). Therefore, these phytochemicals are responsible for the formation of AgNPs, and the formed AgNPs have the mechanisms presented in Figure 4, and their presence in the aqueous extracted honey suggests the ability of the aqueous extracted honey to prepare AgNPs.

### 3.2. Quantitative phytochemical analysis of the extracted Honey

#### 3.2.1.pH Analysis

The tested honey had a pH of 3.9, which is within the limits of the honey standards and it is a consistent finding with Mulugeta *et al.* (2020). The international pH contents for honey are 3.20–4.50, while the pH contents of Ethiopian honey are not well known (Mulugeta, 2020).

#### 3.2.2. Content of Moisture

The moisture content of honey was measured using a sample. 2.0 g of honey was obtained and oven-dried at 70°C for 2 hours. The moisture level of honey was 19.7%, which was less than 20% of the international standard limit. According to Ambaye (2017), the water content of Ethiopian honey is 23% (Amabye, 2017).

#### 3.2.3.Ash Content

The quality of honey is determined by its ash value. Quality honey has an ash concentration of less than 0.6%. The composition of the ash reveals the existence of minerals and uncommon components in the honey. In this study, a higher ash value of 1.04% was obtained. This ash variance is caused by botanical variations and impurities (Amabye, 2017). The ash content of honey was discovered after drying 5.0g of samples in porcelain crucibles at 105°C for 3 hours in an oven. The dried sample was heated to a consistent weight in a furnace at 550°C, and then it was cooled and weighed.

### 3.3.UV–Vis spectroscopy analysis of the extracted Honey

As depicted in Figure 5, the maximum wavelength was 300 nm, which is consistent with the previous finding (Suhandy and Yulia 2021).

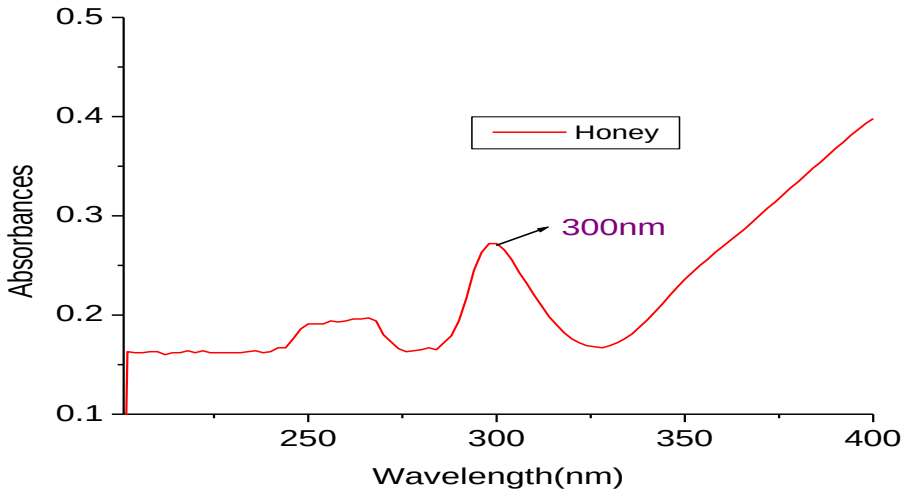


**Figure 5:** UV-Vis spectrum of Honey

### 3.4.Synthesis of Silver Nanoparticles

The binding of AgNPs with flavonoid-rich compounds demonstrated therapeutic potential and is effective against some deadly infectious diseases. Therefore, plant-based metal NPs meet the demand for a less hazardous formulation during drug development and delivery (Singh *et al.*, 2021). Here, the honey phytochemical test was done, which confirmed the presence of flavonoids and other compounds.

The AgNPs were successfully prepared using the aqueous extract of honey. To determine whether the prepared NPs are AgNPs or not, a preliminary investigation was conducted before any optimization. Figure 6 below shows the preliminary test outcomes for the UV-Vis spectroscopy analysis. The synthesis of AgNPs was confirmed by the UV-visible spectrum findings.

In this finding, the prepared AgNPs had a maximum wavelength of 440 nm. The UV-visible spectra of AgNPs have a characteristic peak at 455 nm (Matar *et al.*, 2022). The maximum wavelength, which is related to various literatures, was found between 410 and 450nm (AB, AM, and AM, 2018; Habsi *et al.*, 2019; Othman *et al.*, 2020).

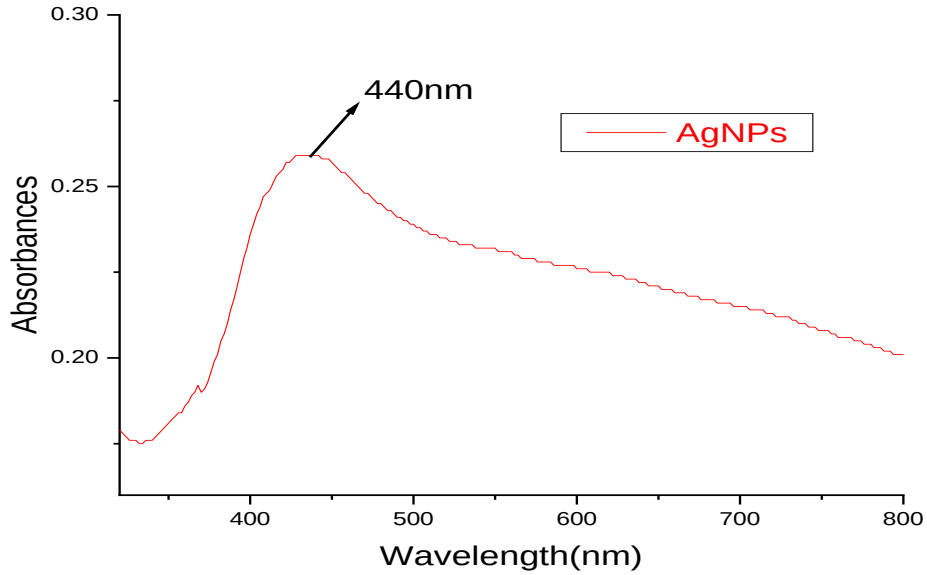


**Figure 6:** UV-visible spectrum of AgNPs

To establish the optimized concentration of AgNPs, the impact of temperature, reaction duration, pH, the ratio of honey to AgNO3 combinations, $AgNO_3$, and honey concentration were studied next to the preliminary study.

### 3.5.Optimization of the silver nanoparticles synthesis

3.5.1.Effects of temperature

The maximum absorbance was found at 80$^{o}$C, as shown in Figure 7. Hence, 80$^{o}$C, was taken as the optimum temperature for further study. Similarly, the rate of synthesis of NPs and their form, size, and other characteristics are all significantly influenced by temperature. The temperature has a significant impact on the size and shape. The rate of reaction accelerates with rising temperature, leading to the synthesis of nucleation centers (Singh *et al.*, 2020).

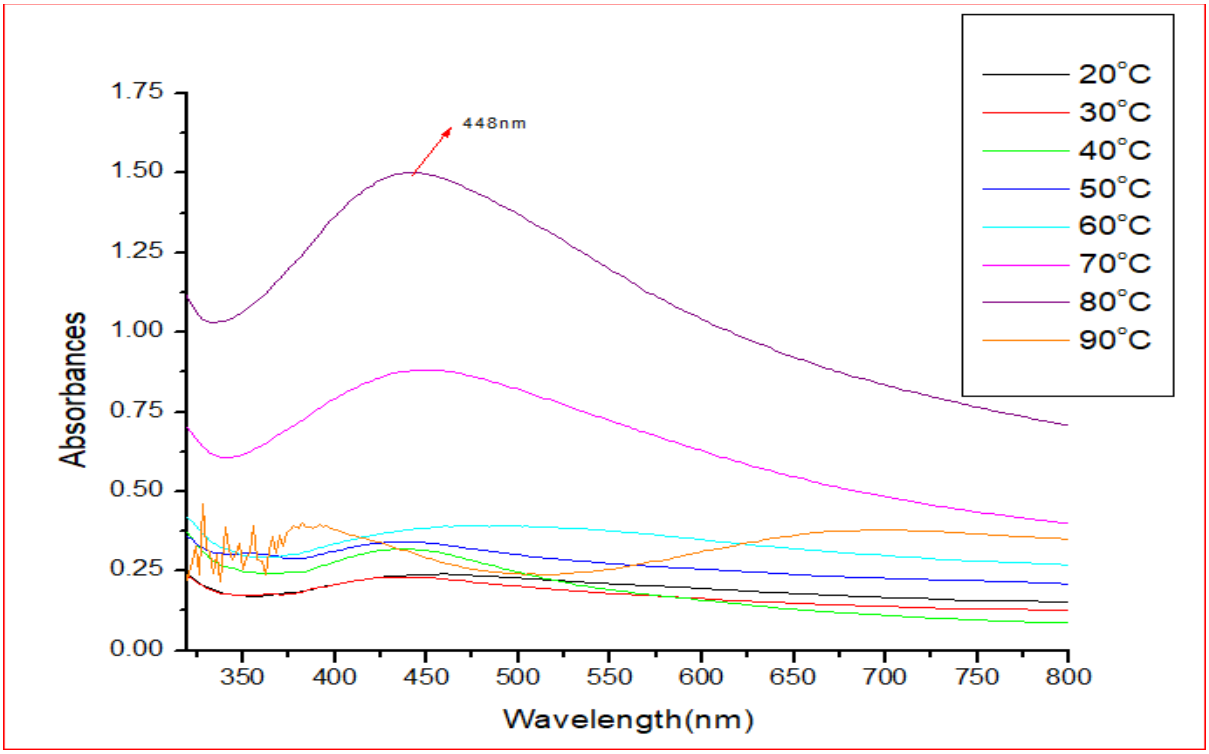


**Figure 7:** Effect of variation in temperature at a fixed pH (6.5), reaction Time (30min), $AgNO_3$ concentration (30mM), and 2% extracted honey using $90^0$C temperature for comparison

3.5.2.Effects of reaction time

The optimum reaction time was found to be 50 minutes. A similar finding was obtained in this study, as shown in Figure 7. A previous study established that when reaction time increased, the rate of AgNPs synthesis increased (Singh *et al.*, 2020).

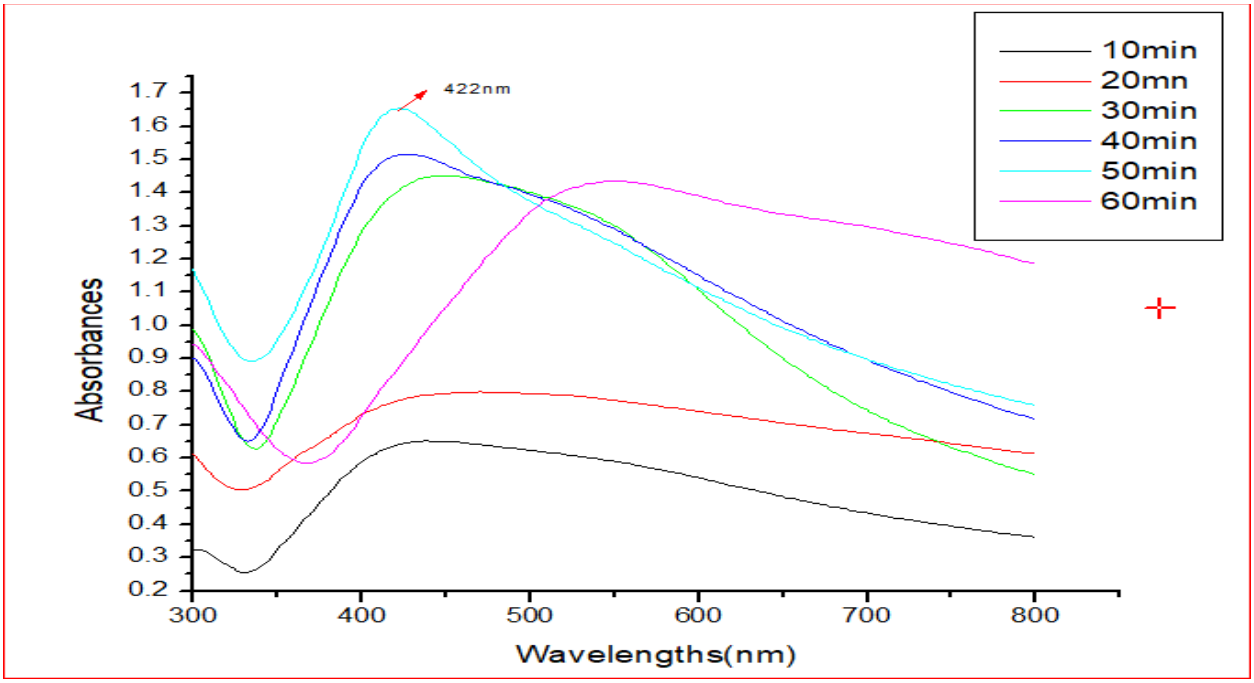


**Figure 8:** Optimization of reaction time at fixed pH (6.5), temperature ($80^0$C), $AgNO_3$ (30mM) and concentration of aqueous extracted honey (2%)

3.5.3.Effects of pH

The silver colloid's UV-vis spectrum was prepared at pH 5, 6, 7, 8, or 9 by employing $AgNO_3$ as a reducing or stabilizing agent in the presence of honey, as shown in Figure 9. The electronic absorption spectrum at pH 5 is greatly widened and lacks any intensity at the plasmon peak absorption at around 406 nm. This implies that at the conditions utilized, the silver ions could not be transformed to AgNPs at pH 5.

When AgNPs were prepared at pH 6 or 7, similar absorption bands with more intensity were obtained. Therefore, it can be said that the pH of the reaction media has direct effects on the synthesis of AgNPs. Only at pH 8, AgNPs were formed in greater quantities. Hence, pH 8 was taken as the optimum pH condition for the preparation of the NPs.

Consistent findings showed that the pH of the reaction is crucial in the production of NPs. Like temperature, it controls the development of nucleation centers. In the previous studies, it was indicated that the formation of metal NPs was enhanced as the pH rose because of an increasing number of nucleation centers. Furthermore, pH plays a significant role in determining how NPs form, both in terms of their morphology and their size (Singh *et al.*, 2020).

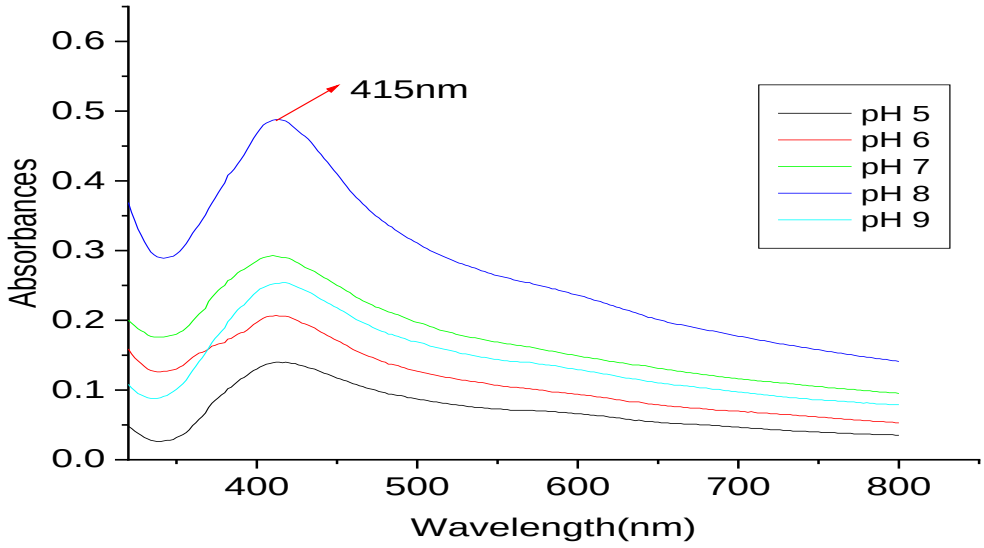


Figure 9: Optimization of pH at fixed reaction time (50min), temperature (800C), AgNO3 concentration (30mM), and 2% extracted honey

3.5.4.Effects of $AgNO_3$ concentration

The intensity of the color grew as the $AgNO_3$ concentration rose. At the lowest concentration of $AgNO_3$ (2 mM), the reaction color was a reddish brown, whereas, at the highest concentration (4 mM), the color became a dark reddish brown. The peak's strength increased in this result as well between 2 and 20 mM, but it decreased after that point. Accordingly, the subsequent rise in $AgNO_3$ concentration is useless. Consequently, as shown in Figure 10, the optimal concentration of $AgNO_3$ was taken to be 20 mM. Similar findings showed that the metal salt concentration has a strong effect on the green preparation of NPs (Othman *et al.*, 2020).

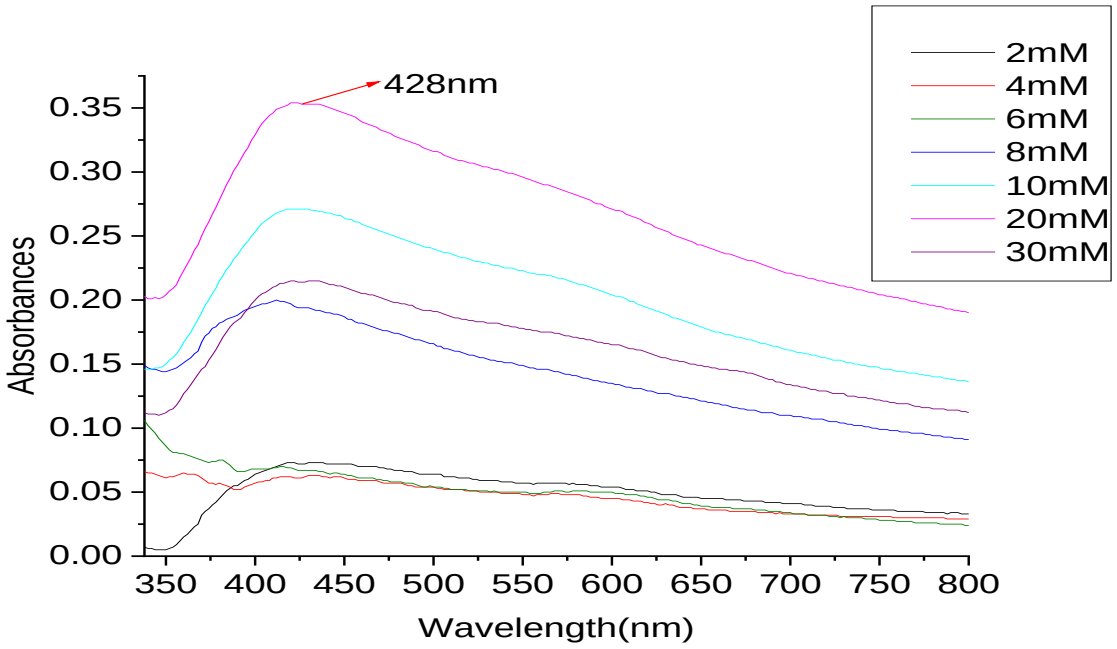


**Figure 10:** Optimization of $AgNO_3$ concentrations at fixed reaction time (50min), pH (8), temperature ($80^0$C), and 2% extracted honey

3.5.5.Effects of Honey concentration

Enhancing honey concentration is crucial to observe honey's effects by varying its amount and observing the effect if its concentration is used as a reducing agent. The optimal honey concentration, according to Figure 11, was 6%. Similar findings indicated that, in concentration range between 2-6%, there is a direct relationship between honey and AgNO3 concentration. However, beyond this concentration range $AgNO_3$ concentration was decreased (Habsi *et al*., 2019).

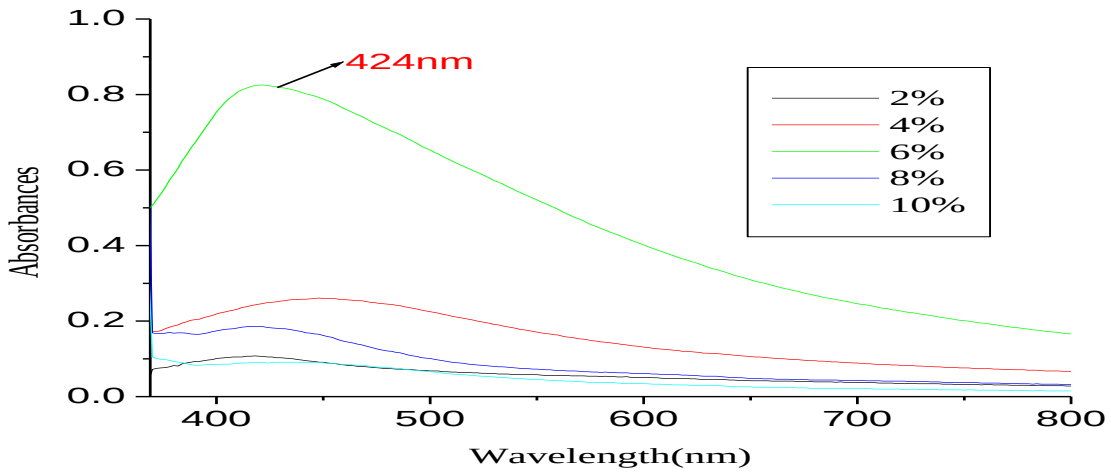


**Figure 11:** Optimization of Honey concentrations at fixed reaction time (50min), pH (8), temperature ($80^0$C), and 20mM $AgNO_3$ concentrations

3.5.6.Effects of volumes of the Honey and $AgNO_3$ solutions

The optimized volume ratio of 6% aqueous extracted honey to $AgNO_3$ was 1:1.5 (Figure 12).

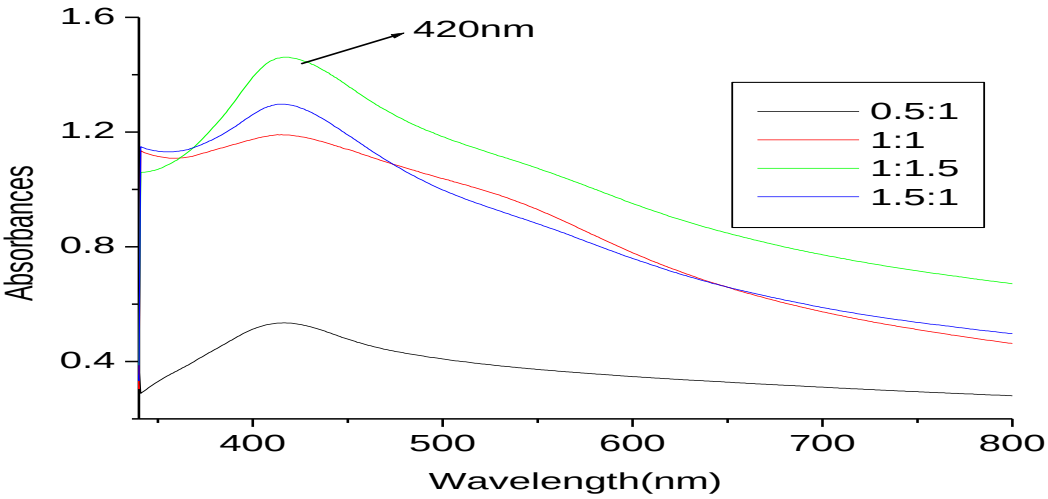


**Figure 12:** Effect of volumes of 20mM $AgNO_3$ and 6% honey on AgNPs synthesis

As per the preliminary study, the optimized AgNPs were prepared at a temperature of $80^o$C, a reaction time of 50 min, a pH of 8, an $AgNO_3$ concentration of 20mM (20ml), 6% aqueous extracted honey (15 ml), and 1.5:1 volume ratio of $AgNO_3$ to 6% aqueous extracted honey.

### 3.6.Characterization of AgNPs and AMP-AgNPs

3.6.1.Visual inspection of synthesized AgNPs

Initially, the color change of the solution mixture was visually inspected in order to identify the synthesis of AgNPs. The solution darkened somewhat when exposed to sunlight, showing that $AgNO_3$ had been converted to AgNPs. As time went on, the color intensity got stronger. This suggests that the amount of AgNPs produced has increased (Kumar *et al.*, 2020).

When exposed to sunlight for various lengths of time, the solution combination underwent a color shift. The mixture of honey and $AgNO_3$ had a yellowish-brown tint, indicating that $Ag^+$ had been converted to $Ag^0$. As the time of the combination extended, so did the color's yellowish-brown hue. Reaction time was a key limiting factor in the formation of $Ag^0$. The presence of sunlight also accelerated the reaction, indicating that light served as a catalyst to speed up the synthesis of $Ag^0$. AgNPs were originally identified by visual inspection of the mixture, and their yellowish-brown color indicates AgNPs' presence (Kumar *et al.*, 2020).

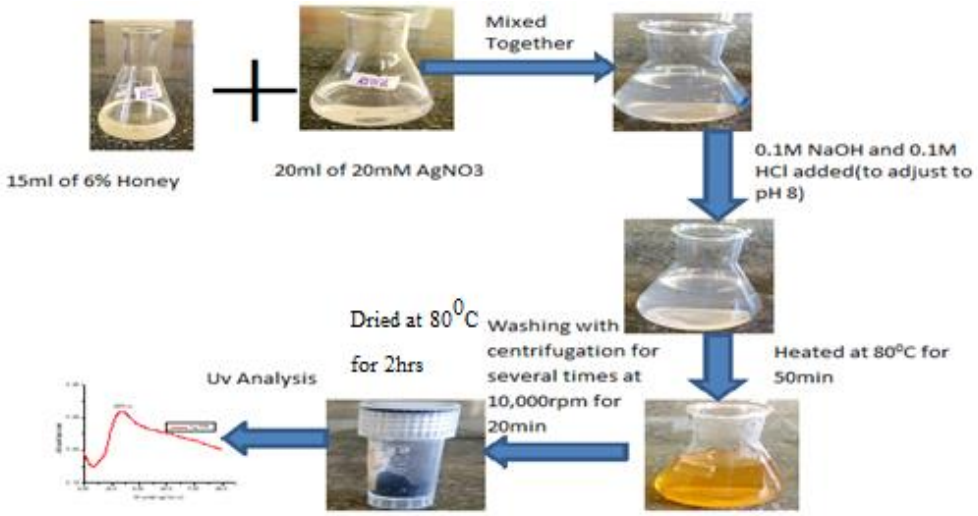


**Figure 13:** Visual illustration of the observed color change during AgNPs synthesis at optimum condition

3.6.2.UV–Vis Spectroscopy of Optimized AgNPs

The optimized AgNPs exhibited a maximum lambda of 430 nm, as shown in Figure 14. The maximum wavelength that we found here is within the range mentioned in several articles. The

most important variables that affect how AgNPs are shaped, structured, and how they work as an antibacterial agent are their optimum parameters (Habsi *et al.*, 2019; Singh *et al.*, 2020).

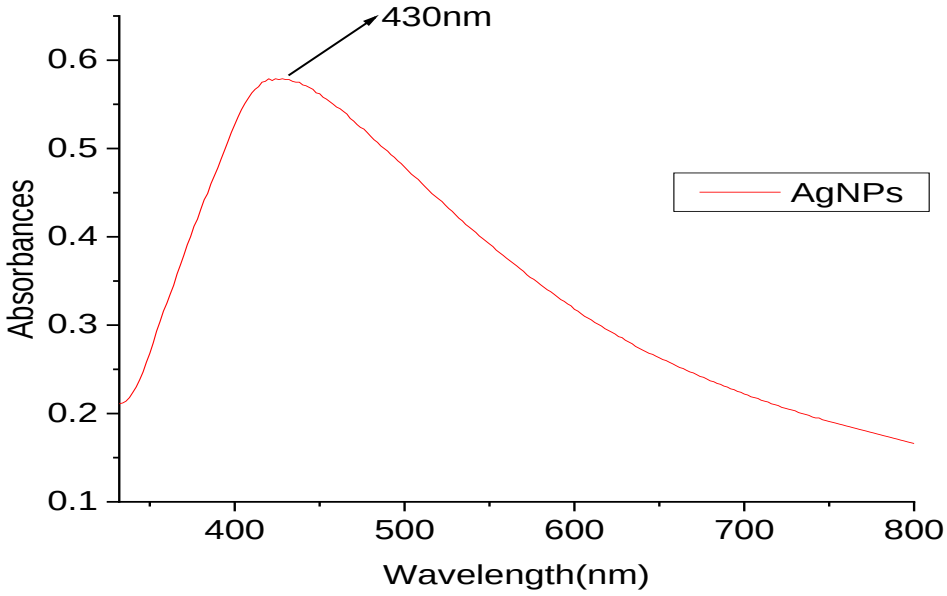


**Figure 14:** Optimized AgNPs at $80^0$C, 50minutes, pH 8, 20mM $AgNO_3$ and 6 % Honey

3.6.3.Fourier-Transform Infrared (FTIR) Analysis

The bands of absorbance were obtained in the wavelength range between 4000 and 400 cm-1 as shown in Figure 15. The aqueous extract of honey's FTIR spectra revealed the existence of distinctive bands for a number of functional groups. The resulting intensity bands were compared to the functional group standard values reported in Table 4 for comparison. It supports the existence of functional groups that might act as stabilizers or be reluctant. As commonly reported reducing or stabilizing agents, phenolic and flavonoids' functional groups are confirmed by the spectra (Matar *et al.*, 2022). The addition of NaOH causes the reduction of Ag ions (H Haiza *et al.*, 2013).

By removing the oxygen from the sugar ring's alpha proton, the base makes it easier for the glucose ring to open, and metal ions can then oxidize glucose to gluconic acid. Sucrose, proteins, and enzymes might also contribute to the reduction (H Haiza *et al.*, 2013).

**Table 4:** Absorption band of functional groups in FTIR spectroscopy of extracted honey(Kędzierska-Matysek *et al.*, 2018)

| Absorption band(cm-1) | Functional group |
|---|---|
| 3300-2500 | OH stretch |
| 1760-1690 | C=O stretching |
| 1320-1210 | C-O stretching |
| 1440-1395 and 950-910 | O–H bending |
| 900–750 | Saccharide configuration |
| 918 | δ (C–H) |

The bands found in aqueous extracted honey at 3264.10 and 2932.53 OH stretch, 1642.01 C=O stretch, 1414.27 O-H bend, 1343.74 and 1251.39 C-O stretch, and 1027.43, 916.77, 863.86, and 773.8 demonstrate some form of saccharide structure, according to this discovery.

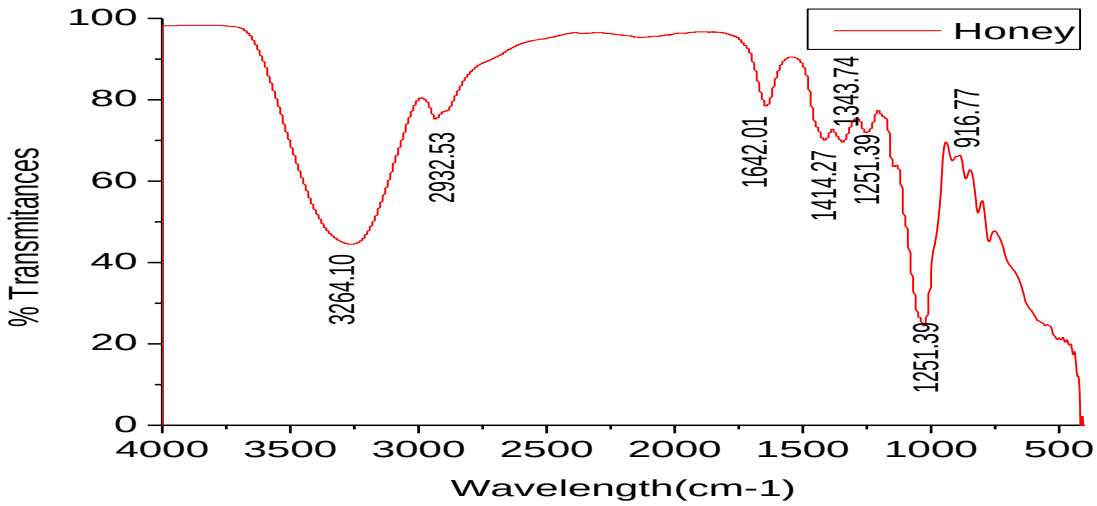


**Figure 15:** FTIR spectrum of Honey

The functional groups for AgNPs were found at 3272.35, 2917.72, 2850.82, 1638.12, 1523.96, 1014.70 and 922.46cm-1. Supporting evidence from the different functional groups present in honey biomolecules and honey containing AgNPs was identified using the FTIR analysis. To find functional groups, the observed intensity bands were compared to the standard values. Representative spectra show absorption peaks in the 4000-500 cm-1 range in both Sidr honey (SH)

and rhododendron honey (RH). The FTIR spectra of SH (alkane) show that the big signal at 3272.56 cm-1 refers to O-H stretching, H-bonded alcohols/phenols, and the small peak at 2930.76 cm-1 pertains to C-H stretching (Matar *et al.*, 2022).

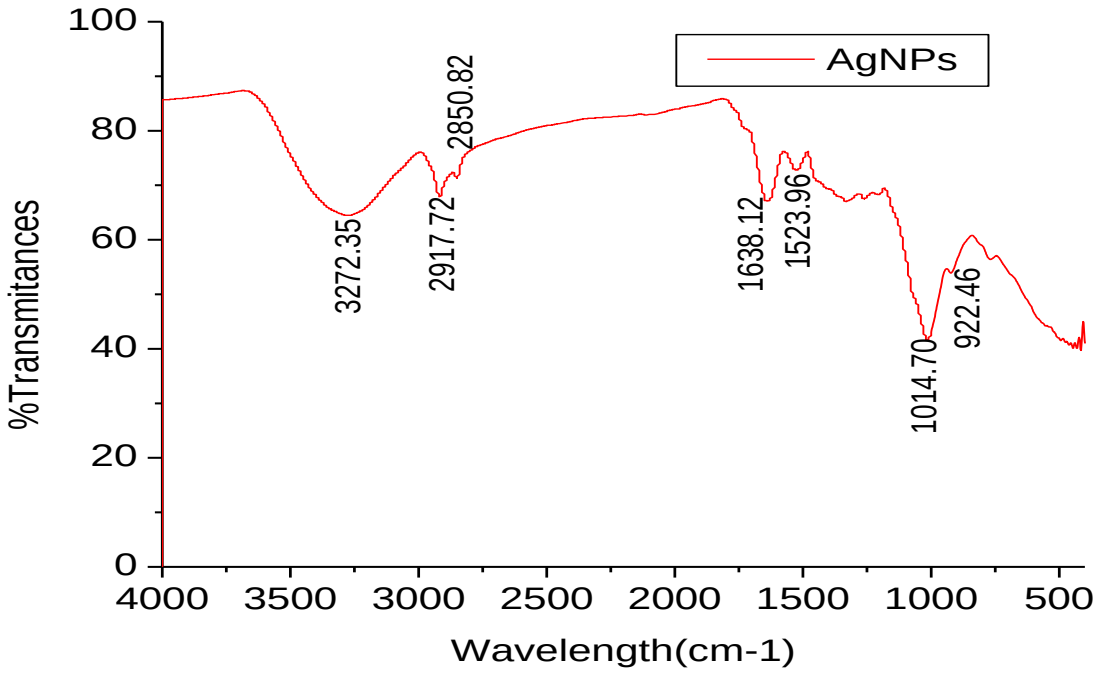


**Figure 16:** FTIR spectrum of AgNPs

In this investigation, the bands seen at 3272.56 cm-1 correspond to H-bonded alcohols and phenols that were subjected to O-H stretching, while the faint peaks at 2930.76 and 2850.82 cm-1 were caused by C-H stretching. The peaks at 1638.12 and 1523.96 cm-1 are a result of vibrations in the protein's amide bonds caused by both carboxyl stretch and N-H deformation. Similar findings, from H Haiza *et al*., (2013) showed that I and II protein amide bands are anticipated to appear as distinct FTIR bands at around 1660 and 1535 cm-1.

The FTIR of AMP trihydrate is shown in Figure 17. The spectrum bands are at 3504.56, 3440.63, 2968.18, 1768.73, 1686.30, 1605.60, 1572.21, 1493.27, 1371.57, etc. Similar findings were observed in AMP antibiotics, with absorption peaks between 3000 and 3360 (O-H stretches), 2800–3000 C≡C stretches, and 1603–1697 C=C conjugation) $cm^{-1}$ corresponds to conjugated

AgNPs. But for the same functional group, we saw variations in absorbance and peaks at various wavenumbers (Murei, 2020). The FTIR detail explanation is clearly seen in appendices III A to D.

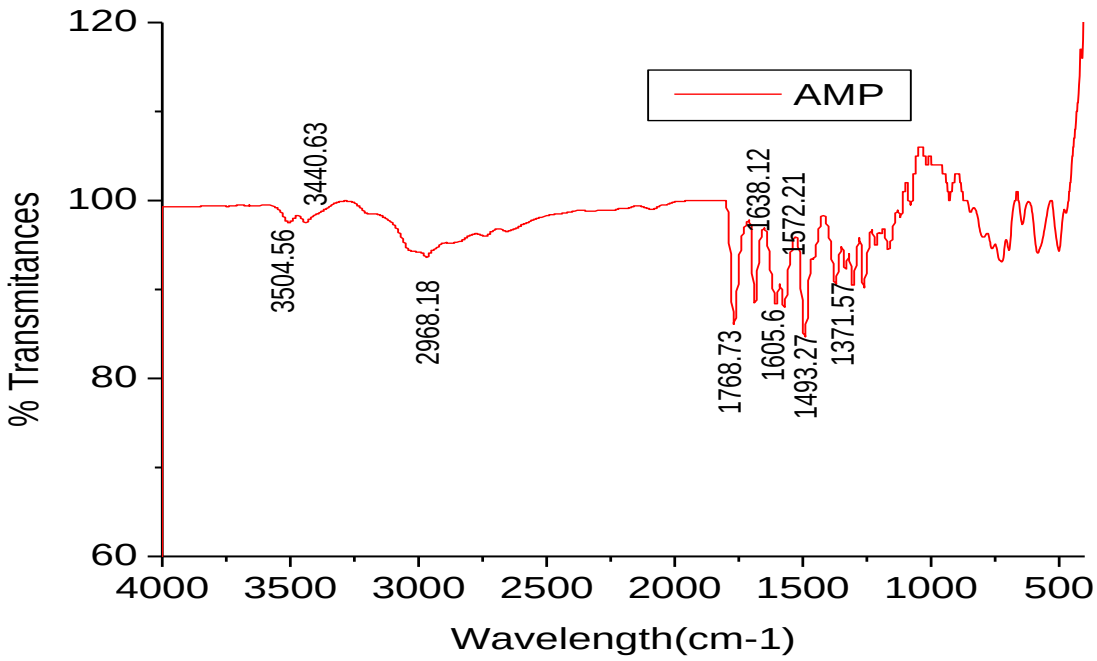


**Figure 17:** AMP trihydrate FTIR spectrum

To comprehend the functional groupings displayed, the final task requiring FTIR is the consequence of AMP-loaded AgNPs. The established FTIR values are 3257.28, 2916.63, 2849.11, 1624.67, 1452.68, 1376.99, 1233.47, 1166.09, and 1031.39, among others. AgNPs can attach to the groups of free amines of a protein or an amino acid residue's carboxylate ion. 1014.7 cm-1, which displays the presence of phosphate ions, is caused by the honey protein's C-O-C symmetric bending and C-O-H bending vibrations. The identification of amide I and II bands, C-O stretching, and the band that is missing as a result of C=O stretching.

Organic phosphates (P=O stretch) are associated with the bands at 1332.31 cm-1, aromatic aryl-O stretch esters are related to the bands at 1260.41cm-1, and phenol C-O stretch is related to the peaks at 1203.81 cm-1. In relation to silicate ions and aliphatic chloro compounds, the bands at 922.46 cm-1 and 769.24 cm-1 (C-Cl stretch) were, respectively. Additionally, bands at 493.32, 475.8, 461.52, 446.36, and 431.1 cm-1 demonstrate the presence of S-S stretches. See the (Appendices IIIB) graph that is appended to this thesis for further details.

As Figure 19 illustrates, there were no incompatibility problems observed in the FTIR characterization. Similar results were observed in this study, namely, that conjugated AgNPs correspond to the functional groups at 3257.28 (O-H stretches), 2916.63 and 2849.11 (C≡C stretches), and 1624.67 (C=C conjugation) cm-1 correspond to conjugated AgNPs. Another finding at 1624.67 and 1526.79 may indicate the presence of (C=N conjugation) and (C=O conjugation), tertiary alcohol or phenol, and OH bend; OH bend shows presence at 1452.68 and 1376.99. Aryl -O stretch and aromatic ethers are also present at 1233.47 and aliphatic phosphates (P-O-C stretch) at 1031.39cm-1. Aryl disulfide (S-S stretch) is also present at 430.08 cm-1.

A spectroscopic examination was carried out to verify the functionalization of AgNPs. To achieve this goal, we captured the FTIR spectra of the NPs before and after functionalization and noted changes in peak shape and position (Rogowska et al., 2017). Plotting the percent transmission against wavenumber from the FTIR spectra revealed that the more light the sample absorbed, the less transmission was seen (Murei, 2020).

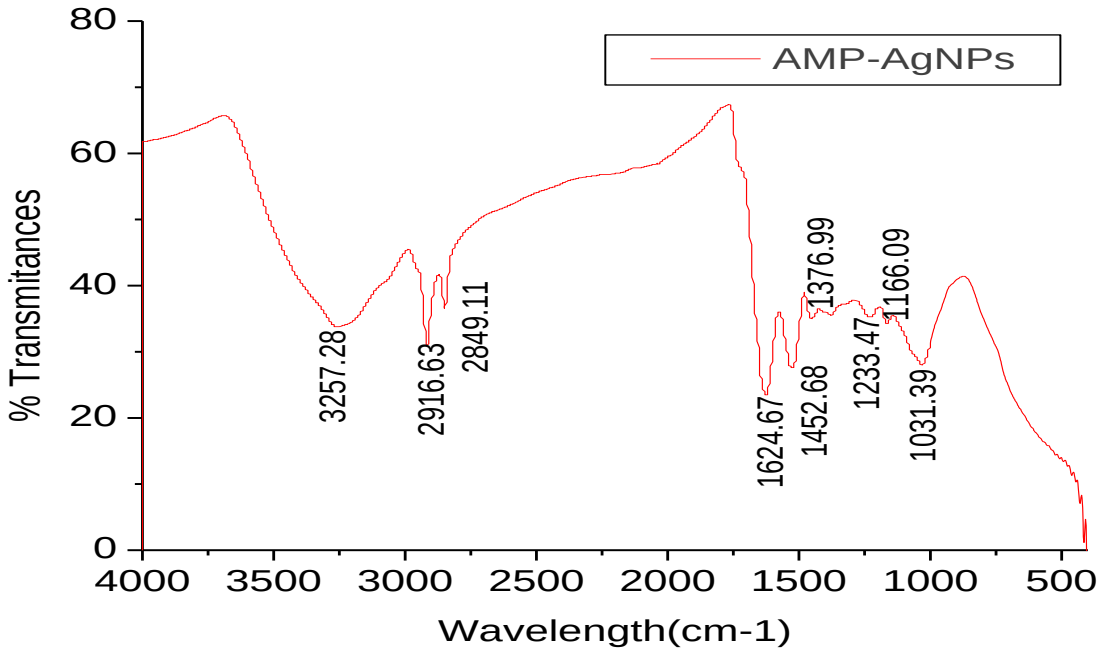


**Figure 18:** FTIR spectrum of AMP loaded AgNPs

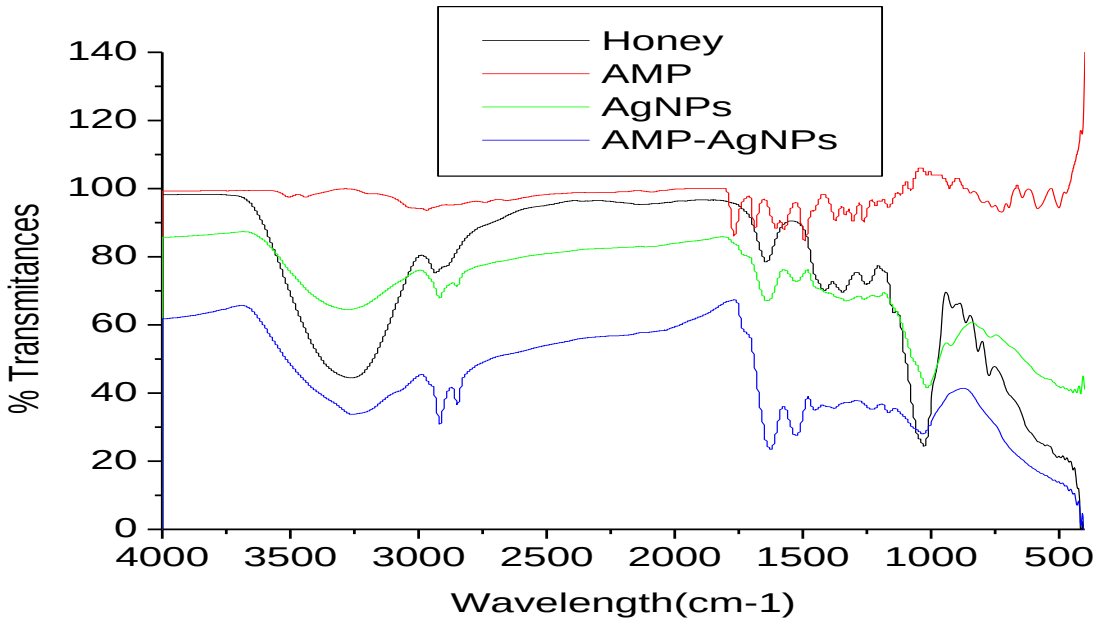


**Figure 19:** FTIR spectrum of Honey, AMP, Honey-AgNPs and AMP-AgNPs

This finding, Compared to the FTIR spectra of AgNPs that had not been changed, numerous significant alterations were found, which may be an indication that functionalization had taken place (see Figure 19 above). New bands that are absent from AgNPs spectra without an AMP appear on the spectrum of AMP loading with AgNPs. The emergence of a peak at 1233.47cm-1 might be a result of a stretching vibration caused by the carboxyl group's C-O bond or by N-H bonds. AMP binding is indicated by a new signal at 2916.63 cm-1 from the stretching vibration of the C-H aromatic ring. By changing the peak's location from 3272.35 cm-1 in the spectrum of AgNPs to 3257.28 cm-1 in the spectrum of AgNPs functionalized with AMP and boosting the peak intensity at 3272.35 cm-1, which likely correlates to the existence of extended vibration O-H in the aromatic ring, it is possible to confirm the presence of the aromatic ring.

As well as confirming the presence of aliphatic fluoro compounds, C-F stretch vibration peak at 1031.39cm-1, there are peaks in the C-H aromatic ring's stretching vibration at 2917.72.0 cm-1 and 2916.63cm-1 and then shifting from 2850.82 to 2849.11 shows the presences of Methoxy, methyl ether O-CH3, and C-H stretch, respectively. However, the change in the peak's position from 1638.12cm-1 to 1624.67cm-1 suggests the existing of stretching vibration coming from the

secondary amine, >N-H bend. This functional group, which may be found in the AMP molecule, may be in charge of attaching to the surface of synthesized AgNPs, which are most likely covered with proteins, peptides, or carbohydrates.

There are also some noticeable differences in the spectra of AgNPs and AgNPs functionalized with AMP, which may be an indication of functionalization. The emergence of bands typical for the aromatic ring at 1452.68 cm-1 obtained from stretching vibration methoxy, O-$CH_3$ stretch, C-H stretch, and at 2917.72cm-1 as well as 2916.63 cm-1 from vibration C-H provided evidence of the AMP's sorption on the surface of the AgNPs.

What's more, there is a shift in the signal from 2917.72 cm-1 to 2916.63cm-1, which is the result of the methyl group's asymmetric stretching vibration. The presence of bands at 3257.28 cm-1, 1526.79 cm-1 and 1452.68cm-1, 1233.47cm-1, and 1031.39cm-1 corresponding to the sequence of O-H stretching vibrations, C=C-C Aromatic ring stretch, Aromatic ethers, aryl -O stretch, and Aliphatic phosphates (P-O-C stretch) are what distinguish the registered spectra for modified AgNPs. The presence of the carbonyl group's stretching vibration (C = O), through which AMP can be linked to AgNPs, is likely responsible for an increase in peak strength at 1624.67 cm-1.

3.6.4.X-ray diffraction (XRD) Analysis

Silver nanoparticles' crystalline size was calculated as shown in Table 2, and it ranges from 16 to 32nm. Furthermore, AgNPs were found to have an average crystal size that ranged from 23.722±7.54 nm (n = 6). As a result, this data has a 95% confidence interval of 1.960s$\bar{x}$ (standard error of the mean) and a 23.7217 ± 6.031 (±25.43%) margin of error value. The same results were reported by prior researchers (Habsi *et al*., 2019). Similarly, AgNPs were discovered to have an average particle size of 18.31 nm (Thiruvengadam and Bansod, 2020).

A consistent finding, from Figure 20 demonstrates, the powerful peaks found at 200 crystallographic planes. There may be crystallographic planes for some impurities. However, there are six major peaks that are similar to the references. Another finding, unassigned peaks discovered in the XRD may be caused by impurities that have not yet reacted with NPs and require greater care during purification (Habsi et al., 2019). The peaks at 3 and 7 in Appendices III indicate the presence of some impurities.

Table 5: Summary of main crystallography peaks and sizes of green synthesized AgNPs (n=6)

| Main at peaks | Sample | d(ang) | Position at 2 theta | FWHM(2θ) | Cos θ | Crystallite size (nm) |
|---|---|---|---|---|---|---|
| 1 | AgNPs | 3.19656 | 27.89 | 0.2203 | 0.2433 | 35.15 |
| 2 | AgNPs | 2.76612 | 32.338 | 0.2177 | 0.2822 | 30.63 |
| 3 | AgNPs | 1.96037 | 46.273 | 0.2224 | 0.4038 | 22.36 |
| 4 | AgNPs | 1.67061 | 54.91 | 0.1744 | 0.4792 | 19.52 |
| 5 | AgNPs | 1.60071 | 57.53 | 0.1759 | 0.5020 | 18.86 |
| 8 | AgNPs | 1.24044 | 76.77 | 0.3968 | 0.6699 | 15.81 |
| Average crystallite size | | | | | | 23.722 |

X-ray diffraction (XRD) is a popular analytical technique for analyzing molecular and crystal structures, qualitative identification of various compounds, quantitative resolution of chemical species, measuring crystallinity, isomorphous substitution, particle sizes, and so on. XRD is the primary method for identifying the presence of crystals at the atomic level (Zhang et al., 2016).

Peaks at 27.61, 32.13, 45.98, 54.56, 57.44, and 67.61 were most likely generated by the 111, 200, 220, 311, 222, and 400 crystallographic planes.AgNPs have a facecentered cubic structure, accordi ng to their XRD patterns.

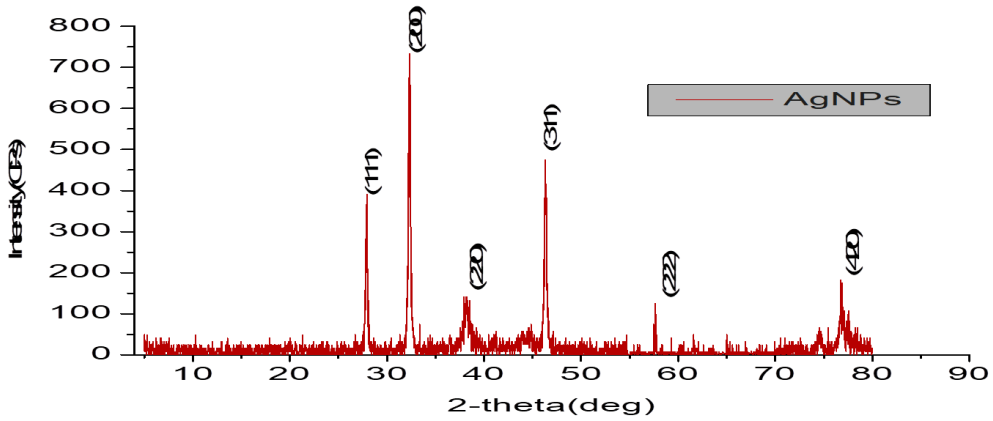


**Figure 20**: XRD Diffraction of honey base synthesized AgNPs

Whereas in this finding, silver crystals have peaks at 27.89, 32.338, 46.273, 54.91, 57.53, and 76.77, which were caused by crystallographic planes of 111, 200, 220, 311, 222, and 420, respectively.

3.6.5.Scanning Electron Microscope (SEM) Analysis

The SEM images of the green synthesized AgNPs are shown in Figure 21 A to D. These AgNPs were examined for size and shape. These experimental results showed that the synthesized AgNPs were found together and had mostly spherical and irregular shapes (Figure 21). Similarly, irregular and low-abundance spherical shapes of AgNPs were seen by Habsi *et al*. (2019).

As shown from the SEM pictures, (clusters were synthesized, which may be due to the aggregate of storage and transport. Consistent with this finding, large AgNPs with an irregular shape were detected on the surface of Abu Twaiq honey, and these AgNPs are influenced by phytochemicals. The SEM pictures of AgNPs prepared using aqueous extracted honey showed particles inclined together, which is consistent with our work. The occurrence was justified since it was caused by the presence of many reducing agents (Habsi *et al*., 2019). Whereas another finding showed that the majority of the AgNPs were well disseminated and free of aggregation, and only a small number of aggregated particles were found. In a study in Turkye, both Sidr honey (SH)-AgNPs and Rhododendron honey (RH)-AgNPs have particle sizes that are, on average, 14.3 nm and 14.7 nm, respectively (Matar *et al.*, 2022).

Additionally, the SEM picture was used to estimate the average AgNPs size, which resulted in a measurement of $49 \pm 0.572$nm.. It is a little bigger than the XRD-measured crystallite size and the published data (Matar et al., 2022). This distinction is very evident because several crystallites were present or had formed within a single particle (Figure 21). Haroon Haiza *et al.*,( 2013), findings demonstrated that the particle size of the AgNPs generated is influenced by the honey concentration. In comparison to a lower honey concentration, a higher honey concentration in the aqueous solution reduces the size of the Ag ions (Haroon Haiza *et al.*, 2013). These findings also provide strong evidence that honey may function as a capping or reducing agent in the synthesis of AgNPs.

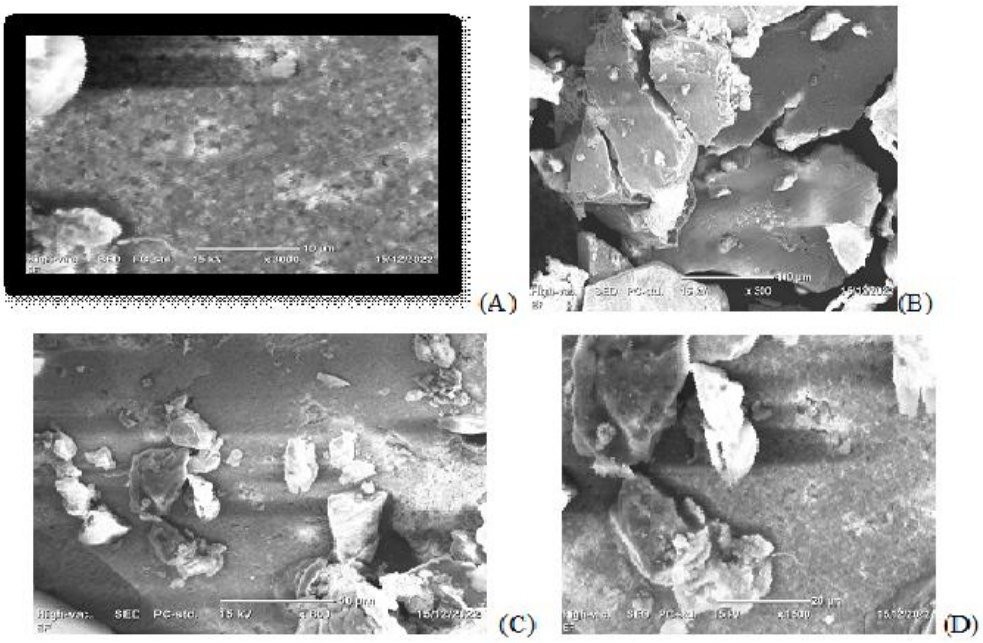


**Figure 21:** SEM Micrographs of honey-AgNPs with their size

3.6.6. Dynamic Light Scattering (DLS)

The average size of the green synthesized AgNPs and the AMP-loaded AgNPs, as shown in Figures 22 A and B, was 46.9667 ±1.027nm and 73.72 ±1.771nm respectively, with a PDI of 0.3563 ±0.0543 for the former and 0.3116 ±0.0217 for the latter. Consistent findings for PDI less than or equal to 0.3 are thought to be suggestive of homogenous particle distribution; this experiment's PDI values demonstrated a homogenous distribution of both blank and drug-loaded NPs (Eltarahony *et al.*, 2018).

According to the findings, AgNPs are uniformly sized and substantially monodisperse. The outcome was encouraging because medication delivery systems are heavily influenced by the PSD of nanocarriers. Additionally, after loading AMP onto the AgNPs, the DLS test was carried out. It was shown that the DLS caused the AgNPs to grow somewhat in size, as expected, with the average AgNPs size reaching 73.72 ±1.771nm. Although the AMP loading increased the AgNPs' particle size as expected, it was found that the AgNPs' PSD was still monodispersed.

It was obvious that the DLS-generated particle size was bigger than the particle size produced by the SEM and XRD data. This is because, when DLS measures the hydrodynamic radius, a fictitious rigid sphere diffuses at the same rate as the particles it is measuring and, as a result, overestimates particle size (Pryshchepa *et al*., 2020), and its hydrodynamic radius is influenced by particle size, shape, particle core, concentration, and roughness (Aldalbahi *et al.*, 2020). Even though DLS is the most frequently employed sizing approach by stakeholders in nanomedicine due to its simplicity and low cost, it is sometimes essential to combine a variety of high-resolution techniques in order to comprehend the PSD of NPs (Caputo *et al.*, 2019).

Additionally, the method produced a biased larger particle size suspended in suspension (Shah Faisal*, *et al*., 2021). The increased measured size of the NPs may be caused by NPs aggregation when they are disseminated in distilled water, in addition to the equipment's low-resolution power. When the size of commercially obtained AgNPs nanopowders was assessed by DLS after being dispersed in distilled water and other solvents, there was aggregation and size increment (Maria Pilar *et al*., 2017).

As another study demonstrates, the hydrodynamic radius of AMP-loaded AgNPs was calculated using the DLS test, which shows that AgNPs had an average diameter of 44.12 ± 2.89 nm. The PDI, which was calculated to determine the PSD, was discovered to be 0.32. The stability of colloidal suspensions was examined using further zeta potential calculations, and it was discovered that +33.42 mV, which suggests that AMP-loaded AgNPs in the suspension phase are stable over a long period of time (Khatoon *et al.*, 2019).

To confirm the AMP adsorption on the surface of AgNPs, physical-chemical tests have been performed. Figure 22 displays two plots that compare the size distribution of AgNPs before and after they have been functionalized with AMP. The increase in the size of AgNPs upon functionalization with AMP suggests that the layer of antibiotic adsorbed on the surface of the green synthesized AgNPs.

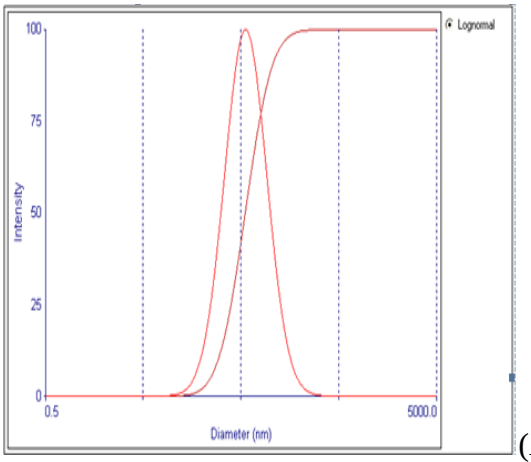

(A)
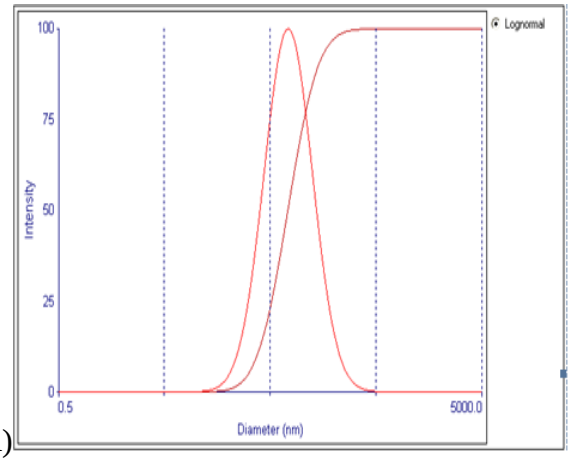

(B)

**Figure 22:** DLS result of AgNPs obtained from reduction of 20mM $AgNO_3$ at $80^0$C, 50min, 6% honey and pH of 8 Before Loading(A) and after Loading of AMP on AgNPs(B).

*3.6.7.*Differential Scanning Calorimetry *(*DSC*)*

Temperature data from 35 to 600 °C, whose rate of heating is 10°C/min, was employed for three procedures. Figure 23 depicts the DSC graph of AMP, which has two endothermic peaks and three exothermic peaks. The endothermic peaks at 102 and $160^o$C served as a representation of the heat flow required to release trapped chemical species from the synthesis process each time. They result from water evaporation and the vaporization of surfactant molecules that were deposited on the surface of AMP. According to Baraldi *et al*., (2014), the vaporization and dehydration of AMP trihydrate resulted in an endothermic process.

This endothermic action of AMP trihydrate is quickly followed by an exothermic peak, which is thought to be related to the partial crystallization of the anhydrous form. The degradation of organic materials could be attributed to the exothermic peaks at 110, 135, and $190^0$C. Where the strong peak was at $190^0$C. Actually, under experimental circumstances, i.e., after the melting of the trihydrate crystals, anhydrous crystals can form because of factors including a slow heating rate and the presence of trihydrate water molecules still in the system (Baraldi *et al.*, 2014). AMP trihydrate displayed a high melting temperature, proving that it is not easily broken down at low temperatures.

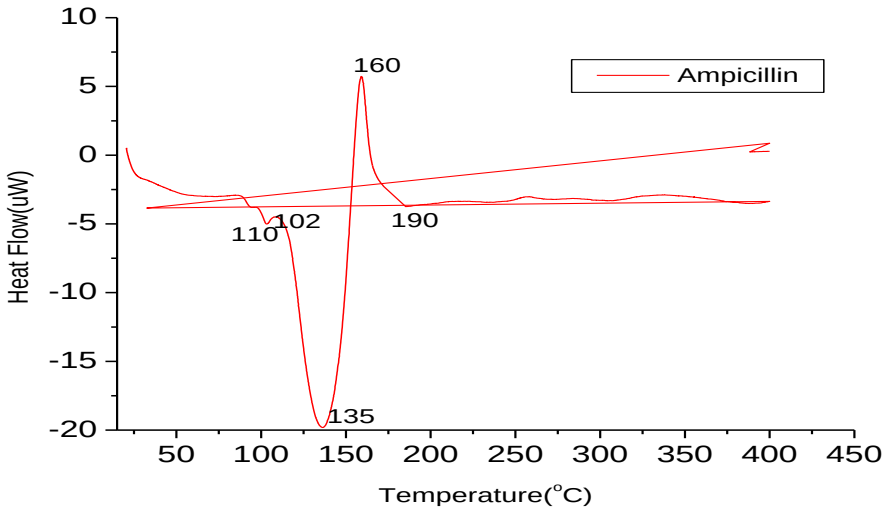


**Figure 23:** Differential scanning Calorimetry of ampicillin trihydrate

The DSC graph displays three endothermic peaks and four exothermic peaks, as shown in Figure 24. The heat flow per time to eliminate trapped chemical species from the synthesis process was represented by the endothermic peaks at 134, 360, and 455$^{o}$C. They are attributable to the evaporation of water and volatile surfactant molecules deposited on the surface of AgNPs during green synthesis. A minor low-temperature endothermic peak at 134°C was noticed as a result of the loss of water molecules that had been adsorbed on the surface of AgNPs during synthesis. A massive, high-temperature endothermic peak occurs when silver nitrate is transformed to AgNPs at 134, 360, and 485$^{o}$C. The endothermic peak at the above temperature is related to the conversion of silver nitrate to AgNPs.

The synthesis of AgNPs and the degradation of organic materials could be attributed to the exothermic peaks at 166, 310, 390, and 485$^{0}$C. Where the strong peaks were at 160$^{0}$C. The DSC results showed that AgNPs' biological components are capable of being reduced using extracted honey. According to Sampaio and Viana (2018), organic molecules predominantly degraded between 80°C and 500°C. AgNPs displayed a high melting temperature, proving that they are not easily broken down at low temperatures.

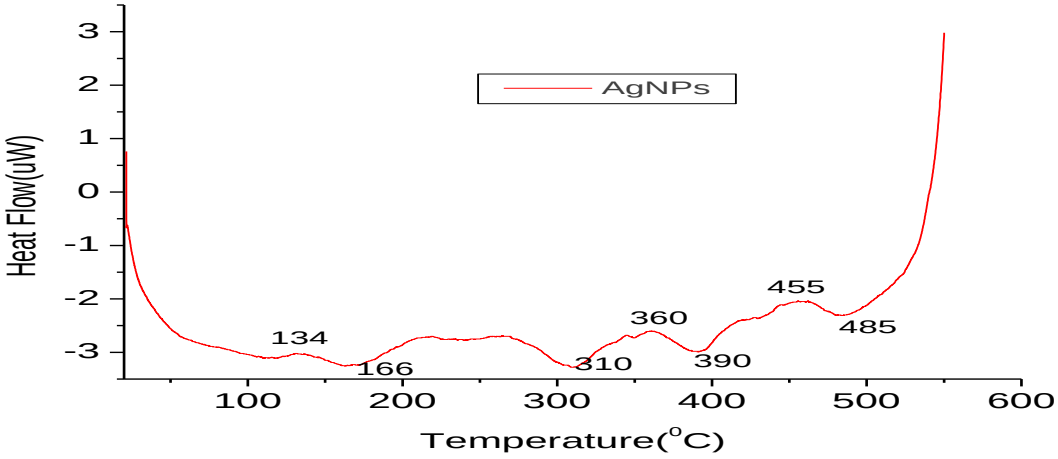


**Figure 24:** Differential scanning Calorimetry of silver nanoparticles

Figure 25 depicts the DSC graph, which each has three endothermic and exothermic peaks. The endothermic peaks at 350, 366, and 460$^{o}$C served as a representation of the heat flow required each time to release trapped chemical species from the synthesis process. They resulted from water and volatile surfactant molecules that were deposited on the surface of AMP-AgNPs during loading, which causes evaporation.

A low-temperature endothermic peak was seen around 350°C due to the loss of water molecules that were adsorbed on the surface of AMP-AgNPs during loading. The exothermic peak at 78,384 and 490$^{0}$C may be linked to the deterioration of organic components from AMP-loaded AgNPs. Finally, AMP-loaded AgNPs were highly heat resistances.

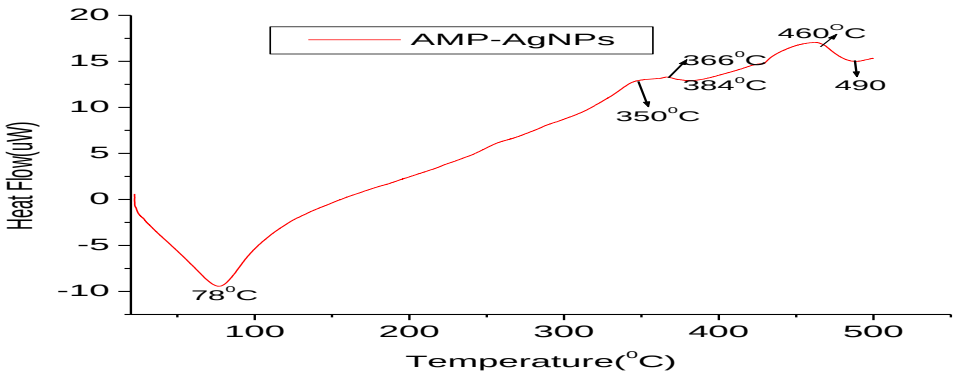


**Figure 25:** Differential scanning Calorimetry of ampicillin loaded silver nanoparticles

### 3.7.Ampicillin Loading with Silver Nanoparticles

#### 3.7.1.Standard Ampicillin Calibration Curve

The calibration curve for AMP in this study was prepared by plotting absorbance versus concentration with an equation of $Y= 0.0294X+ 0.0004$, $R^2 = 0.9997$; where Y, X, and $R^2$ denoted absorbance, concentration in mg/ml in the supernatant, and correlation coefficient, respectively (Appendix I) for determining the unknown AMP concentration in the supernatant. This calibration curve was used to optimize concentration and time.

#### 3.7.2.Optimization for Ampicillin Loading

##### 3.7.2.1.Effects of AMP Concentration

Since the principle of drug loading on AgNPs is surface adsorption (Sekar *et al.*, 2013), the surface can be saturated at high AMP concentrations. At a concentration of 3 mg/ml, this was thought to be the ideal concentration ratio in this investigation. The AMP-to-AgNPs mixing ratio demonstrated a promising result. This finding suggests that the amount of AgNPs is crucial for the transportation of AMP. It was exciting to see that as AMP increased, the concentration went from 1 to 3 mg/ml, and the associated EE and DL capacities improved even though the amount of AgNPs concentration remained constant (12 mg). As demonstrated in Table 6, increasing the amount of AMP added to AgNPs from 1 to 3 mg/ml caused an increase in EE and LC. However, as AMP concentration was further increased to 5mg/ml, EE and LC started to drop, indicating that the saturation point for the AMP carrying capacity of AgNPs had been achieved, as shown in Table 6.

**Table 6:** Drug loading and encapsulation efficiency of AgNPs with different AMP Concentrations

| AMP concentration (mg/mL) | Total amount of AMP added (mg) | Amount of AMP loaded (mg) | EE (%) | LC (%) |
|---|---|---|---|---|
| 1.5 | 3 | 2.64 | 88.00 | 22.00 |
| 2 | 4 | 3.67 | 91.75 | 38.92 |
| 2.5 | 5 | 4.68 | 93.60 | 39.00 |
| 3 | 6 | 5.77 | 96.17 | 48.08 |
| 5 | 10 | 2.79 | 60.08 | 23.25 |

While the concentration of AgNPs stays constant, the ratio of AMP to AgNPs is constantly increasing until it reaches 3mg/ml. Table 6 illustrates the positive EE of the synthesized AgNPs. 3 mg/ml (out of a total of 6 mg) was chosen as the ideal level for this study since the concentration of AgNPs remained constant when AMP was increased to 6 mg/ml in 2 ml. In light of this, as indicated by EE above, the maximum DL is reached at 3 mg/ml (for a total of 6 mg in 2 ml).

3.7.2.2. Effects of incubation time

Initially, AMP was loaded on AgNPs for 24 hours, and the DL was assessed by taking samples every 6 hours. After 6 hours of incubation, the lowest levels of EE and LC were detected, while the highest quantity was detected after 24 hours. For optimum loading and the greatest synergistic effect against AMP-resistant *E. coli*, AMP should be incubated for 24 hours on prepared AgNPs. However, another test is still needed to confirm the maximum drug LC of AgNPs against time. Following that, another 36 hours of loading were done to determine the effects of time on the DL capacity of AgNPs. To establish the maximum drug LC against time, more tests were done using the same procedures as shown in Table 7. Out of all of these tests, 24 hours was chosen as the ideal incubation period to have a good effect against AMP-resistant *E. coli*.

**Table 7:** Drug loading and encapsulation efficiency of AgNPs with different incubation times

| Incubation period (hrs) | Total amount of AMP added (mg) in 2ml | Amount of AMP loaded (mg) | EE (%) | LC (%) |
|---|---|---|---|---|
| 6 | 6 | 5.41 | 90.17 | 45.10 |
| 12 | 6 | 5.48 | 91.33 | 45.67 |
| 18 | 6 | 5.65 | 94.17 | 47.10 |
| 24 | 6 | 5.78 | 96.33 | 48.17 |
| 36 | 6 | 5.46 | 91.00 | 45.50 |

### 3.8. Drug release study

3.8.1.Calibration curve for drug release test

For all solutions of AMP in all buffer conditions, the absorbance readings were obtained and plotted (Y-axis) against concentration of solutions (X-axis) (Appendix II, A through E). Then, equations for linear regression and correlation coefficients were obtained for each calibration curve (Table 8).

**Table 8:** Correlation coefficients ($R^2$) and regression equations of calibration curves of AMP in different buffer solutions

| S.No | Buffer solutions' pH | Linear Regression Equation* | Correlation Coefficient ($R^2$) |
|---|---|---|---|
| 1 | 1.2 | Y = 0.0727X + 0.0023 | 0.9998 |
| 2 | 6 | Y =0.0798X + 0.0084 | 0.9995 |
| 3 | 7.3 | Y=0.0731X + 0.0011 | 0.9996 |
| 4 | 7.4 | Y =0.0794X + 0.0074 | 0.9992 |
| 5 | 8 | Y= 0.0778x + 0.01 | 0.9994 |

Note: X represents the concentration in µg/mL, and Y is the absorbance

3.8.2.Drug release test

AMP-loaded AgNPs quickly disintegrated in the bag for dialysis at pH 1.2, whereas they did not at the pH 7.4 medium. Figure 26 demonstrated that at a pH of 1.2 as opposed to 7.4, AMP was released more quickly and completely dissolved in 6 hours. At a pH of 1.2, AMP displayed a burst release in the first six hours. Faster AMP release rates were found, with 16.18%, 42.18%, and 92.44% of the drug being released after 1, 3, and 6 hours, respectively. This may be related to an acidic medium with a pH lower than 3, where the dissolving rate constants rose linearly. Beyond this pH, all penicillins have a constant dissolution rate. Due to the amide's side-chain intramolecular assault on the β-lactam molecule, the acidic solution instability of penicillin is well recognized (Tsuji *et al.*, 1978).

Another reason is that AgNPs are very unstable in acidic environments and are therefore likely to disintegrate into their ions (Mbanga, Cukrowska, and Gulumian, 2022). The *in vitro* drug release of AMP-AgNPs at pH 7.4 shows a biphasic mechanism with a first release and subsequent controlled release of the remaining drug molecules. Then, over the course of 96 hours, a sustained release of AMP was seen. AgNPs' surface-bound or weakly trapped drugs may be the cause of the initial rapid release since they can quickly diffuse into the release medium.

The leftover medication contained in the inner region of the AgNPs will travel slowly over time, which may explain the eventual sluggish release. Furthermore, the pH had an impact on the release rate. According to this study, an acidic medium (pH 1.2) demonstrated the fastest release within 6 hours. More than 92.44 ±0.136 and 84.82±0.255% of the total loaded drug content were released within 6 hours and 96 hours, respectively. The slowest release, however, was observed at the highest pH medium (pH 7.4). Only 20.32 ±0.867% and 73.98 ±4.237% of the LC were released in 6 hours and 96 hours, respectively.

At pH 7.3, the AMP-loaded AgNPs' colloid solution remained steady, and controlled drug release occurred. The estimated percentage of AMP released in 96 hours was 78.27 ±0.364%, indicating that over 21% retention of the AMP within AgNPs. Only 72.2% of the AMP was released within the first three days at pH values of 7.4. This shows that AMP-loaded AgNPs are stable at physiological pH, which is helpful because it prevents AMP from being released during blood circulation. Compared to a pH of 7.4, the AMP release rate accelerated when the pH value was the

lowest. At pH 6, around 84% of the medication was released in less than 72 hours; at pH 7.3, about 78.27%, and at pH 8, 85% of the AMP was released within 24 hours. AMP was released entirely within the first 6 hours at a much lower pH value of 1.2.

Time altered the release of AMP from AgNPs, a finding similar to Flory et al. (2013), with an initial burst release over the first three to six hours followed by a slow release rate throughout the research. AMP-loaded AgNPs can be released in a sustained manner, but they must be modified and protected if they encounter a basic environment (Fontana *et al.*, 1998).

Similarly, at pH 7.4 and pH 1.1, esterases greatly accelerate AMP release from polyethylcyanoacry late (PECA) NPs, with 70% quickly released and 30% strongly bound (Fontana et al., 1998). This is a consistent finding: a pH greater than 7 makes AMP in the solution less stable. It is possible to use any of the three items, but for solution stability, the pH must be reduced to 7 or lower (Jaeger and Smith, 2021). Another finding showed that, as pH increases, the rate of ion release decreases (Flory *et al.*, 2013). The most pronounced pH-dependent changes in surface charge and aggregated particle size were observed in honey-stabilized AgNPs (Badawy *et al.*, 2010).

AgNPs demonstrated poor attachment efficiency at high pH but significantly greater attachment efficiency at neutral pH (Flory *et al.*, 2013). Additionally, AgNPs' increased solubility around neutral pH, and specifically AgNPs were highly soluble at pH 6.5 (Molleman and Hiemstra, 2017), may make the full release of the AMP possible at this particular pH level.

Another finding was that, below pH 3, the rates considerably increased as the acidity of the solution rose due to the hydrogen ion's back migration towards the solid surface. Above pH 3, the dissolution rates from the revolving discs were independent of the bulk solution's pH. Accordingly, at pH 1-3 in the stomach, it is anticipated that the solids will dissolve very quickly (Fontana *et al.*, 1998; Tsuji *et al.*, 1978). At pH 3, the electrostatically stabilized AgNPs showed significant aggregation (Badawy *et al.*, 2010).

The findings of this investigation indicate that AgNPs are efficient AMP carriers with regulated AMP release behavior. According to the release profile observed, the medicine will be delivered quickly to have antibacterial effects and slowly over time to promote long-term healing. By avoiding the toxic and harmful systemic effects brought on by high AMP concentrations, it can

also improve patient compliance. AgNPs produced using aqueous extracted honey is thus a suitable candidate for the AMP drug delivery system. Similar results, such as AgNPs, can be thought of as ionic delivery systems, operating similarly to medication delivery systems in that the silver ions contained within the NPs are delivered to, and then released at or close to, biological target areas (Flory *et al.*, 2013). pH 6,7.3 and 7.4 as shown in Figure 26, are optimal for the regulated release of AMP-loaded AgNPs. This is due to the fact that the release is almost ready to be released in a controlled manner.

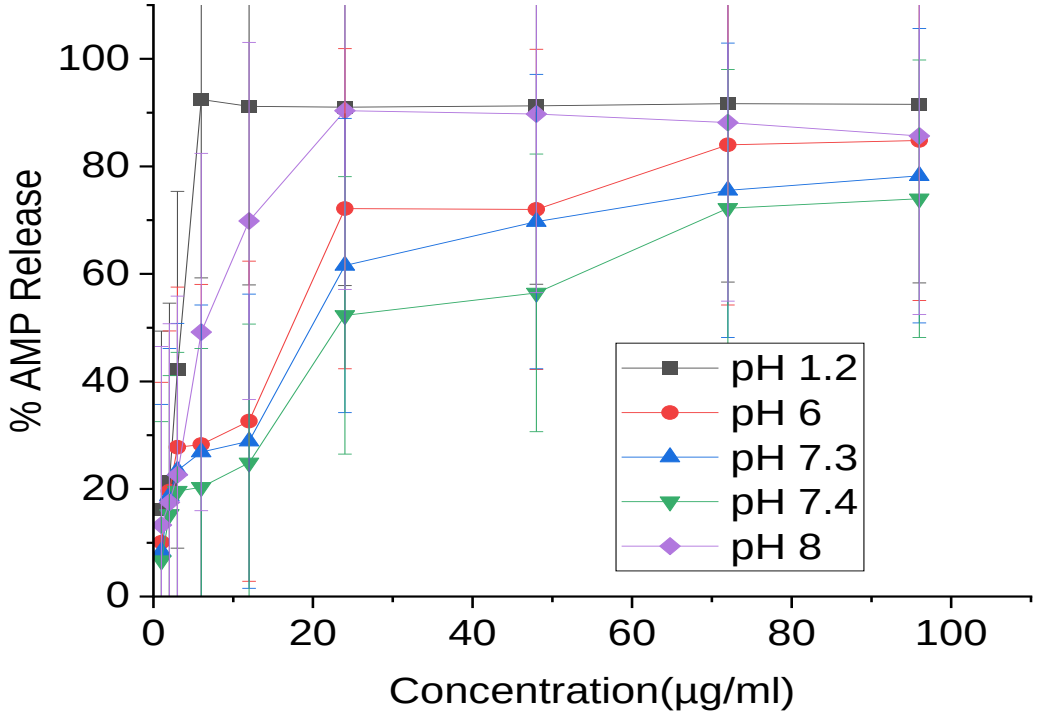


Figure 26:% Cumulative drug releases of AMP from AMP loaded AgNPs in different pH conditions.

### 3.9.*In Vitro* antimicrobial susceptibility test(AST)

As indicted in Table 6.our AST revealed a 95.66% increase in antimicrobial efficacy of AMP-AgNPs over AMP alone, but only a 77.04% increase when compared to AgNPs alone. The green synthesis of AgNPs alone displayed antibacterial effectiveness against AMP-resistant *E.coli* and

increased AMP activity when bound with AgNPs, whereas the negative control had no inhibitory effect

As reported by CLSI, AST of AMPs by using the disk-diffusion method results in zone diameter breakpoints of ≥17, 14–16, and ≤13 mm, indicating susceptibility, intermediate, or resistance of bacteria to AMP (CLSI, 2020), respectively. Therefore, according to this guideline, *E.coli* was found to be resistant to AMP as the diameter of the ZOI around the AMP-impregnated disc was≤13mm. However, upon conjugation with green synthetic AgNPs, the ZOI diameter increases to 17.2±1.686mm (n=5) falling into the category of susceptibility threshold. From this, we can conclude that AgNPs can enhance the activity of AMP against AMP-resistant *E.coli.*

AgNPs can improve the antibacterial effectiveness of antibiotics (Kolár *et al.*, 2016). AgNPs-amplified AMP antibiotic action (Murei, 2020). Antibiotics and AgNPs have strong synergistic effects against *E. coli* at 5 and 2.5 mg/L concentrations (Kolár *et al.*, 2016). The outcomes shown in Table 7 are the antibacterial activities of AMP, AgNPs, and AMP-loaded AgNPs against AMP-resistant *E. coli.*

Mutations in the target gene prevent antibiotics from working, leading to alternative approaches (Singh *et al.*, 2020). Newly developed nanomedicine is cheap and environmentally friendly, i.e., the green synthesis method (El Shafey, 2020), but as shown in each section above, other NPs synthesis methods are expensive, produce fewer NPs, and are not more environmentally friendly. This disruption of the cell wall facilitates entry into the bacterial cell, an effect not achieved by AMP alone (Agarwal, Venkat Kumar, and Rajeshkumar, 2017; El Shafey, 2020).

One of the most effective approaches to treat bacterial illnesses that are resistant to medication is metal NPs (Sreedharan and Singh, 2019). NPs have a strong affinity for cell membranes due to their high surface-to-volume ratio (Prasad, 2008). NPs target multiple pathways to kill bacteria, making them difficult to resist (Singh *et al.*, 2020).

The antibacterial properties of NPs change with changes in NPs' size, shape, and oxidation state (Mokhena *et al.*, 2018). According to reports, the antibacterial activity of NPs rises with smaller sizes and falls with larger sizes. Shape-wise, triangular and spherical NPs have remarkable antibacterial capabilities, although the underlying mechanisms are still unclear. According to

reports, the majority of metal NPs from transition (d-block) elements are effective antibacterial substances. This is because they quickly reduce and oxidize in the presence of reducing and oxidizing chemicals, respectively, and have high oxidation numbers (Singh *et al.*, 2020).

In the presence of AgNPs, the antibacterial effects of AMP, kanamycin, erythromycin, and chloramphenicol were increased against test microorganisms. On the strains put to the test, AMP had the most potentiating effects. The outcomes demonstrated that combining antibiotics with AgNPs led to improved antibacterial activities (Mohammed *et al.*, 2010). Consistent with our study (Kolár *et al*., (2016), we discovered that the presence of AgNPs enhanced the antibacterial activity of AMP against *E. coli.*

There have also been reports showing the dose-dependent efficacy of AMP-conjugated AgNPs against multidrug-resistant strains, including *E. coli* (Id *et al*., 2018). It has also been reported that the ZOI of AMP was increased by 75% compared to *E. coli* strains that were evaluated with AgNPs present (Mohammed *et al.*, 2010). In another finding, AgNPs in combination with AMP and vancomycin increased antibacterial activity against methicillin-resistant *Staphylococcus aureus* (MRSA) (ATCC 25,923), *beta-lactamase-producing Klebsiella pneumonia* (ATCC 700,603), and *beta-lactamase* and both antibiotics showed increased uptake of produced AgNPs by *E. coli* (ATCC 35.218)(Murei, 2020).

**Table 9:** Summary of Antimicrobial Susceptibility Test

| S.No | Test Material | Amount of loaded material per disc(2ml) | ZOI [a] Diameters[b](mm) | In vitro AST Breaking point (CLSI, 2020) | Fold increase % $= \frac{(d-c)*100}{c}$ |
|---|---|---|---|---|---|
| 1. | DW | 2ml | $6.00 \pm 0.00$ | NA | |
| 2. | Honey | 10%,20%,30% | $6.00 \pm 0.00$ | Insignificant | |
| 3. | AgNPs | 10µg | $10.00 \pm 0.6673$ | R | 77.04 |
| 4. | AMP(c) | 10µg | 8.00±2.63 | R | 95.66 |
| 5. | AgNPs-AMP(d) | 20µg | 17.2 ±1.686 | S | |

[a] -the measured ZOI diameter includes the disc diameter

[b] -the diameter is the mean of three tests

Note: Breaking points for AMP in *E.coli*: R: ≤ 13 mm, I: 14-16mm, S: ≥17mm (CLSI, 2020), NA: Not Applicable, DW: Distilled water, CLSI: Clinical Laboratory Standards Institutes

As previously mentioned, AgNPs antibacterial activity has been loss of cell integrity through direct contact with the cell wall, formation of ROS, and release of $Ag^{+}$ antibacterial ions, mainly, but this has yet to be clarified(Chmielewska *et al.*, 2021).

Contact with AgNPs together with the cell wall is based on electrostatic attraction, as bacteria can have a negative charge and metal oxides can have a positive charge. This can disrupt the outer membrane of *E. coli* cells, allowing material, proteins, and genetic material to leak out. This can be facilitated due to the small size of the green synthesized AgNPs, which provides a large surface area for contact with bacteria (Singh et al., 2020). This scenario might also work in this case as the AgNPs have an average size of $23.722 \pm 7.54$nm (determined from XRD data) and $49 \pm 0.572$nm (determined from SEM data).

The surface of the synthesized AgNPs is rough, which may increase the likelihood of direct contact killing as surface roughness increases the likelihood of bacterial attachment to the NPs(Chang *et al.*, 2021). As for the formation of ROS, after their generation (mostly $H_2O_2$) they can penetrate the bacterial cell wall and disrupt metabolic processes(Chmielewska *et al.*, 2021). It contributes significantly in protein, enzyme modification, and RNA/DNA damage (Singh *et al.*, 2020); while, it plays an important role in protein, enzyme modification, and RNA/DNA damage(Chmielewska *et al.*, 2021). As an opportunity, *E. coli* also has a thin peptidoglycan layer, which facilitates the entry of ions from the NPs into the bacterium, leading to cell wall disruption (Morigi *et al.*, 2012). This broad mechanism makes it difficult for microbes to acquire resistance to these NPs (Wang and Hu, 2017).

AgNPs have antibacterial effects due to their mechanism of action. For example, the antimicrobial efficacy of AgNPs in AMP-AgNPs conjugates was assessed in contrast MDR *E.coli*, *Staphylococcus aureus*, and *Klebsiella spp.* (tolerant to AMP), justified as AgNPs damage bacterial cell walls by forming ROS or by mechanical damage through surface defects. Damage to

cell membranes was confirmed by release assays showing the release of RNA, DNA and other substances(Chmielewska *et al.*, 2021).

The effectiveness of the antibiotics and aqueous extracted honey in various concentrations was evaluated against *E. coli* American Type Culture Collection (ATCC: 25922). The strain of the bacteria was kept at 37 $^{0}$ C for 24 h under aerobic conditions. The antibacterial effect was tested by 10 %( H1), 20% ($H_2$) and 30% ($H_3$) of honey concentration. The findings of the test were presented in the following Figure 27.

As Figure 27 shows, honey has no antibacterial effect at the stated concentrations, but its effect was dependent on its concentration i.e. as the concentration increases its antibacterial effect was increased as Figure 27 clearly shows. The effect of the honey from the Figure 27 is null for the resistant *E. coli* strains. Additionally, the AST were done against *E.coli b*y using AMP, AgNPs, and AMP-AgNPs. According to these results, antibacterial effect was more pronounced in AMP-AgNPs compared to others. Similarly, the ZOI for AMP, AgNPs and AMP-AgNPs 6.00mm, 10.00±0.6673mm and 17.2 ±1.686mm respectively. These results indicates that the antibacterial effect of AMP loaded AgNPs has synergistic than others. Finally, ATCC: 25922 types *E. coli* was the resistant strain that has more resistant against AMP but, *E.coli* strain was killed easily by AgNPs and AMP loaded AgNPs.

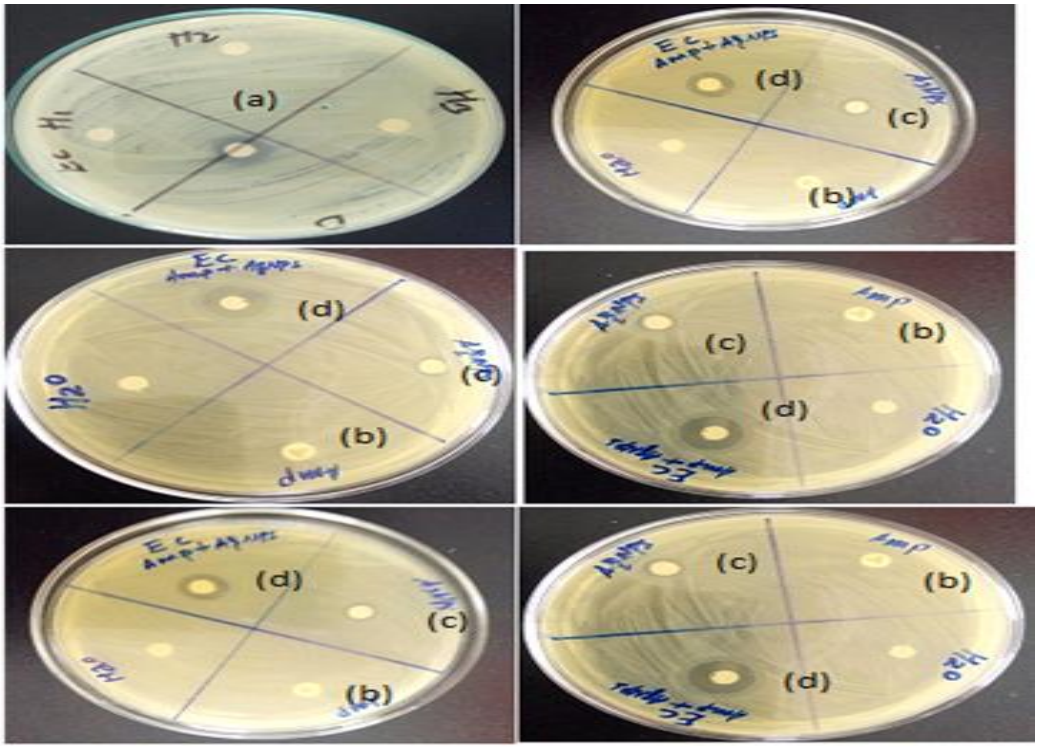


Figure 27: Antibacterial effects of extracted honey (a), AMP (b), AgNPs(c), AMP-AgNPs (d)

Note: 10 µg of AMP was used as the positive control, distilled water as the negative control, and H1, H2, and H3 were utilized to represent concentrations of 10%, 20%, and 30% of honey, respectively.

## 4. Conclusion

In this study, AgNPs were synthesized using an eco-friendly process using aqueous extracted honey. UV/Vis, FTIR, and XRD spectrophotometers all verified that AgNPs were actually formed. The anticipated crystallite length of AgNPs XRD result was 23.722 ±7.54nm, and their common diameter changed into $49 \pm 0.572$nm. as per the SEM result; whereas the DLS result was higher after loading; i.e 46.9667 ±1.027nm before loading whereas 73.72 ±1.771nm after loading. The AMP-loaded AgNPs were also characterized and as a result, the powerful loading of the AMP changed the FTIR and UV/Vis spectrum of the unloaded AgNPs and the free AMP.

The AMP release test results revealed that the AMP-loaded AgNPs were stable at physiological pH and released the AMP in a sustained manner at the pH value of an environment with newborn meningitis caused by *E. coli*, making the AgNPs a good option for AMP delivery. However, the AMP-loaded AgNPs were unstable at an acidic pH (pH 1.2). The findings of this investigation demonstrated that aqueous extracted honey-based AgNPs can be a suitable nanocarrier for AMP delivery to enhance its efficacy against resistant *E.coli*. The result of AST showed that both AMP-loaded and free AgNPs were active against AMP-resistant *E. coli*, and loading AMP enhanced their activity against AMP-resistant *E.coli*. The average ZOI for AgNPs and AMP-loaded AgNPs was 10.00±0.6673 and 17.2 ±1.686mm, respectively, while honey and AMP ZOIs were insignificant. Hence, from this study, we concluded that honey-based AgNPs are a good delivery vehicle for AMP against AMP-resistant *E. coli*.

## 5. Suggestion for Further Work

The results of this study points to the need for additional research in the following areas:

- ✓ *In vivo* effectiveness and toxicity study
- ✓ Stability study
- ✓ Studies on surface chemistry

## References

AB, A.M., *et al*.,(2018) 'New Synergistic Potential of Silver Nanoparticles and it is Application in Pharmaceutical Production Areas', *Journal of Biotechnology & Biomaterials*, 08(04). Available at: https://doi.org/10.4172/2155-952x.1000288.

Agarwal, H., *et al*., (2017) 'A review on green synthesis of zinc oxide nanoparticles – An eco-friendly approach', *Resource-Efficient Technologies*, 3(4), pp. 406–413. Available at: https://doi.org/10.1016/j.reffit.2017.03.002.

Ahmad, M. and Khan, A.U. (2019) 'Journal of Global Antimicrobial Resistance Global economic impact of antibiotic resistance : A review', *Integrative Medicine Research*, 19, pp. 313–316. Available at: https://doi.org/10.1016/j.jgar.2019.05.024.

Akbar, S. *et al.* (2020) 'An overview of the plant-mediated synthesis of zinc oxide nanoparticles and their antimicrobial potential', *Inorganic and Nano-Metal Chemistry*, 50(4), pp. 257–271. Available at: https://doi.org/10.1080/24701556.2019.1711121.

Aldalbahi, A. *et al.* (2020) 'Greener Synthesis of Zinc Oxide Nanoparticles: Characterization and Multifaceted Applications', *Molecules*, 25(18), pp. 1–14. Available at: https://doi.org/10.3390/molecules25184198.

Amabye, T.G. (2017) 'Phytochemical and biochemical compostion of wild honey a case study in Estern zone areas in tigray', *MOJ Food Processing & Technology*, 4(3), pp. 88–94. Available at: https://doi.org/10.15406/mojfpt.2017.04.00094.

Asaduzzaman, M. *et al.* ,(2015) 'Analysis of Biochemical Composition of Honey and its Anti-Oxidant, Phytochemical and Anti-Bacterial Properties', *Biomedical and Pharmaceutical Reseach*, 4(4), pp. 69–81. Available at: http://www.academia.edu/15224880/Analysis_of_Biochemical_Composition_of_Honey_and_its_Anti-Oxidant_Phytochemical_and_Anti-Bacterial_Properties.

Badawy, A.M.E.L. *et al.* (2010) 'Impact of Environmental Conditions ( pH , Ionic Strength , and Electrolyte Type ) on the Surface Charge and Aggregation of Silver Nanoparticles Suspensions', 44(4), pp. 1260–1266.

Bahiru, M.W. (2022) ‘COLLEGE OF HEALTH SCIENCE SCHOOL OF PHARMACY DEPARTMENT OF PHARMACEUTICS AND SOCIAL PHARMACY A Thesis Submitted to the Department of Pharmaceutics and Social Pharmacy , School of Pharmacy , College of Health Sciences , Addis Ababa University for the parti’, pp. 1–95.

Baraldi, C. *et al.* (2014) ‘Characterization of polymorphic ampicillin forms’, *Journal of Pharmaceutical and Biomedical Analysis*, 100, pp. 329–340. Available at: https://doi.org/10.1016/j.jpba.2014.08.021.

Van De Beek, D. *et al.* (2012) ‘Advances in treatment of bacterial meningitis’, *The Lancet*, 380(9854), pp. 1693–1702. Available at: https://doi.org/10.1016/S0140-6736(12)61186-6.

Blanco Massani, M. *et al.* (2018) ‘Chromosomal Sil system contributes to silver resistance in E. coli ATCC 8739’, *BioMetals*, 31(6), pp. 1101–1114. Available at: https://doi.org/10.1007/s10534-018-0143-1.

Boisseau, P. and Loubaton, B. (2011) ‘Nanomedicine, nanotechnology in medicine’, *Comptes Rendus Physique*, 12(7), pp. 620–636. Available at: https://doi.org/10.1016/j.crhy.2011.06.001.

Brudzynski, K. and Sjaarda, C. (2014) ‘Antibacterial Compounds of Canadian Honeys Target Bacterial Cell Wall Inducing Phenotype Changes , Growth Inhibition and Cell Lysis That Resemble Action of b -Lactam Antibiotics’, *PLOS ONE*, 9(9), p. 106967. Available at: https://doi.org/10.1371/journal.pone.0106967.

Caputo, F. *et al.* (2019) ‘Measuring particle size distribution of nanoparticle enabled medicinal products, the joint view of EUNCL and NCI-NCL. A step by step approach combining orthogonal measurements with increasing complexity’, *Journal of Controlled Release*, 299(December 2018), pp. 31–43. Available at: https://doi.org/10.1016/j.jconrel.2019.02.030.

Chang, T. *et al.* (2021) ‘A novel methodology to study antimicrobial properties of high-touch surfaces used for indoor hygiene applications-A study on Cu metal’, *PLoS ONE*, 16(2 February), pp. 1–25. Available at: https://doi.org/10.1371/journal.pone.0247081.

Chmielewska, S.J. *et al.* (2021) ‘Bactericidal properties of rod-, peanut-, and star-shaped gold nanoparticles coated with ceragenin CSA-131 against multidrug-resistant bacterial strains’,

*Pharmaceutics*, 13(3), pp. 1–27. Available at: https://doi.org/10.3390/pharmaceutics13030425.

Cokcetin, N.N. *et al.* (2016) 'The Antibacterial Activity of Australian Leptospermum Honey Correlates with Methylglyoxal Levels', *PLOS ONE*, pp. 1–13. Available at: https://doi.org/10.1371/journal.pone.0167780.

Combarros-Fuertes, P. *et al.* (2020) 'Honey: Another alternative in the fight against antibiotic-resistant bacteria?', *Antibiotics*, 9(11), pp. 1–21. Available at: https://doi.org/10.3390/antibiotics9110774.

Dadgostar, P. (2019) 'Antimicrobial resistance: implications and costs', *Infection and Drug Resistance*, 12(1), pp. 3903–3910. Available at: https://doi.org/10.2147/IDR.S234610.

Elkrewi, E. *et al.* (2017) 'Cryptic silver resistance is prevalent and readily activated in certain Gram-negative pathogens', *Journal of Antimicrobial Chemotherapy*, 72(11), pp. 3043–3046. Available at: https://doi.org/10.1093/jac/dkx258.

Eltarahony, M. *et al.* (2018) 'Biosynthesis, Characterization of Some Combined Nanoparticles, and Its Biocide Potency against a Broad Spectrum of Pathogens', *Journal of Nanomaterials*, 2018, pp. 1–17. Available at: https://doi.org/10.1155/2018/5263814.

Famuyiwa, T.O. *et al.* (2021) 'Pharmacovigilance and Pharmacoepidemiology Drug Release Studies of SC-514 PLGA Nanoparticles', *Pharmacovigilance and Pharmacoepidemiology*, 4(1), pp. 1–21.

Flory, J. *et al.* (2013) 'Influence of pH on the transport of silver nanoparticles in saturated porous media: Laboratory experiments and modeling', *Journal of Nanoparticle Research*, 15(3), pp. 1–56. Available at: https://doi.org/10.1007/s11051-013-1484-x.

Fontana, G. *et al.* (1998) 'Preparation , characterization and in vitro antimicrobial activity of ampicillin-loaded polyethylcyanoacrylate nanoparticles', *Biomaterials*, 19, pp. 1009–1017.

Friedman, N.D., *et al.*, (2016) 'The Negative Impact of Antibiotic Resistance', *Clinical Microbiology and Infection*, 22(5), pp. 416–422. Available at: https://doi.org/10.1016/j.cmi.2015.12.002.

Geilich, B.M. *et al.* (2015) ‘Silver nanoparticle-embedded polymersome nanocarriers for the treatment of antibiotic-resistant infections’, *Nanoscale*, 7(8), pp. 3511–3519. Available at: https://doi.org/10.1039/c4nr05823b.

Geta, K. (2019) ‘Factors, impacts and possible solutions of antibiotic resistance’, *World Scientific News*, 138(2), pp. 225–247.

Ghai, I. *et al.* (2018) ‘Ampicillin permeation across OmpF, the major outer-membrane channel in Escherichia coli’, *Journal of Biological Chemistry*, 293(18), pp. 7030–7037. Available at: https://doi.org/10.1074/jbc.RA117.000705.

Green, K.J., *et al*.,(2020) ‘Development and validation of a new microplate assay that utilises optical density to quantify the antibacterial activity of honeys including Jarrah , Marri and Manuka’, *PLOS ONE*, pp. 1–25. Available at: https://doi.org/10.1371/journal.pone.0243246.

Gupta, A. *et al.* (2020) ‘HHS Public Access’, *Mem Inst Oswaldo Cruz*, 48(2), pp. 415–427. Available at: https://doi.org/10.1039/c7cs00748e.Combatting.

Guruvu, N. *et al.* (2022) ‘Synergistic antimicrobial activity of honey combined with silver nanoparticles topically applied in experimentally infected wounds in Wistar albino rats’, *National Journal of Physiology, Pharmacy and Pharmacology*, 12(1), p. 1. Available at: https://doi.org/10.5455/njppp.2022.11.07239202120072021.

Habsi, F.S. Al *et al.* (2019) ‘Green synthesis, characterization and optimization of silver nanoparticles using honey and antimicrobial study with food supplements’, *Indian Journal of Natural Products and Resources*, 10(2), pp. 150–157.

Hadiya, S. *et al.* (2018) ‘Levofloxacin-loaded nanoparticles decrease emergence of fluoroquinolone resistance in Escherichia coli’, *Microbial Drug Resistance*, 24(8), pp. 1098–1107. Available at: https://doi.org/10.1089/mdr.2017.0304.

Haiza, H *et al.* (2013) ‘Green synthesis of silver nanoparticles using local honey’, *Trans Tech Publications Ltd*, 4, pp. 87–98. Available at: https://doi.org/10.4028/www.scientific.net/NH.4.87.

Haiza, Haroon *et al.* (2013) ‘Green Synthesis of Silver Nanoparticles Using Local Honey’, *Nano*

*Hybrids*, 4, pp. 87–98. Available at: https://doi.org/10.4028/www.scientific.net/nh.4.87.

Hasan, T.H. *et al*.,(2020) 'Mechanisms of antibiotics resistance in bacteria', *Systematic Reviews in Pharmacy*, 11(6), pp. 817–823. Available at: https://doi.org/10.31838/srp.2020.6.118.

Hernando-Amado, S. *et al.* (2019) 'Defining and combating antibiotic resistance from One Health and Global Health perspectives', *Nature Microbiology*, 4(9), pp. 1432–1442. Available at: https://doi.org/10.1038/s41564-019-0503-9.

Id, N.J.B. *et al.* (2018) 'Antibacterial Activities of Azole Complexes Combined with Silver Nanoparticles', *molecules*, 23(361), pp. 1–17. Available at: https://doi.org/10.3390/molecules23020361.

Israili, Z.H. (2014) 'Antimicrobial properties of honey', *American Journal of Therapeutics*, 21(4), pp. 304–323. Available at: https://doi.org/10.1097/MJT.0b013e318293b09b.

Jaeger, E.C. and Smith, A.C. (2021) 'Physical Description', *Introduction to the Natural History of Southern California*, pp. 8–12. Available at: https://doi.org/10.1525/9780520330870-002.

Jelinkova, P. *et al.* (2019) 'Nanoparticle-drug conjugates treating bacterial infections', *Journal of Controlled Release*, 307(April), pp. 166–185. Available at: https://doi.org/10.1016/j.jconrel.2019.06.013.

Jin, Y. *et al.* (2021) 'Synergistic and On-Demand Release of Ag-AMPs Loaded on Porous Silicon Nanocarriers for Antibacteria and Wound Healing', *ACS Applied Materials and Interfaces*, 13(14), pp. 16127–16141. Available at: https://doi.org/10.1021/acsami.1c02161.

Jubeh, B., *et al*.,(2020) 'Resistance of gram-positive bacteria to current antibacterial agents and overcoming approaches', *Molecules*, 25(12), pp. 1–23. Available at: https://doi.org/10.3390/molecules25122888.

Juraj Majtan, *et al.*,(2020) 'of Honey against Planktonic and Biofilm-Embedded Bacteria', *Molecular*, 25, pp. 1–13.

Kariuki, S., *et al*., (2021) 'Antimicrobial Resistance in Endemic Enteric Infections in Kenya and the Region, and Efforts Toward Addressing the Challenges', *The Journal of Infectious Diseases*,

224(Supplement_7), pp. S883–S889. Available at: https://doi.org/10.1093/infdis/jiab457.

Kędzierska-Matysek, M. *et al.* (2018) 'Application of FTIR spectroscopy for analysis of the quality of honey', *BIO Web of Conferences*, 10(March), p. 02008. Available at: https://doi.org/10.1051/bioconf/20181002008.

Khan, E. *et al.* (2015) 'Molecular structure, spectral analysis and hydrogen bonding analysis of ampicillin trihydrate: A combined DFT and AIM approach', *New Journal of Chemistry*, 39(12), pp. 9800–9812. Available at: https://doi.org/10.1039/c5nj01779c.

Khan, S.U.S.U. *et al.* (2019) 'Antimicrobial potentials of medicinal plant's extract and their derived silver nanoparticles: A focus on honey bee pathogen', *Saudi Journal of Biological Sciences*, 26(7), pp. 1815–1834. Available at: https://doi.org/10.1016/j.sjbs.2018.02.010.

Khatoon, N. *et al.* (2019) 'Ampicillin Silver Nanoformulations against Multidrug resistant bacteria', *Scientific Reports*, 9(1), pp. 1–10. Available at: https://doi.org/10.1038/s41598-019-43309-0.

Kolár, M. *et al.* (2016) 'Strong and nonspecific synergistic antibacterial efficiency of antibiotics combined with silver nanoparticles at very low concentrations showing no cytotoxic effect', *Molecules*, 21(1), pp. 1–17. Available at: https://doi.org/10.3390/molecules21010026.

Kora, A.J. and Rastogi, L. (2013) 'Enhancement of antibacterial activity of capped silver nanoparticles in combination with antibiotics, on model gram-negative and gram-positive bacteria', *Bioinorganic Chemistry and Applications*, 2013(1), p. 7. Available at: https://doi.org/10.1155/2013/871097.

Kumar, A.S. *et al.* (2020) 'Optical and antimicrobial properties of silver nanoparticles synthesized via green route using', *Green Processing and Synthesis*, 1(9), pp. 268–274.

Laallam, H. *et al.* (2015) 'Modeling the synergistic antibacterial effects of honey characteristics of different botanical origins from the Sahara Desert of Algeria', *Frontiers in Microbiology*, 6(NOV), pp. 1–12. Available at: https://doi.org/10.3389/fmicb.2015.01239.

Liu, Y. *et al.* (2021) 'Escherichia coli causing neonatal meningitis during 2001–2020: A study in

eastern China', *International Journal of General Medicine*, 14, pp. 3007–3016. Available at: https://doi.org/10.2147/IJGM.S317299.

Livermore, D.M., *et al*.,(2018) *Surveillance of antimicrobial resistance*, *British Medical Journal*. Available at: https://doi.org/10.1136/bmj.317.7159.614.

Mandal, M.D. and Mandal, S. (2011) 'Honey: Its medicinal property and antibacterial activity', *Asian Pacific Journal of Tropical Biomedicine*, 1(2), pp. 154–160. Available at: https://doi.org/10.1016/S2221-1691(11)60016-6.

Maria Pilar Vinardell *, *et al*.,(2017) 'In vitro comparative skin irritation induced by nano and non-nano zinc oxide', *Nanomaterials*, 7(3), p. 56. Available at: https://doi.org/10.3390/nano7030056.

Matar, G.H. *et al.* (2022) 'An Investigation of Green Synthesis of Silver Nanoparticles Using Turkish Honey Against Pathogenic Bacterial Strains', *Biointerface Research in Applied Chemistry*, 13(2), pp. 1–11. Available at: https://doi.org/10.33263/BRIAC132.195.

Mbanga, O., *et al*.,(2022) 'Dissolution kinetics of silver nanoparticles: Behaviour in simulated biological fluids and synthetic environmental media', *Toxicology Reports*, 9(February), pp. 788–796. Available at: https://doi.org/10.1016/j.toxrep.2022.03.044.

Merker, M. *et al.* (2020) 'Evolutionary Approaches to Combat Antibiotic Resistance: Opportunities and Challenges for Precision Medicine', *Frontiers in Immunology*, 11(August), pp. 1–7. Available at: https://doi.org/10.3389/fimmu.2020.01938.

Moges, F. *et al.* (2014) 'The growing challenges of antibacterial drug resistance in Ethiopia', *Journal of Global Antimicrobial Resistance*, 2(3), pp. 148–154. Available at: https://doi.org/10.1016/j.jgar.2014.02.004.

Mohammed *et al.* (2010) 'Biogenic synthesis of silver nanoparticles and their synergistic effect with antibiotics: a study against gram-positive and gram-negative bacteria', *Nanomedicine: Nanotechnology, Biology, and Medicine*, 6(1), pp. 103–109. Available at: https://doi.org/10.1016/j.nano.2009.04.006.

Mokhena, T. *et al.* (2018) ‘We are IntechOpen , the world ’ s leading publisher of Open Access books Built by scientists , for scientists TOP 1 %’, *Intech*, pp. 225–240. Available at: https://www.intechopen.com/books/advanced-biometric-technologies/liveness-detection-in-biometrics.

Molchanova, N., *et al*., (2017) ‘Advances in development of antimicrobial peptidomimetics as potential drugs’, *Molecules*, 22(9), pp. 1–60. Available at: https://doi.org/10.3390/molecules22091430.

Molleman, B. *et al*., (2017) ‘Time, pH, and size dependency of silver nanoparticle dissolution: The road to equilibrium’, *Environmental Science: Nano*, 4(6), pp. 1314–1327. Available at: https://doi.org/10.1039/c6en00564k.

Morigi, V. *et al.* (2012) ‘Nanotechnology in Medicine: From Inception to Market Domination’, *Journal of Drug Delivery*, 2012, pp. 1–7. Available at: https://doi.org/10.1155/2012/389485.

Mulugeta, E. (2020) ‘Journl of Agricultural Science and Food Research Physicochemical Analysis and Determination of the Levels of Some Heavy Metals in Honey Samples Collected from Three District Area of East Goj- jam Zone of Amhara Region , Ethiopia’, *Journl of Agricultural Science and Food Research*, 11(4 November), p. 279. Available at: https://doi.org/10.35248/2593-9173.20.11.279.

Murei, A. (2020) ‘Functionalization and antimicrobial evaluation of ampicillin , penicillin and vancomycin with Pyrenacantha grandiflora Baill and silver nanoparticles’, *Scientific Reports*, 10(0123456789), pp. 1–14. Available at: https://doi.org/10.1038/s41598-020-68290-x.

Murugaiyan, J. *et al.* (2022) ‘Progress in Alternative Strategies to Combat Antimicrobial Resistance: Focus on Antibiotics’, *Antibiotics*, 11(2), pp. 1–37. Available at: https://doi.org/10.3390/antibiotics11020200.

Nishio, E.K. *et al.* (2016) ‘Antibacterial synergic effect of honey from two stingless bees : Scaptotrigona bipunctata’, *scientificreports*, (January 2015), pp. 1–8. Available at: https://doi.org/10.1038/srep21641.

Othman, A.M. *et al.* (2020) ‘Correction to: Biosynthesis and characterization of silver

nanoparticles induced by fungal proteins and its application in different biological activities (Journal of Genetic Engineering and Biotechnology, (2019), 17, 1, (8), 10.1186/s43141-019-0008-1)', *Journal of Genetic Engineering and Biotechnology*, 18(1), pp. 1–13. Available at: https://doi.org/10.1186/s43141-020-0022-3.

Pal, S.L. *et al.* (2011) 'Nanoparticle : An overview of preparation and characterization', *Journal of Applied Pharmaceutical Science*, 01(06), pp. 228–234.

Percival, S.L., *et al.*,(2019) 'Silver, biofilms and wounds: resistance revisited', *Critical Reviews in Microbiology*, 45(2), pp. 223–237. Available at: https://doi.org/10.1080/1040841X.2019.1573803.

Prasad, S. (2008) 'Nanotechnology in Medicine and Antibacterial Effect of', *Digest Journal of Nanomaterials and Biostructures*, 3(3), pp. 115–122.

Pryshchepa, O., *et al.*, (2020) 'Silver nanoparticles: Synthesis, investigation techniques, and properties', *Advances in Colloid and Interface Science*, 284, pp. 87–100. Available at: https://doi.org/10.1016/j.cis.2020.102246.

Puzniak, L. *et al.* (2021) 'Real-world use of ceftolozane/tazobactam: a systematic literature review', *Antimicrobial Resistance and Infection Control*, 10(1), pp. 1–20. Available at: https://doi.org/10.1186/s13756-021-00933-8.

Regea, G. (2018) 'Review on Antibiotics Resistance and its Economic Impacts', *Journal of Pharmacology & Clinical Research*, 5(5), pp. 1–11. Available at: https://doi.org/10.19080/JPCR.2018.05.55567.

Rogowska, A. *et al.* (2017) 'Silver nanoparticles functionalized with ampicillin', *Electrophoresis*, 38(21), pp. 2757–2764. Available at: https://doi.org/10.1002/elps.201700093.

Samuel Kariuki, and G.D. (2015) 'NIH Public Access', *NIH Public Access*, 1323(1), pp. 43–55. Available at: https://doi.org/10.1111/nyas.12380.Antibacterial.

Sanmuham, V. *et al.* (2021) 'Effect of silver nanopowder on mechanical, thermal and antimicrobial properties of kenaf/hdpe composites', *Polymers*, 13(22), pp. 1–14. Available at: https://doi.org/10.3390/polym13223928.

Sanseverino, I. *et al.* (2018) 'Amr__Jrc_Technical__Report_Final_Online_15Jan.2019', *JRC Science Hub*, pp. 1–109. Available at: https://doi.org/10.2760/82376.

Sekar, R.P. *et al.* (2013) 'Formulation and Evaluation of Azathioprine Loaded Silver Nanopartilces for The Treatment of Rheumatoid Arthritis', *Asian Journal of Biomedical and Pharmaceutical Sciences*, 3(23), p. 28.

El Shafey, A.M. (2020) 'Green synthesis of metal and metal oxide nanoparticles from plant leaf extracts and their applications: A review', *Green Processing and Synthesis*, 9(1), pp. 304–339.

Shah Faisal*, *et al.*, (2021) 'Green Synthesis of Zinc Oxide (ZnO) Nanoparticles Using Aqueous Fruit Extracts of Myristica fragrans: Their Characterizations and Biological and Environmental Applications', *ACS Omega*, 6(14), pp. 9709–9722. Available at: https://doi.org/10.1021/acsomega.1c00310.

Shah, K.N. (2022) 'Studies on phytochemical composition of wild honey from Melghat province', *Journal of Pharmacognosy and Phytochemistry*, 11(1), pp. 235–238.

Shaker, M.A. and Shaaban, M.I. (2017) 'Formulation of carbapenems loaded gold nanoparticles to combat multi-antibiotic bacterial resistance: In vitro antibacterial study', *International Journal of Pharmaceutics*, 525(1), pp. 71–84. Available at: https://doi.org/10.1016/j.ijpharm.2017.04.019.

Sharma, R., *et al.*, (2020) 'A review on biogenic synthesis, applications and toxicity aspects of zinc oxide nanoparticles', *EXCLI Journal*, 19, pp. 1325–1340. Available at: https://doi.org/10.17179/excli2020-2842.

Singh, A. *et al.* (2020) 'Green synthesis of metallic nanoparticles as effective alternatives to treat antibiotics resistant bacterial infections: A review', *Biotechnology Reports*, 25, p. e00427. Available at: https://doi.org/10.1016/j.btre.2020.e00427.

Singh, M. *et al.* (2021) 'Biomimetic synthesis of silver nanoparticles from aqueous extract of saraca indica and its profound antibacterial activity', *Biointerface Research in Applied Chemistry*, 11(1), pp. 8110–8120. Available at: https://doi.org/10.33263/BRIAC111.81108120.

Sreedharan, S.M. and Singh, R. (2019) 'Ciprofloxacin functionalized biogenic gold nanoflowers as

nanoantibiotics against pathogenic bacterial strains', *International Journal of Nanomedicine*, 14, pp. 9905–9916. Available at: https://doi.org/10.2147/IJN.S224488.

Stabryla, L.M. *et al.* (2021) 'Role of bacterial motility in differential resistance mechanisms of silver nanoparticles and silver ions', *Nature Nanotechnology*, 16(September), pp. 996–1003. Available at: https://doi.org/10.1038/s41565-021-00929-w.

Suhandy, D. and Yulia, M. (2021) 'The use of UV spectroscopy and SIMCA for the authentication of Indonesian honeys according to botanical, entomological and geographical origins', *Molecules*, 26(4), pp. 1–13. Available at: https://doi.org/10.3390/molecules26040915.

Thapa, R. *et al.* (2017) 'Enzyme-mediated formulation of stable elliptical silver nanoparticles tested against clinical pathogens and MDR bacteria and development of antimicrobial surgical thread', *Annals of Clinical Microbiology and Antimicrobials*, 16(1), pp. 1–10. Available at: https://doi.org/10.1186/s12941-017-0216-y.

Thiruvengadam, V. *et al.*,(2020) 'Characterization of silver nanoparticles synthesized using chemical method and its antibacterial property', *Biointerface Research in Applied Chemistry*, 10(6), pp. 7257–7264. Available at: https://doi.org/10.33263/BRIAC106.72577264.

Tsang, K.K. *et al.* (2017) 'The anti-inflammatory and antibacterial action of nanocrystalline silver and manuka honey on the molecular alternation of diabetic foot ulcer: A comprehensive literature review', *Evidence-based Complementary and Alternative Medicine*, 2015, pp. 1–20. Available at: https://doi.org/10.1155/2015/218283.

Tsuji, A. *et al.* (1978) 'Physicochemical properties of amphoteric β-lactam antibiotics I: Stability, solubility, and dissolution behavior of amino penicillins as a function of pH', *Journal of Pharmaceutical Sciences*, 67(8), pp. 1059–1066. Available at: https://doi.org/10.1002/jps.2600670810.

Tuem, K.B. *et al.* (2018) 'Drug Resistance Patterns of Escherichia coli in Ethiopia: A Meta-Analysis', *BioMed Research International*, 2018, pp. 1–14. Available at: https://doi.org/10.1155/2018/4536905.

Tuem, K.B. *et al.* (2019) 'Antimicrobial resistance patterns of uropathogens isolated between 2012

and 2017 from a tertiary hospital in Northern Ethiopia', *Journal of Global Antimicrobial Resistance*, 18, pp. 109–114. Available at: https://doi.org/10.1016/j.jgar.2019.01.022.

US Department of Health and Human Services (1992) 'Toxicology and Carcinogenesis Studies of Ampicillin Trihydrate in F344/N Rats', *National Toxicology Program Technical Report Series*, 409(275), pp. 1–171.

Vallet-Regí, M.,*et al*., (2019) 'Nanomaterials as promising alternative in the infection treatment', *International Journal of Molecular Sciences*, 20(15), pp. 1–18. Available at: https://doi.org/10.3390/ijms20153806.

Wang, L., Hu, C. and Shao, L. (2017) 'The-antimicrobial-activity-of-nanoparticles--present-situati', *International journal of nanomedicine*, 12, pp. 1227–1249. Available at: https://www.ncbi.nlm.nih.gov/pmc/articles/PMC5317269/pdf/ijn-12-1227.pdf.

Weng, J., *et al*., (2020) 'In vitro release study of the polymeric drug nanoparticles: Development and validation of a novel method', *Pharmaceutics*, 12(8), pp. 1–18. Available at: https://doi.org/10.3390/pharmaceutics12080732.

Y., E. *et al.* (2013) 'Antibacterial effects of Apis mellifera and stingless bees honeys on susceptible and resistant strains of Escherichia coli, Staphylococcus aureus and Klebsiella pneumoniae in Gondar, Northwest Ethiopia', *BMC Complementary and Alternative Medicine*, 13(1), pp. 1472–6882. Available at: http://www.embase.com/search/results?subaction=viewrecord&from=export&id=L52825320%5Cnhttp://www.biomedcentral.com/1472-6882/13/269%5Cnhttp://dx.doi.org/10.1186/1472-6882-13-269%5Cnhttp://sfx.hul.harvard.edu/sfx_local?sid=EMBASE&issn=14726882&id=doi:10.11.

Zhang, X.F. *et al.* (2016) 'Silver nanoparticles: Synthesis, characterization, properties, applications, and therapeutic approaches', *International Journal of Molecular Sciences*, 17(9), pp. 5–6. Available at: https://doi.org/10.3390/ijms17091534.

**Appendices**

**Appendices I: Ampicillin Calibration Curves for loading Study**

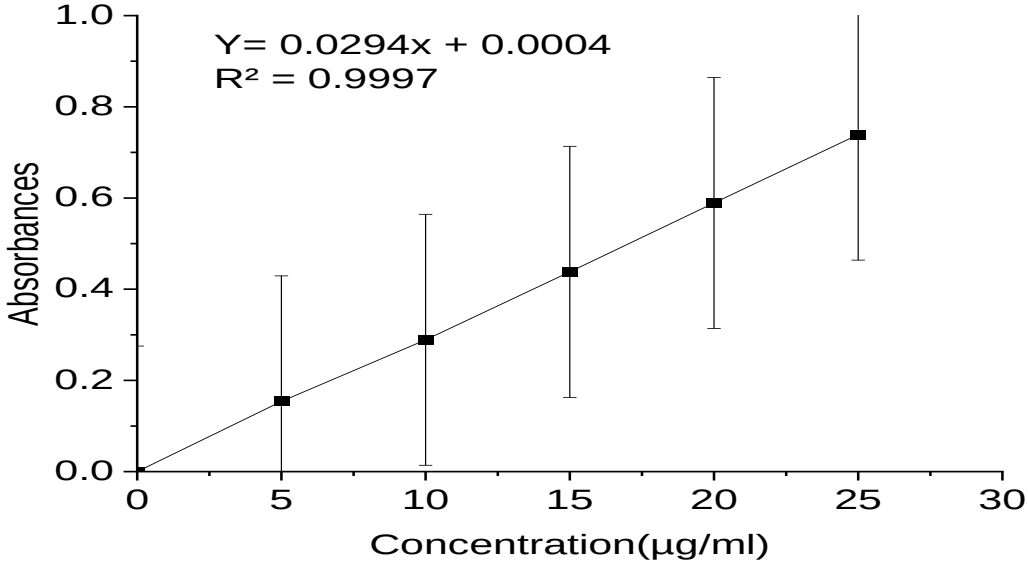


## Appendices II: Ampicillin Calibration Curves for Release Study

A. Standard calibration curve of pure ampicillin at λmax of 222nm in buffer solution with pH value of 1.2.

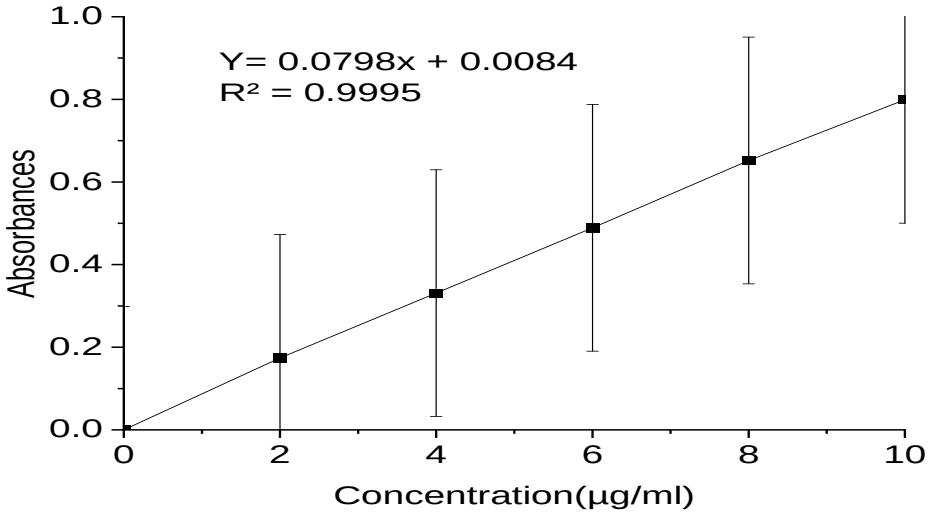

B. Standard calibration curve of pure ampicillin at λmax of 224nm in buffer solution with pH value of 6.0.

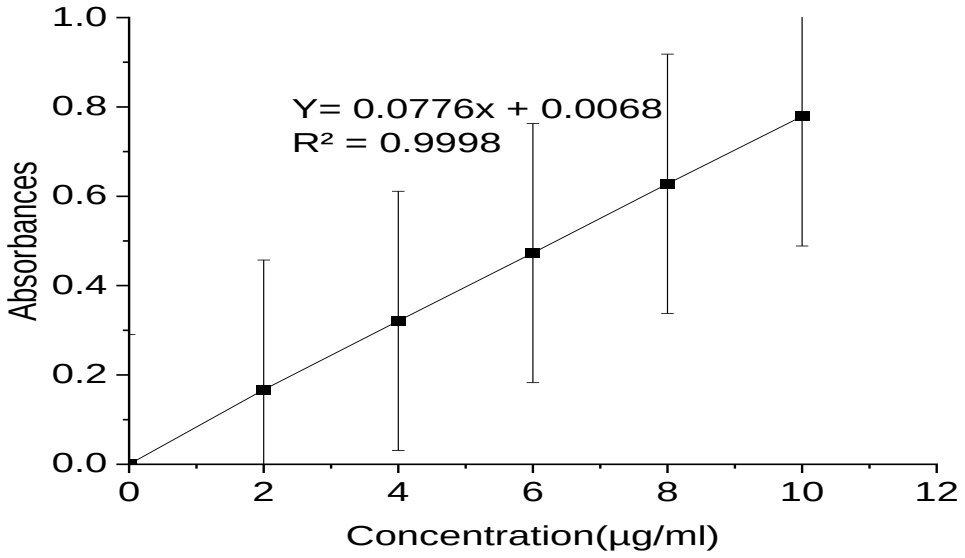


C. Standard calibration curve of pure ampicillin at λmax of 220nm in buffer solution with pH value of 7.3.

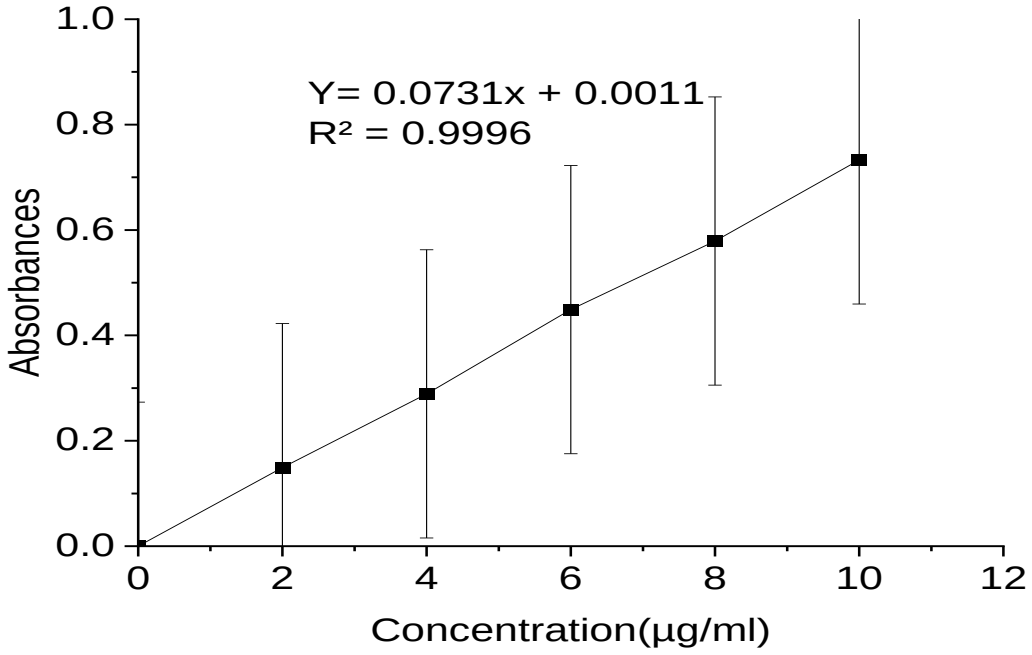

D. Standard calibration curve of pure ampicillin at λmax of 218nm in buffer solution with pH value of 7.4.

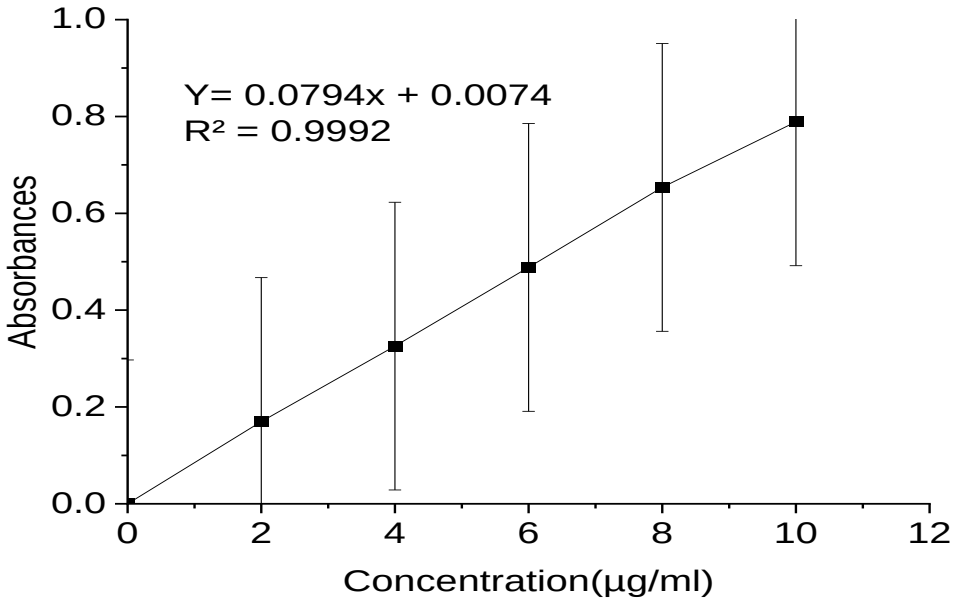


E. Standard calibration curve of pure ampicillin at λmax of 222nm in buffer solution with pH value of 8.

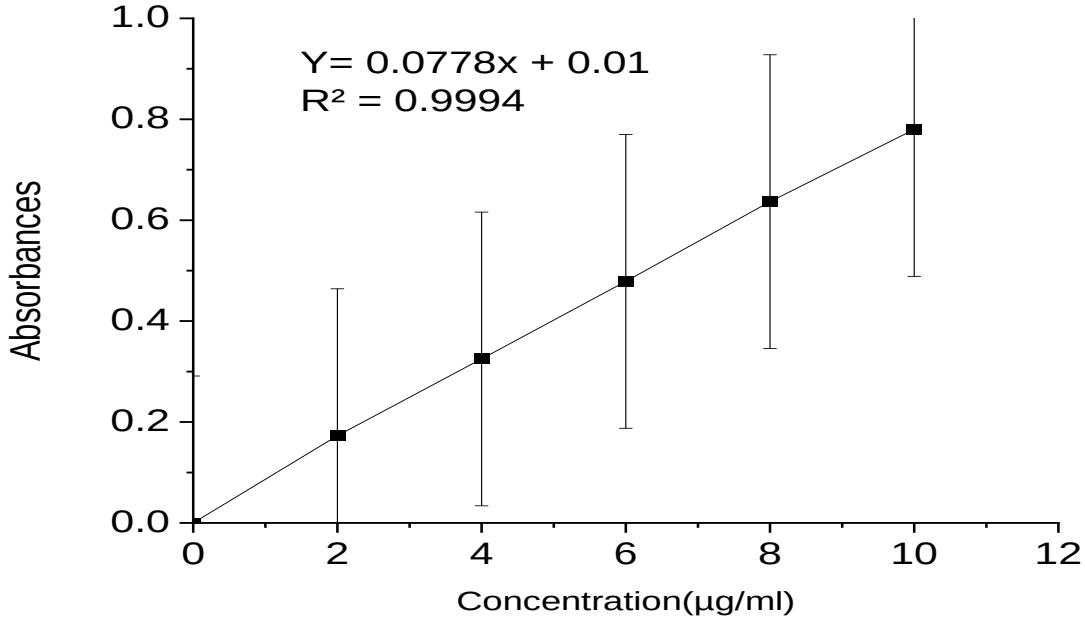

**Appendices III: FTIR analysis of AMP (A), Free AgNPs (B), Honey (C) and AMP Loaded AgNPs (D) Data**

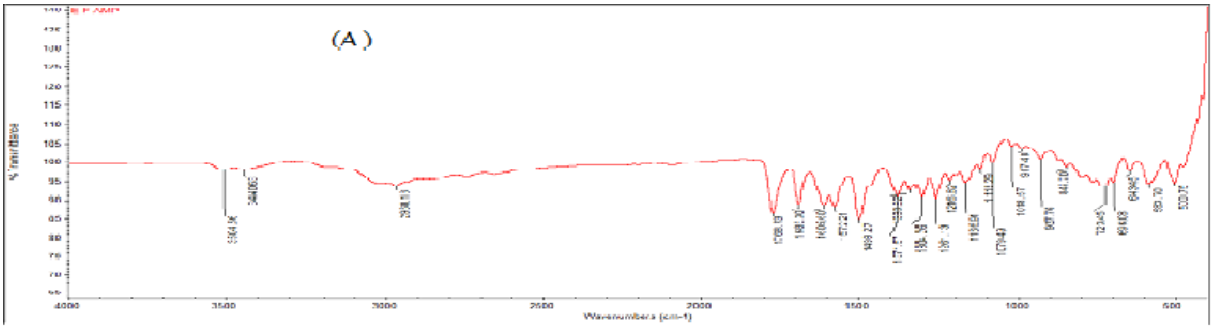


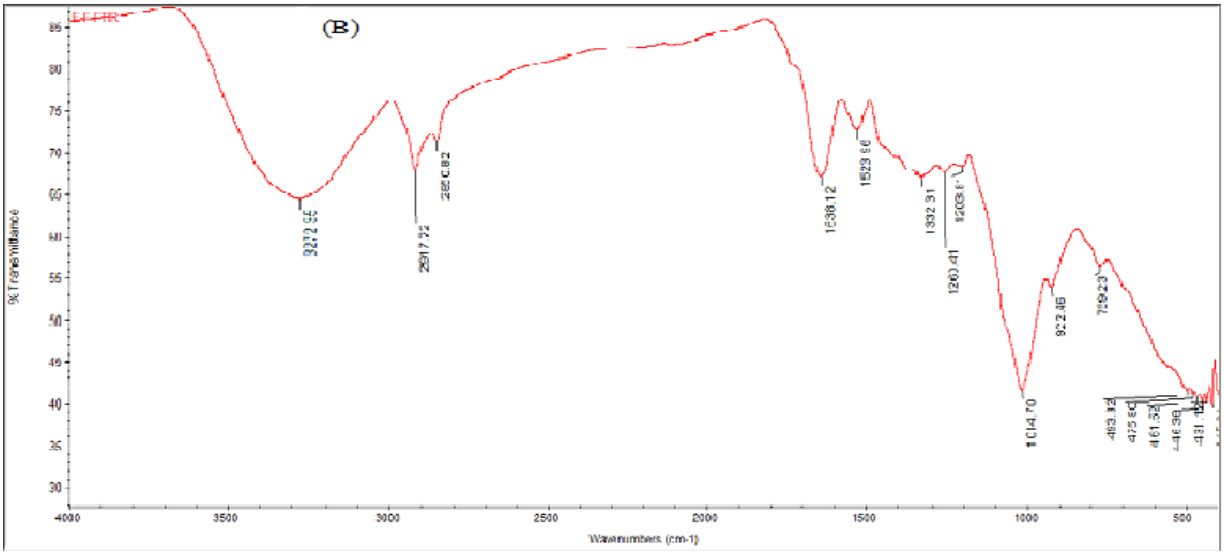


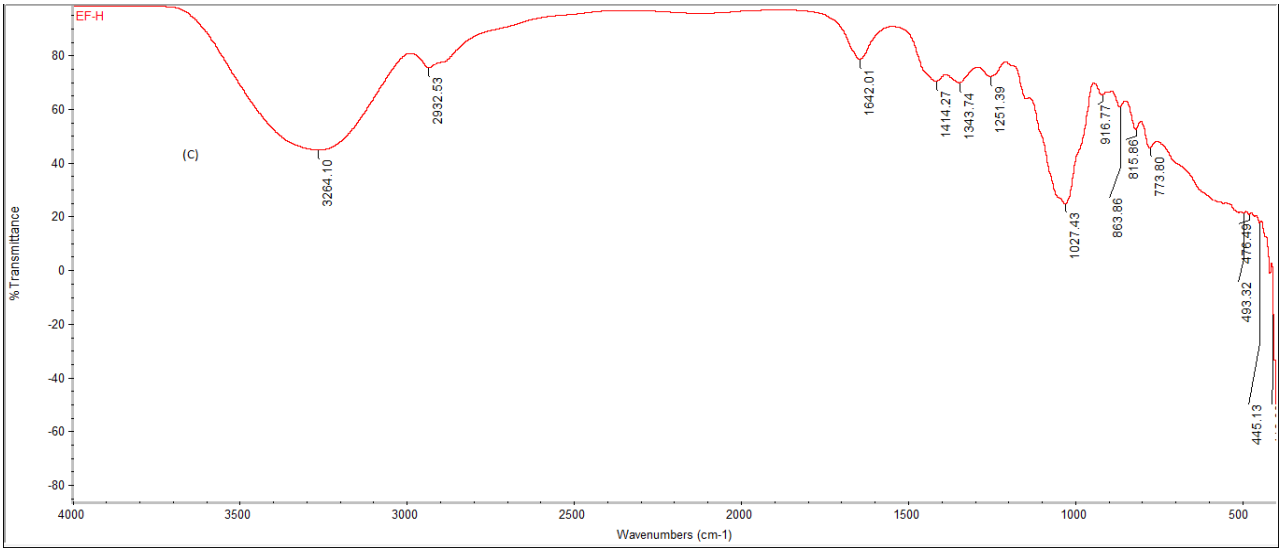

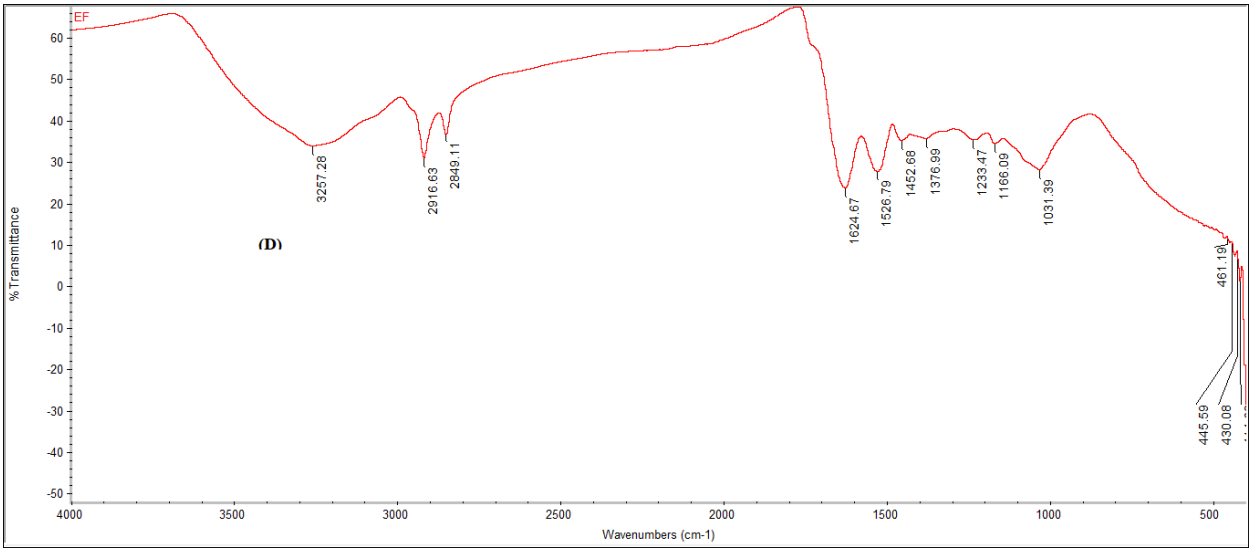


# Appendices IV: XRD analysis of AgNPs Data